Kestrel

Transition into a new era

Alfred Gessow Rotorcraft Center
Department of Aerospace Engineering
University of Maryland
College Park, MD 20740, USA

University of Maryland
Alfred Gessow Rotorcraft Center
Department of Aerospace Engineering
College Park, Maryland 20742

Transitioning into a New Era

Elena Shrestha, Graduate Student

Michael Avera, Graduate Student

Tyler Fean, Graduate Student

Camli Badrya, Graduate Student

Jonathan Chambers, Graduate Student

Dr. Inderjit Chopra, Faculty Advisor

Chin Gian Hooi, Graduate Student

Dr. J. Gordon Leishman, Faculty Advisor

Dr. V.T. Nagaraj, Faculty Advisor

AHS Graduate Student Design Team
Alfred Gessow Rotorcraft Center
University of Maryland
College Park, MD 20742, USA

To the American Helicopter Society,

The University of Maryland Graduate Design Team hearby grants AHS the permission to distribute this report as they see fit.

Thank You,

UMD Design Team

ACKNOWLEDGMENTS

The University of Maryland graduate team wishes to acknowledge the following people for their assistance and guidance throughout this design process:

Professors:

Dr. Inderjit Chopra – Alfred Gessow Professor, Director of Alfred Gessow Rotorcraft Center (AGRC), Dept. of Aerospace Engineering, University of Maryland, College Park

Dr. J. Gordon Leishman – Minta Martin Professor of Engineering, Dept. of Aerospace Engineering, University of Maryland, College Park

Dr. Vengalattore T. Nagaraj – Senior Research Scientist, Dept. of Aerospace Engineering, University of Maryland, College Park

Dr. Derek Paley – Willis H. Young Associate Professor, Dept. of Aerospace Engineering, University of Maryland, College Park

Dr. James Baeder – Associate Professor, Dept. of Aerospace Engineering, University of Maryland, College Park

Industry Professionals:

Mark Alber – Manager, Advanced Concepts, Sikorsky Aircraft

Dr. Ashish Bagai – Program Manager, Tactical Technology Office, Defense Advanced Research Projects Agency

Dr. Andy Bernhard – Chief Engineer, Sikorsky Aircraft

Dr. Hao Kang – Research Aerospace Engineer, U.S. Army Research Laboratory, Aberdeen Proving Ground, MD

Charley Kilmain – Director, Rotor and Drive System Design, Bell Helicopter Textron, Inc.

Dr. James Wang – Vice President of Research and Technology, AgustaWestland

Special Thanks to:

Daniel Brown	Dr. Ananth Sridharan	Joseph Schmaus	William Staruk
Graham Bowen-Davies	Bharath Govindarajan	Elizabeth Weiner	Jaime Reel
Dr. Vikram Hrishikeshavan	Dr. Derrick Yeo	Dr. Anish Sydney	Dr. Joe Milluzo
James Lankford	Maryland State Police	Advanced Helicopter Concepts	

Contents

List of Tables

List of Figures

1 Vehicle Configuration Selection

In response to the American Helicopter Society's 2014 Student Design Competition Request for Proposal (RFP), the University of Maryland Graduate Team proudly presents the *Kestrel*, a dual-rotor tailsitter aircraft that represents a leap forward in Vertical Takeoff and Landing (VTOL) aircraft performance.

The current fleet of VTOL aircraft is dominated by the single main rotor configuration, which provides good hovering capabilities but is inadequate for long range and high speed missions. This performance shortfall was the inspiration for the United States Defense Advanced Research Projects Agency (DARPA) to commence the VTOL X-Plane program in February 2013 [1]. The objective of the VTOL X-Plane program is to foster the design and development of advanced technologies, subsystems, vehicle designs and configurations to advance the fundamental capabilities of VTOL aircraft. The VTOL X-Plane program does not stipulate any specific mission because it seeks to demonstrate significant improvement in the areas of hover time, maximum airspeed, range, and useful load capabilities. Also in mind, is a focus to overcome typical performance issues of current rotorcraft that limit capabilities such as retreating blade stall, advancing blade compressibility effects, high parasite drag, thrust download penalties, and losses from complex aerodynamic interactions.

1.1 Performance Requirements

The 2014 AHS Student Design Competition RFP has followed DARPA's requirements and set goals almost identical to the VTOL X-Plane program. There are four main performance requirements:

- Sustained forward flight between 300 kts and 400 kts.
- Aircraft hovering efficiency within 25% of the ideal power loading.
- Aircraft lift-to-drag ratio of 10 or higher.
- Useful load fraction of at least 40% of gross weight with a payload fraction no less than 12.5% of gross weight.

The goals represent a jump in VTOL aircraft performance. Today's rotorcraft typically have maximum speeds around 170 kts, lift-to-drag ratios around 4, hover efficiencies near 60% of ideal, and empty weight fractions greater than 60%. The vehicle must also be capable of a minimum -0.5 G to 2.0 G load factor and should weigh between 10,000 lb and 12,000 lb, with scalability potential down to 4,000 lb and up to 24,000 lb. The use of new technologies is encouraged, with the provision that any new technologies or subsystems must be mature sufficiently enough within 52 months to be integrated on a technology demonstrator for safe and reliable flight. The powerplant selection was restricted to existing available engines.

The RFP retained the non-mission specific nature of the X-Plane program, however, to compare all designs, a representative mission profile was given and is discussed in Chapter 2.

1.2 Assessment of Potential Configurations

The rationale for the selection of a tailsitter configuration to fulfill the requirements of the RFP is presented with a thorough evaluation of alternate configurations. The key design drivers were based on the requirements for high speed flight and incorporating advanced aerodynamic features. Decision analysis tools were used to provide an additional foundation for the selection of a tailsitter.

1.2.1 Conventional Single Main Rotor

The first aircraft configuration evaluated was the single main rotor (SMR) with a tail rotor as shown in Fig. 1.1(a). The large open main rotor provides a lower disk loading and a lower power requirement to hover. This configuration has had decades of operation and offers a low empty weight, good mechanical reliability, and low maintenance and

production costs. However, its use of an edgewise oriented rotor in forward flight limits its high speed capabilities. The SMR configuration has lower range capabilities when compared to designs that utilize fixed-wings for lift in forward flight. Because high maximum forward flight speed is a key requirement of the RFP, the single main rotor configuration was not considered for the *Kestrel*.

(a) Maryland State Police AugustaWestland 139.

(b) Boeing CH-47, Boeing CH-46, Piasecki CH-21, Piasecki H-25.

Figure 1.1: a) Single main rotor and b) tandem rotor helicopters.

1.2.2 Tandem Rotors

Tandem rotor configurations utilize two large open rotors rotating in opposite directions. Four examples of tandem rotor aircraft are shown in Fig. 1.1(b). These aircraft have high payload capabilities because of their low disk loading and greater range of allowable center of gravity travel. These qualities are well suited to cargo transport missions but not for high speed forward flight. As with the single main rotor configuration, tandem rotor aircraft suffer from retreating blade stall and compressibility effects that arise from using an edgewise rotor in forward flight. Because of this, the maximum speed of tandem rotor aircraft is low, and therefore, this configuration was not considered for the *Kestrel*.

1.2.3 Compound Configurations

Compound configurations consisting of thrust augmentation, such as the Sikorsky X-2, and both lift and thrust augmentation, such as the Airbus Helicopters X^3 shown in Fig. 1.2(a), fly much faster than SMR helicopters and can maintain a level attitude in high speeds reducing parasitic drag. The wings and auxiliary propellers offset the lift and thrust needed from the main rotor making it more efficient. However, because compound configurations still use one or two rotors in edgewise flight, they still have limited maximum airspeed capabilities and incur significant drag from the rotor hub. Therefore, a compound configuration was not selected for the *Kestrel*.

1.2.4 Slowed Rotor

The slowed rotor configuration, as shown in Fig. 1.2(b), has very similar characteristics to the thrust and lift augmented compound configuration. However, the slowed rotor configuration has a main rotor that is slowed significantly when compared to the thrust and lift augmented compound configuration. In forward flight, the main rotor is unpowered and is in an autorotative state. This condition significantly decreases the power required for forward flight leading to higher lift-to-drag ratios. However, the slowed rotor aircraft cannot sustain hovering flight which is a requirement in the RFP mission profile. The main rotor and hub also contribute a significant amount of drag, limiting the slowed rotor maximum airspeed potential. Because of these disadvantages, the slowed rotor configuration was not chosen for the *Kestrel*.

(a) Airbus Helicopters X^3.

(b) Carter PAV.

Figure 1.2: a) Compound and b) slowed rotor configurations.

1.2.5 Stopped Rotor

Stopped rotor configurations consist of a main rotor, at least two fixed-wings and a turbine or propeller powered thruster, as shown in Fig. 1.3(a). The main rotor provides lift and VTOL capabilities. In forward flight the rotor is completely stopped and lift is provided by the rotor acting as a set of wings. In some designs, one blade of the main rotor is pitched 180° such that both of the leading edges of the blades point forward and the rotor blades form a third lifting surface. Several sets of fixed wings produce more drag and weigh more than a single fixed-wing. The blades of the main rotor are a design compromise between high aspect ratio flexible blades and lower aspect ratio rigid wings. Prior stopped rotor concepts suffered from stability issues in the transition phase, and the concept was never truly been validated through rigorous flight testing. Because of these disadvantages, the stopped rotor configuration was not considered for the *Kestrel*.

(a) Boeing X-50 Dragonfly.

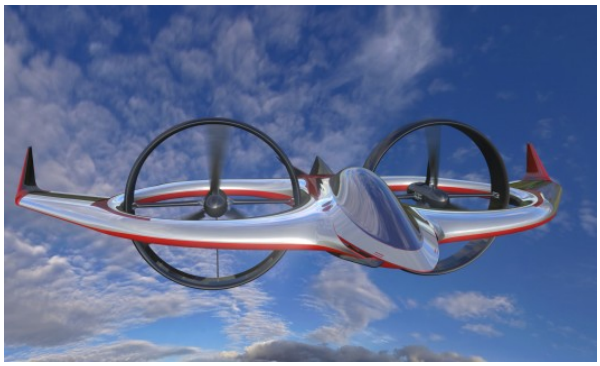

(b) AugustaWestland Project Zero.

Figure 1.3: a) Stopped rotor and b) fan-in-wing configurations.

1.2.6 Fan-In-Wing

Even though several fan-in-wing configurations have been designed and flown, none have ever entered production. A recent version of the fan-in-wing configuration is the AugustaWestland Project Zero, as shown in Fig. 1.3(b). In VTOL mode, these rotor systems provide thrust and control. To transition into forward flight mode, both rotors tilt 90° to maintain axial flight. This approach has the distinct advantage of resolving stall and compressibility issues associated

with rotors in edgewise flight. However, the size of the rotors are restricted to fit into the wing platform. This size limitation artificially limits the rotor efficiency when compared to a configuration with lower disk loading because it does not have this constraint. Also, in forward flight the two large openings which accommodate the rotors produce extra drag over a traditional fixed-wing aircraft. Any devices used to cover up the holes in forward flight to reduce drag would increase the empty weight of the aircraft. The fan-in-wing was not chosen because the RFP requires a high lift-to-drag ratio and hover efficiency.

1.2.7 Tandem Lift-Fan

Another version of the fan-in-wing configuration uses turbine powered forward thrust and a lift fan embedded in each wing for vertical lift. The Ryan XV-5, shown in Fig. 1.4(a), uses directed jet thrust from its two turbojet engines to power the two, three foot diameter lift fans. Because of the small area of the fans, the XV-5's high disk loading of 42.9 lb sf^{-2} leads to issues of ground crew safety and lower hover efficiency. While capable of high maximum cruise speeds, a fan-in-wing configuration similar to the XV-5 was not chosen for the *Kestrel* because of its poor hover efficiency.

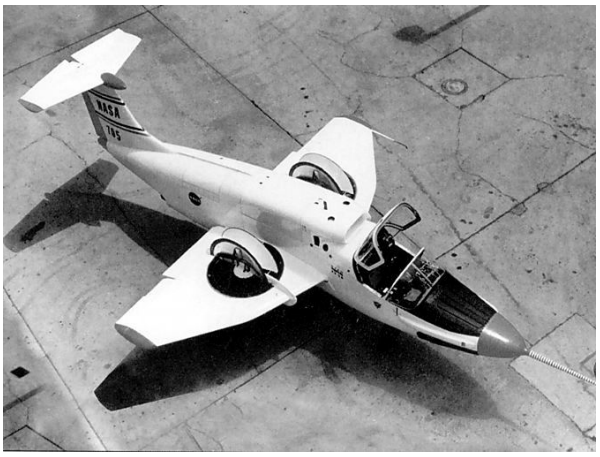

(a) Ryan XV-5.

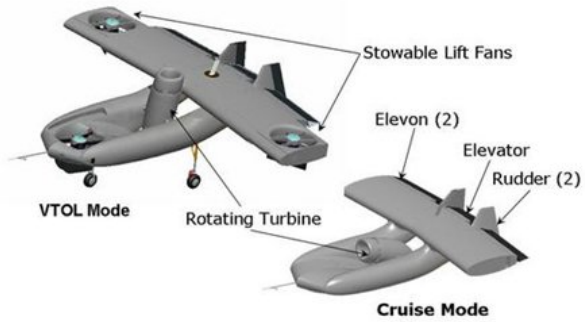

(b) Aurora Flight Sciences Excalibur.

Figure 1.4: Fan-in-wing configurations.

1.2.8 Tilting Turbine

The final fan-in-wing design explored was the Aurora Flight Sciences *Excalibur*, as shown in Fig. 1.4(b), which uses three lift fans and one rotating turbine engine. In hovering mode, the *Excalibur* rotates its turbojet engine downward, extends two stowable lift fans outboard of its wing, and uses a nose lift fan to produce thrust. To transition into cruise mode, the turbine engine rotates to provide propulsive thrust, stows its two wing-mounted lift fans, and covers up its nose lift fan. In forward flight, the body produces some amount of lift. This configuration has a relatively high empty weight by utilizing four systems for lift in hover. Also, the lift fans have lower hovering efficiencies. Therefore, this fan-in-wing configuration was not considered for the *Kestrel*.

1.2.9 Tiltrotor

The tiltrotor, shown in Fig. 1.5(a), combines the hovering capability of a rotary-wing aircraft and the forward flight capability of a fixed-wing aircraft. This configuration offers significant advantages over other VTOL aircraft with

respect to maximum speed, range, and endurance. A drawback to all tiltrotors is the additional systems required to support and rotate the proprotors. These additional systems increase the empty weight and mechanical complexity of the aircraft. Another drawback to the tiltrotor design is that tiltrotors have a relatively high download penalty in VTOL from rotor downwash impinging on the wings and fuselage. This configuration is a feasible option to satisfy the requirements of the RFP. However the inherent empty weight and download penalties of a tiltrotor lead to considerable inefficiencies. It was decided that this configuration would only allow for incremental advancements of existing aircraft, and not the radical improvements required by the RFP. Therefore, the tiltrotor configuration was not selected.

(a) AgustaWestland 609. (b) AeroVironment Skytote.

Figure 1.5: a) Tiltrotor and b) tailsitter configurations.

1.2.10 Tailsitter

The tailsitter configuration has a similar rotor-wing-fuselage layout as a traditional fixed-wing aircraft, except that when at rest, the tailsitter stands on its rear empennage. Past versions of the tailsitter were propelled by jet thrust and coaxial counter rotating rotors. In hover the aircraft is oriented vertically, as shown in Fig. 1.5(b), and transitions to level flight either by the use of control surfaces submerged in the rotor wash, cyclic control of the main rotor system, or by using small control jets. The tailsitter is a mechanically efficient design in that it uses the same propulsion system for hover and forward flight, keeping the vehicle empty weight low. Open rotor versions maintain the high efficiency of a rotor system, while keeping the rotor in sustained axial flight to eliminate vibration, stall, and compressibility issues of edgewise rotor designs. Because of their clean fuselage and axially oriented rotors, tailsitter configurations in the 1950s had estimated maximum speeds of up to 500 kts. Unlike a tiltrotor, the tailsitter does not require any heavy hydraulic system to rotate the rotors from axial flight. The tailsitter also does not suffer from the large thrust download penalty that tiltrotors have. With the tailsitter's wing and rotor orientation, the wings actually benefit from the extra airflow produced by the rotor downwash increasing their lift and efficiency.

The tailsitter configuration is not without its own disadvantages. It requires a large footprint to maintain stability while at rest on the ground. Typically, the rear stabilizers are used for the landing gear and are larger in size and increase drag compared to typical rear stabilizers of fixed-wing aircraft. Also, because the entire aircraft rotates, the transition maneuver is more complex than that of a tiltrotor aircraft which maintains a level attitude. However, the tailsitter configuration presented the best potential to meet and exceed the RFP performance requirements and offered several distinct advantages over other configurations. Its disadvantages are addressed and thoroughly resolved in the following chapters.

1.3 Decision Analysis

After conducting a survey of past VTOL aircraft configurations, eleven candidates were selected for a more detailed selection process which utilizes Pugh Matrices and the Analytical Hierarchy Process to arrive at a final design configuration.

1.3.1 Pugh Decision Matrix

Stuart Pugh's decision matrix is an effect method for comparing alternatives when the alternatives are not refined enough to produce quantitative data. The method involves repetitive assessment of each alternative's potential to meet the requirements and converges on the strongest solution. The Pugh method is most effective when each member of the decision team individually performs it and the results are compiled into one final matrix.
To implement the Pugh method for the design of the *Kestrel*, the RFP requirements were decomposed into 23 unique performance criteria from which each configuration would be assessed. From the set of vehicle configurations that were investigated, 11 were downselected to conduct Pugh decision methodology. The V-22 Osprey tiltrotor was chosen as the baseline to which the remaining 10 configurations were evaluated against. A value ranging from -3 to 3 was assigned to each configuration for each of the 23 evaluation criteria. A value of -1 or 1 represented that a design was marginally better or marginally worse than the tiltrotor for that specific criteria. Similarly, a value of -2 or 2 meant a design was distinctly better or distinctly worse, and a value of -3 or 3 meant a design was significantly better or significantly worse compared to a tiltrotor. The resulting compiled Pugh matrix is shown in Table 1.1. The top three design configurations were the tailsitter, the fan-in-wing, and the slowed-rotor configurations. These three, along with the baseline tiltrotor, were chosen for further decision analysis using the Analytical Hierarchy Process.

	Design Configuration	Weight	Tilt-rotor	Tail-sitter (tandem)	Tail-sitter (contra)	Co-axial Compound (X2)	SMR Compound (X3)	Tilt-wing	Fan-in-wing (tilted)	Fan-in-wing (hybrid)	Tilting ducted fan	Slowed Rotor	Tip-driven	Stopped Rotor
	Example		V-22	Puffin	Pogo	X2	X3	CL-84	Project Zero	Excalibur	AD-150	Carter PAV	XV-1	S-72
RFP Requirement	Evaluation Criteria													
FM > 0.75	Low Disk loading	5	0	1	-1	2	2	0	1	-1	-1	1	2	2
	Low Downwash	3	0	1	-1	1	2	0	1	-1	-1	1	2	2
300-400 knots	High Forward speed	5	0	3	3	1	1	2	1	3	3	1	-1	1
	Forward flight efficiency	4	0	1	2	-2	-2	1	0	2	1	1	-2	-2
L/D > 10	Range	4	0	2	2	-1	-1	-1	1	2	1	1	-1	-1
	High Wing Loading	3	0	3	3	-1	-1	1	1	3	2	-2	-1	-1
	Low Drag	5	0	1	1	-2	-2	0	-1	2	1	1	-1	-1
G-limit	G-limit/Acceleration	3	0	2	2	1	1	0	0	2	1	1	0	0
Useful load	Mechanical complexity	3	0	1	1	1	1	-2	0	-1	-3	1	-1	-2
	Low Empty weight	5	0	1	1	-1	-1	-1	-2	-1	-1	-1	-1	-1
	Payload Access	2	0	-3	-3	0	0	0	0	0	0	0	0	0
	High Payload	3	0	-2	-2	-1	-1	-1	-2	-2	-2	0	-1	0
OTHERS	Controlability	3	0	-1	-2	0	0	0	-1	-2	-1	0	0	0
	Compactness	1	0	3	3	1	1	0	-1	1	0	-2	-1	0
	Autorotation/Gliding	5	0	0	-1	2	2	0	0	0	0	3	2	2
	Transition	3	0	-1	-1	3	3	-1	0	1	0	1	3	2
	Maturity of Technology	2	0	-1	-1	2	2	-1	-1	-1	-2	-1	-3	-3
	Operational Cost	1	0	1	1	1	1	-1	0	0	-1	0	-1	0
	Vibration	2	0	0	1	-1	-1	0	-1	0	0	1	-1	1
	Acoustics	2	0	0	2	-1	-1	0	0	-1	0	1	-1	1
	Safety	5	0	-1	-1	2	2	0	1	1	0	1	-1	1
	Manufacturability	2	0	1	1	2	2	0	1	1	-1	1	-1	-1
	Scalability	2	0	3	3	2	2	0	2	1	3	0	-1	0
			Total	50	36	30	33	-7	2	37	5	46	-22	7

Table 1.1: Pugh decision matrix.

1.3.2 Analytical Hierarchy Process

The Analytical Hierarchy Process (AHP) is a mathematical technique for decision making which uses pairwise comparisons considering both subjective and objective factors to rank alternatives. Similar to Pugh's decision matrix, the AHP is useful method for evaluating alternatives when quantitative data is not yet available. The first execution of AHP determined the relative importance of each evaluation criteria. The RFP's main performance requirements were broken down into six specific design criteria; low disk loading, high top speed, low total aircraft drag, low empty weight fraction, high safety characteristics, and high stability during transition maneuvers. Each of these criteria were individually compared against the rest of the criteria one at a time using an AHP matrix. A value lower than one represents a criteria that is less important than the criteria that it is compared against. The opposite is true for values higher than one which represent a more important criteria. The importance factors are compiled into one AHP matrix and the eigenvectors of this matrix become the weighting factors for a second execution of AHP. This second execution compares the final four design configurations against one another.

For the second deployment of AHP, each design configuration was compared individually against the remainder of the configurations based on its capabilities for each of the six evaluation criteria. Using the same importance scales from the first AHP deployment, this AHP deployment constructs six AHP matrices. This results in six sets of configuration rankings, one for each of the evaluation criteria. The top-ranked vehicle for a specific criteria has the best relative performance, and the lowest-ranked configuration for a specific criteria had the worst relative performance

All six rankings were compiled into one final AHP matrix, which uses the weighting factors from the first AHP deployment to determine a final score of the four design configurations, as shown in Table 1.2. The tailsitter, fan-in-wing, and powered slow rotor concepts all scored higher than the tiltrotor, with the tailsitter configuration receiving the highest score.

	Low DL		Top Speed		Low Drag		Low Wempty		Safety		Transition		
	Weight	Score	Weight	Score	Weight	Score	Weight	Score	Weight	Score	Weight	Score	
Tilt Rotor	0.19	0.20	0.19	0.17	0.19	0.13	0.19	0.13	0.19	0.19	0.04	0.10	0.16
Tail Sitter	0.19	0.12	0.19	0.47	0.19	0.40	0.19	0.45	0.19	0.10	0.04	0.04	**0.30**
Fan-In-Wing	0.19	0.23	0.19	0.28	0.19	0.37	0.19	0.18	0.19	0.26	0.04	0.17	0.26
Slowed Rotor	0.19	0.45	0.19	0.08	0.19	0.10	0.19	0.24	0.19	0.45	0.04	0.29	0.27

Table 1.2: Analytical Hierarchy Process matrix.

1.4 Final Selection

From the initial vehicle survey consisting of historical and alternative designs, 11 potential configurations were selected for decision analysis. The Pugh decision method narrowed the set of potential designs down to four, which were then ranked by the AHP. From the objective survey and decision analysis tools, the tailsitter was chosen as the best design for the *Kestrel*. Its fixed-wing forward flight efficiency would allow for lift-to-drag ratios of 10 or higher. Its rotors would provide hover efficiency of 75% or higher. Its axial flow rotors and streamlined fuselage presented high potential maximum speed capability, and a mechanically simpler drive system would lead to a low empty vehicle weight. The following chapters discuss the design and development of the *Kestrel*.

The *Kestrel* is an unmanned vehicle due to the unconventional configuration of the tailsitter. As was discovered in the 1950s, if a pilot were present, the control of the vehicle would be extremely challenging because the pilot would have trouble getting accustomed to the changing vehicle orientation during VTOL, hover, and forward flight. This leads to higher pilot workloads and pilot disorientation. Acknowledging the levels of risk associated with manned flight of this vehicle design, it was decided that the unmanned version under the the control of modern control systems could pilot the vehicle more safely and efficiently.

1.5 Hypothetical Manned Configuration

The tailsitter configuration was selected to have the best performance potential for the *Kestrel* as an unmanned version with remote piloting capabilites. In the case where a pilot is required, a hypothetical manned version would require certain modifications to be operated successfully. The Federal Aviation Authority (FAA) daytime Visual Flight Reference (VRF) Minimum Equipment List (MEL) of avionics would need to be installed with provisions for the pilot, including a gimbaled seat to provide adequate seating orientation in both helicopter and airplane modes, and a host of safety equipment. The total weight of the avionics, pilot and accompanying systems needed for manned flight is approximated to weigh 638 lb. The manned vehicle would have a 3.8% increase in empty weight fraction.

2 Tailsitter Sizing

The *Kestrel* was designed to have relatively high maximum forward airspeed capability while maintaining the hovering efficiency of an open-rotor VTOL aircraft. As a tailsitter configuration, the *Kestrel* combines some design aspects of a fixed-wing aircraft with a traditional helicopter. As such, it requires a performance analysis and weight estimations that represent this hybrid aircraft design. The method routine used for the *Kestrel* is based upon Tishchenko's helicopter sizing methodology [3] with modifications for fixed-wings, where appropriate. The sizing method was used to conduct trade studies for engine selection, cruise range, and best operating altitude. The sizing analysis produced an initial vehicle design and performance profile which was then used for more detailed design.

2.1 Description of Sizing Method

Tishchenko's methodology consists of a number of elements for performance estimations and component weight determination based upon historical trends of rotorcraft data including American and Russian military rotorcraft. These approximations were constructed from a minimal set of sizing parameters that represent trends from helicopters of all sizes. These are utilized early in the design stage. Because Tishchenko's method pertains specifically to conventional helicopter configurations, modifications were made to the methodology to represent the *Kestrel's* tailsitter configuration, as described next.

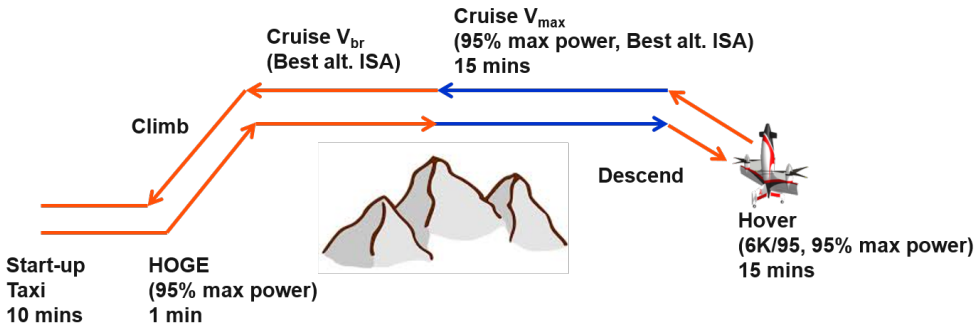

Figure 2.1: RFP mission profile.

The RFP provided a mission profile against which all design entries would be evaluated. Each mission segment was decomposed into altitude, power setting, time, speed, and mode of flight; a diagram of the mission profile is shown in Fig. 2.1. This mission profile is fairly unique in that it does not specify a cruise range for segments 4 and 10, as shown in Table 2.1, nor does it prescribe an operating altitude for that mission. The airspeed for segments 5 and 9 are required to be performed at 300–400 kts; the specific airspeed for these segments were initially decided by the vehicle sizing routine and subsequent performance analysis. The climb, descent, best range cruise, and maximum airspeed cruise segments utilized fixed-wing methods while the hover, idle, and takeoff segments utilized methods for open-rotors.

The sizing process consisted of compiling mission segment parameters from the RFP such as segment type, flight time per segment, range, power setting, and flight altitude. Also, initial determinations of rotor and wing geometries were made, along with initial airframe weight estimates. The sizing routine used these initial values as inputs to calculate empty weight, fuel weight, payload weight and individual subsystem weights, taking into account altitude, drivetrain loses, propeller efficiencies, and accessory losses. Values of rotor disk loading, number of blades, wing area, wing ratio, rotor solidity, rotor tip speed, and blade loading, were selected from parametric sweeps with the sizing method. Because the RFP stresses hovering efficiency and forward flight efficiency over specific payload or range capabilities, the selection of these values were left as inputs for the sizing routine, and final values were determined from the design of the proprotor, which is described in detail in Chapter 4. The sizing routine was also used to conduct parametric sweeps to determine the characteristics of the engine, the cruise range, and the best operating altitude.

Segment Number	Segment Type	Time (min)	Condition
1	Start-up/Warm-up/Taxi	10	Engine Idle, SLS
2	HOGE Take Off	1	95% MCP, SLS
3	Climb		To Best Alt., Vbroc
4	Cruise Out 1		Vbr, Belt Alt., ISA
5	Cruise Out 2 (Dash)	15	Max. Sustained Speed, 95% MCP, Best Alt., ISA
6	Descend		To SLS, Vbroc
7	Hover	15	HOGE w/Full Payload, 95% MCP, SLS
8	Climb		To Best Alt., Vbroc
9	Cruise In 1	15	Max. Sustained Speed, 95% MCP, Best Alt., ISA
10	Cruise in 2		Vbr, Best Alt., ISA
11	Descend		To SLS, Vbroc
12	HOGE Land	1	95% MCP, SLS
13	Shutdown/Taxi	5	Engine Idle, SLS

Table 2.1: Specified mission profile segments from the RFP.

The steps executed in the sizing method were as follows:

1. Rotor and wing geometric values, which partially come from the proprotor design, were used as inputs.
2. The mission profile, as given by the RFP, was decomposed into airspeed, range, power setting, altitude and flight time for each individual segment. Because the RFP does not specify a maximum cruise airspeed, cruise range, or operating altitudes, these parameters were outcomes from the sizing studies.
3. The initial empty weight and fuel weight were estimated such that the aircraft met the requirements of the RFP.
4. The power required for a given segment was calculated using the rotor and wing geometries from Step 1.
5. The power available and specific fuel consumptions for the same segment were calculated using the engine model, which takes into account manufacturer specifications, specific fuel consumption degradation from partial power settings, and power lapse rates from atmospheric conditions, as discussed in Section 2.1.1.
6. Steps 4 and 5 were repeated for each mission segment in succession to determine the total fuel weight required for the mission, including 20 min of reserve fuel.
7. Individual system weights and aircraft empty weight were calculated from weight estimations using historical data, as discussed in Section 2.1.2, and using results from Steps 4 through 6.
8. The aircraft empty weight was checked for convergence versus the initial estimation. The weights determined at Step 7 were used as starting points for successive design iterations. Steps 3 through 7 were repeated until the empty weight of the aircraft had converged.
9. The payload weight was then determined as the useful load minus the final calculated fuel weight.

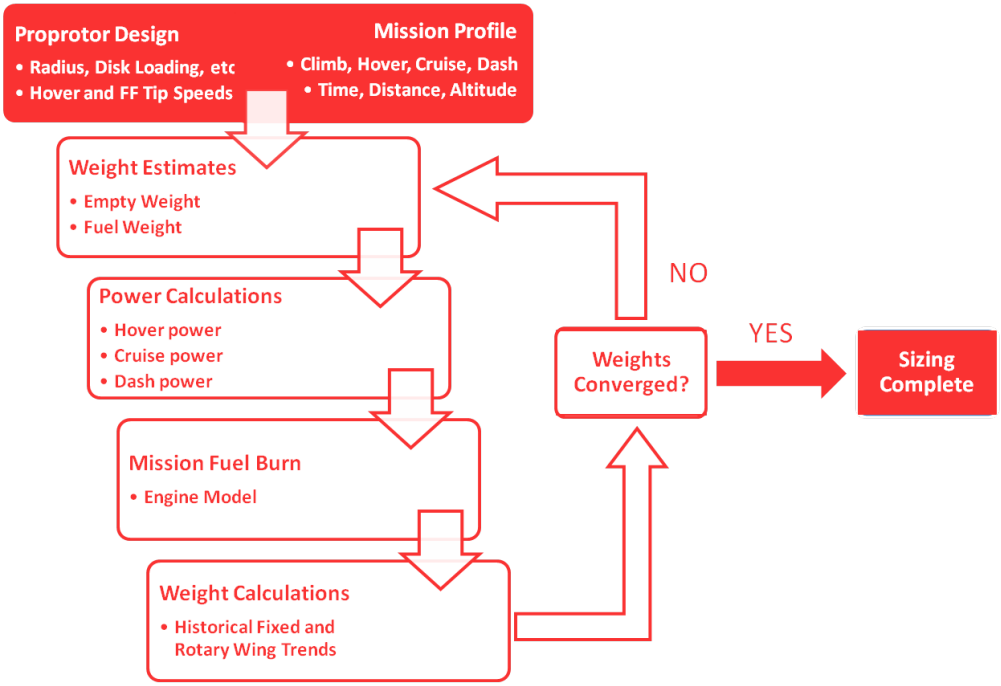

Figure 2.2: Sizing routine workflow.

2.1.1 Engine Model

The RFP requires the use of existing engine technology. In lieu of an exact engine performance model from a manufacturer, a representative engine performance model was constructed. Building an engine model is critical for calculating the SFC at different power settings, altitudes, and ambient air temperatures. This representative model was used to determine the best operating altitude for the mission profile, as described in Section 2.2.3. The power output from a turboshaft engine decreases with decreasing ambient air density, which decreases with increasing altitude and temperature. Lapse rates from [3] were used in the engine model to account for these effects.

To represent the SFC degredation as a function of power, a typical turboshaft engine curve [5], as shown in Fig. 2.3, was used. A database of engines was constructed from the manufacturer's specifications, which typically only specify takeoff rated power, takeoff rated fuel consumption, and engine dry weight. In cases where the Maximum Continuous Power (MCP) was not provided, the MCP was estimated to be 85% of the specified takeoff power rating. Data for each engine was fitted to the curve in Fig. 2.3 to determine the SFC at a specific engine power setting from performance calculations of each mission profile segment.

2.1.2 Airframe Weight Model

A key component of the preliminary design is the determination of the weight of the aircraft. In the early stages of aircraft design, when the exact composition of the vehicle constantly evolves, it is necessary to use approximate models to find reasonable values for the component weights. Such an approach allows for the subsequent assessment of vehicle performance and begins the process of selecting the final geometric sizing parameters and subsystem design.

For the design of the *Kestrel*, Tishchenko [3] weight estimations were employed in combination with estimations from AFDD [6]. Tishchenko's method is robust in that it provides equations for the estimation of subsystem weights while requiring only a minimal set of design parameters to be known. Weights for components, such as the wings and rotor

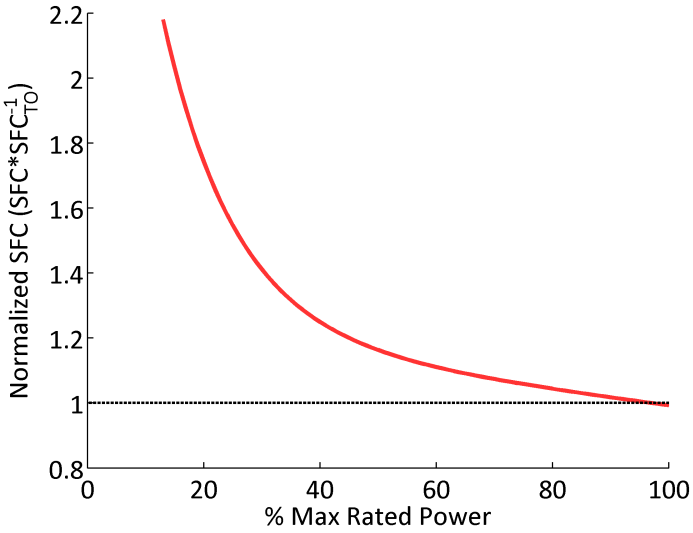

Figure 2.3: SFC degradation at partial power settings.

hubs were estimated from [6] and were used to appropriately represent the unique construction of the wing and rotor hub of the tailsitter components. The components typically must have high stiffness to prevent whirl flutter instabilities, and also include internal supports and rotor cross-shafting for safety in a one engine inoperative (OEI) situation.

Most empirical weight models utilize a technology factor to represent the efficiency of a subsystem's design. Therefore, the technology coefficients of the empirical weight formulas in the sizing routine were calibrated against the XV-15 tiltrotor aircraft so that the resulting system weights from the sizing routine closely predict the reported weights. The XV-15 was chosen for calibration because of its relatively similar weight and airframe layout to the *Kestrel*. The lack of mechanisms and hydraulic systems were taken into account, as well as the extra weight onboard the XV-15 for research equipment that the *Kestrel* would not typically be outfitted with. Also taken into account were the technological advancements in materials, manufacturing, and aircraft design.

As the design of the *Kestrel* progressed and more specifications were finalized, the weight estimations used in the sizing routine were replaced with more appropriate values. These parameters included the weight of the engine and transmission determined by a weight buildup of the final transmission design.

More accurate weight and drag estimations were also used in place of original empirical estimates once the detailed specifications were determined. As discussed in Chapter 4, it was determined that the *Kestrel's* maximum airspeed was limited by the proprotor aerodynamics. This limitation was taken into account for dash segments of the mission.

2.2 Trade Studies

The sizing routine was used for parametric studies in the selection of the final design parameters. The wing and blade geometric parameters were determined by aerodynamic optimization based upon maximizing hover and cruise efficiencies instead of maximizing vehicle weight using the sizing routine. This ensures that the *Kestrel* was designed to meet the specific RFP requirements. The range of the cruise segments, the operating altitude, and the engine were chosen using the sizing methodology described in Section 2.1.

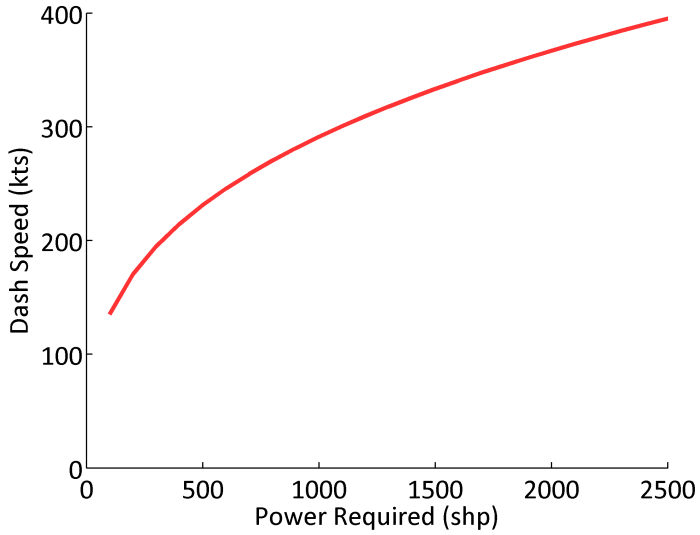

Figure 2.4: Rotor power required to achieve 300–400 kts dash speed.

2.2.1 Engine Selection

Two engines were chosen for the *Kestrel* to provide a safety margin and redundancy. The use of three or more engines would be unnecessary and would have resulted in a higher empty weight of the entire vehicle. Routine and unscheduled maintenance required to keep the engines operational will also increase with the use of more engines over the use of a single engine. However, it is very common for operational rotorcraft to utilize two engines and, therefore, current locations that already field turbine rotorcraft will be well equipped to service the *Kestrel*. The merits of using two engines for the *Kestrel's* design results in increased safety from redundancy over a single engine, and a lower aircraft empty weight than a three or more engine setup.

Research was conducted to compile a database of engines to use in sizing and performance calculations to determine the best available engine for the *Kestrel*. Figure 2.4 shows the calculated power required to achieve dash speeds from 300–400 kts. From these results, it was determined that engines with approximately 1,000 shp to 2,500 shp MCP ratings were appropriate.

From the engine database, the engines with the best power-to-weight ratios near the aforementioned power range were selected to conduct further sizing studies, and also to assess the maximum cruise speed and best range cruise capabilities of the *Kestrel* for each engine. Table 2.2 details the MRP rating, dry weight, and power-to-weight ratio of the selected engines. Figure 2.5 shows the results of the engine study in terms of maximum dash speed versus maximum cruise range. The payload-to-fuel weight ratio was held constant for all configurations in this study.

As discussed later in Chapter 4 it was determined that the *Kestrel* was limited to a maximum airspeed of 350 kts by the growing helical Mach number of the proprotor. Therefore, to maximize *Kestrel's* mission profile performance, a further study was conducted to assess the engine performance with the dash segment speeds held constant at 350 kts. Although some engines may have more than enough power to achieve 350 kts in forward flight, operation at power settings lower than takeoff rated power generaly degrade fuel consumption. As shown in Fig. 2.6, the Rolls-Royce/Turbomeca RTM322-01/9 gave the highest range capabilites. While producing even better cruise capabilites, the CTS800-4N and the T58-GE-100 engines do not provide enough power to reach the 350 kts maximum airspeed.

Figure 2.7 shows the RTM322-01/9 and Table 2.3 lists the engine specifications. The RTM322 family of engines has been in service since 1995 aboard the AugustaWestland AW101 Merlin, NH Industries NH90, and the AgustaWestland

Table 2.2: Summary of downselected engine specifications.

Engine	MRP/Takeoff Power (shp)	Dry Weight (lb)	Power-to-Weight Ratio (shp lb^{-1})
T55-L-712	3750	750	5.00
RTM322-01/9	**2397**	**503**	**4.86**
T55-L-7C	2850	590	4.83
CT7-8A	2520	537	4.69
T58-GE-100	1500	335	4.48
T58-GE-16	1870	443	4.22
CTS800-4N	1360	408	3.33

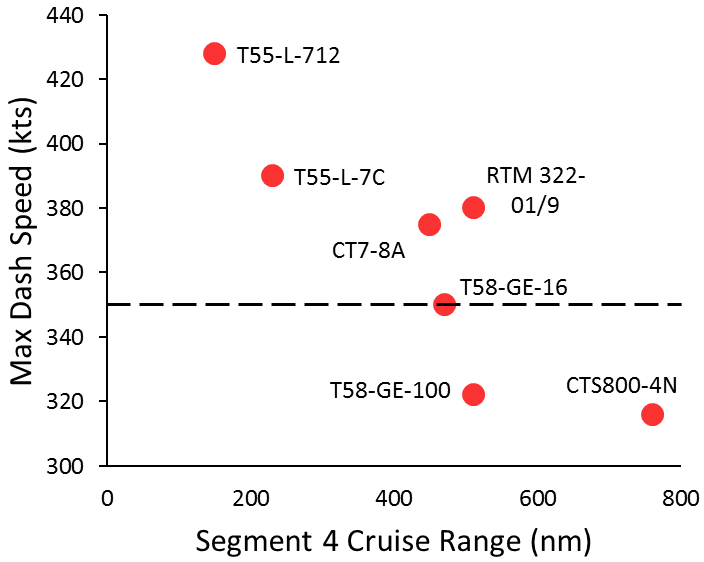

Figure 2.5: Dash and cruise capabilities of downselected engines.

Table 2.3: Specifications of the Rolls-Royce/Turbomeca RTM322-01/9 turboshaft engine.

OEI Continuous Power	2,415 shp
Takeoff Power	2,397 shp
Max Continuous Power	2,227 shp
Dry Weight	503 lb
Power-to-Weight Ratio	4.765 shp lb^{-1}
Takeoff SFC	0.420 shp lb hr^{-1}
Length	44.4 in
Width	25.9 in
Height	23.8 in

WAH-64 Apache. The RTM322-01/9 consists of 3 axial and 1 centrifugal compressor stages with a total pressure ratio of 15.0, annular reverse flow combustors, a two stage gas generator turbine, and a two stage power turbine. Should the proprotor design allow for higher maximum cruise speeds in future revisions of the *Kestrel*, the RTM322-01/9 has enough built-in growth potential to provide enough power to sustain a maximum of 380 kts.

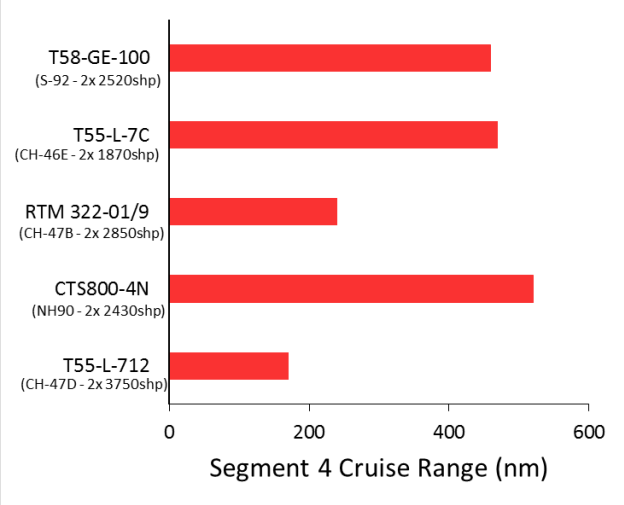

Figure 2.6: Cruise capabilities of downselected engines with prescribed 350 kts dash speed.

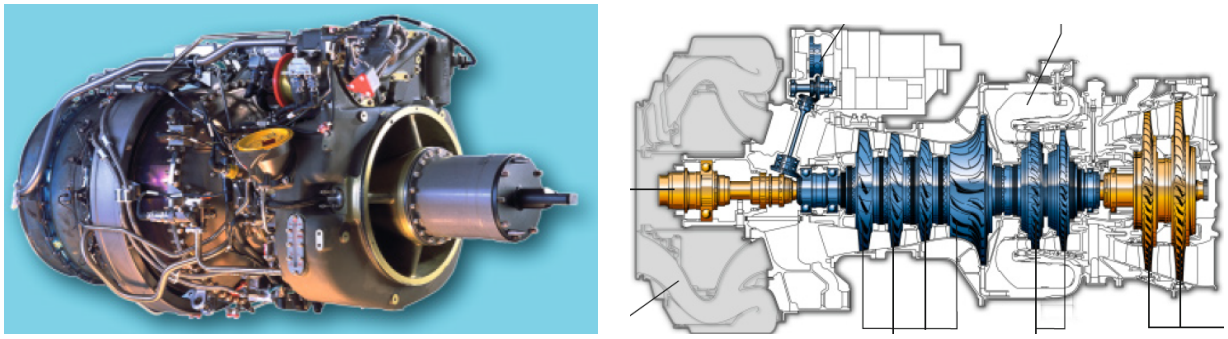

Figure 2.7: Rolls-Royce/Turbomeca RTM322-01/9 turboshaft engine.

The *Kestrel's* total takeoff power at SLS conditions is 4,794 shp. With a design gross weight of 10,500 lb, the *Kestrel's* power-to-weight ratio of 0.46 shp/lb is much greater than the AW101, NH90, and WAH-64, which also use the RTM322 engine. The AW609, XV-15, and V-22 tiltrotors also have lower power-to-weight ratios at 0.24 shp/lb, 0.23 shp/lb, and 0.26 shp/lb respectively. The *Kestrel's* power-to-weight ratio is significantly higher because it is sized for high-speed forward flight which requires a significantly higher amount of power. The *Kestrel's* maximum airspeed is approximately 50 kts higher than that of the slightly larger XV-15 tiltrotor. Parasitic drag increases with the cube of forward airspeed, so the *Kestrel* requires 600 shp more to reach 350 kts than it would for 300 kts. As discussed in Section 14, not only does the excess power allow the *Kestrel* to reach higher airspeeds, but the *Kestrel* can hover at a higher density altitude than most other helicopters including the XV-15. The practical utility of the *Kestrel's* higher hover ceiling is discussed in Chapter 14.

The RTM322 family of engines, however, are not rated for operating in a vertical orientation such as is necessary for a tailsitter. In fact, as of May 2014, the Pratt & Whitney PT6C-67A (1,938 shp T.O.) installed in the AugustaWestland AW609 and the Rolls-Royce Liberty AE1107C (6,830 shp T.O.) installed in the Bell/Boeing V-22 are the only production engines rated for vertical orientation. The XV-15 tiltrotor and the Canadair CL-84 tiltwing both used modified Lycoming T53 turboshaft engines that were not mass-produced for vertical operation. Recently, it has been reported that for the production version of the AW609, the P&W PT6C-67A will increase in power to 2,400 shp. However,

since no details on the progress of the development of this upgrade were available, it was not selected. Because the only engines available for vertical operation output too little or too much power for the *Kestrel's* design, the selected RTM322-01/9 will need to modified for vertical operation. For the *Kestrel*, the lubrication and scavenging systems would need to be upgraded such that the oil is dispersed properly and picked up properly by sump pump pickups [8]. Modifying an existing engine to be rated for vertical operation is not a trivial task, however it has been done in the past. As more tiltrotor designs are developed through VTOL aircraft development programs such as JMR, X-Plane, and Clean Sky, the design and modification process of converting engines will become an alternate version offered by manufacturers, as is the case with the PT6C-67A. As such, the use of the RTM322-01/9 with these minor (non-core related) modifications satisfies the RFP's requirement for using current engine technology.

2.2.2 Determination of Cruise Range

The distance for cruising at V_{BR} for segments 4 and 10, as shown in Table 2.1, was not defined by the RFP and so became an outcome from the vehicle design. To determine this distance, a parametric sizing sweep of fuel weight to payload weight ratio was conducted. Because the RFP mandated a minimum useful load fraction and a minimum payload weight fraction, the ratio of fuel weight to payload weight was varied. The resulting payload and range capabilites are shown in Fig. 2.8. All data points meet the 40% useful load and 12.5% minimums set by the RFP. The maximum possible cruise segment 4 range of 250 nm was chosen for the *Kestrel* to maximize the operating radius of the RFP mission profile. Payload range capabilities for payload configurations other than MTOGW and payload weight fractions are presented in 2.8.

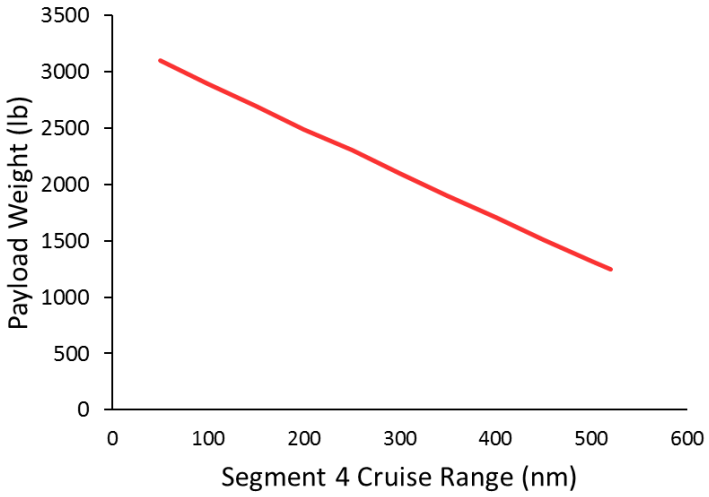

Figure 2.8: Payload range capabilities.

2.2.3 Selection of Best Operating Altitude

The operating altitude of the mission profile was also unspecified by the RFP, so it was chosen in a similar manner as was done for the cruise range. A parametric sizing sweep was conducted by operating altitude and calculating the resultant fuel weight fraction. Operating in a fixed-wing flight mode requires less power at higher altitudes because of the reduction in parasite drag. A tradeoff is that operation at higher altitudes requires more fuel to climb to these altitudes. Another factor, is that the power available from the engines decreases with altitude, causing the maximum rate of climb to decrease, and further increasing the time to climb as well as the fuel burned. However, an optimized

operating altitude would allow for the best useful load fraction.

Figure 2.9 shows the results of the altitude sweep showing total fuel weight as a function of the operating altitude for a maximum cruise speed of 350 kts. The choice of the maximum cruise speed was determined by the proprotor design as described in Chapter 4. The least amount of fuel required to complete the mission profile occurs at an operating density altitude of approximately 9,186 ft ISA.

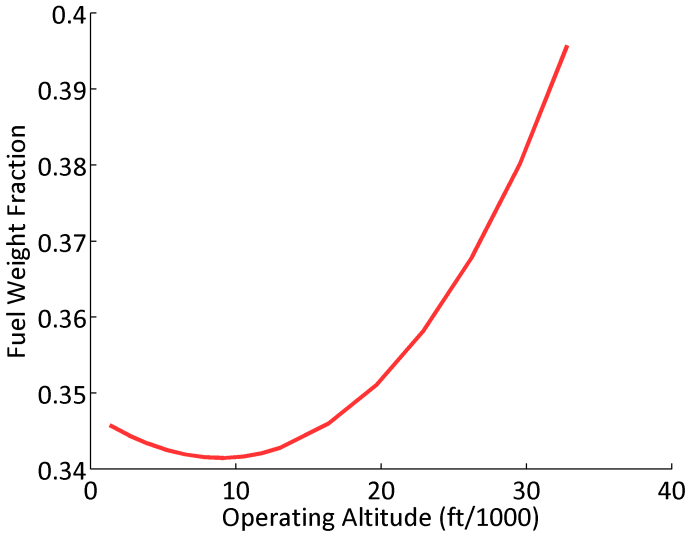

Figure 2.9: Fuel weight fraction as a function of operating altitude.

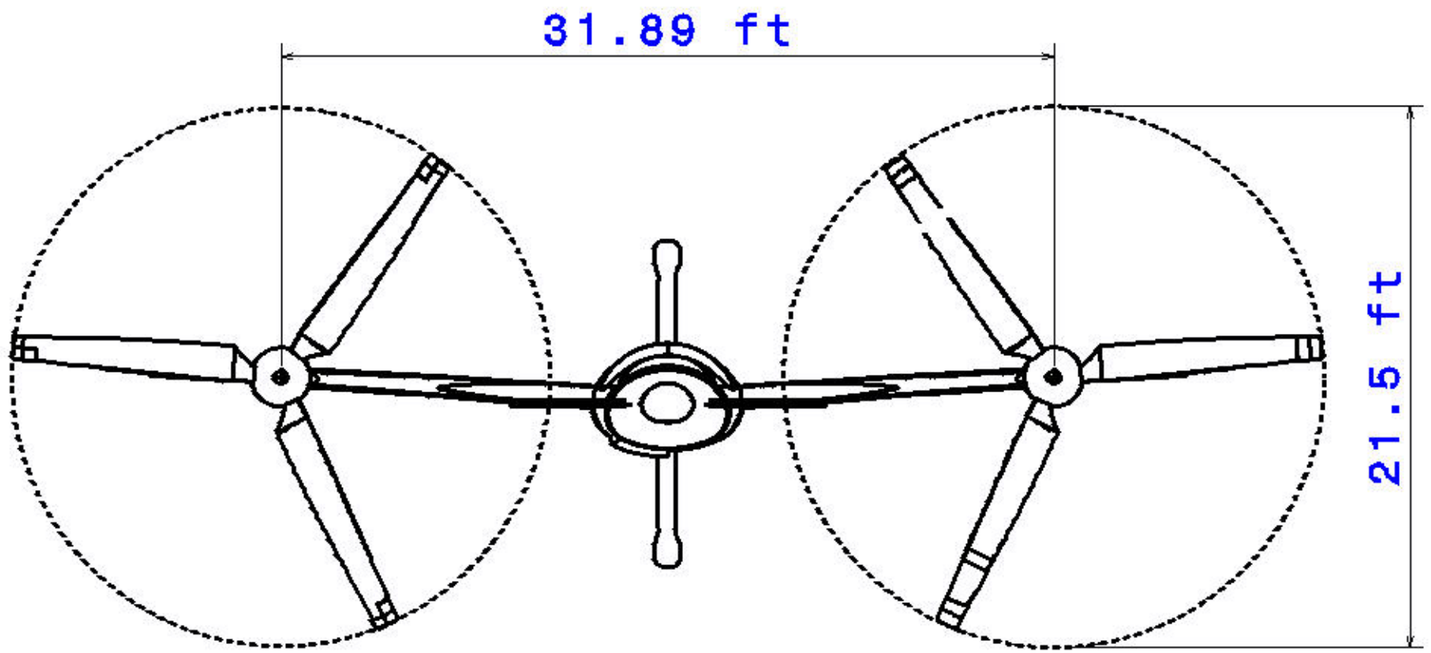

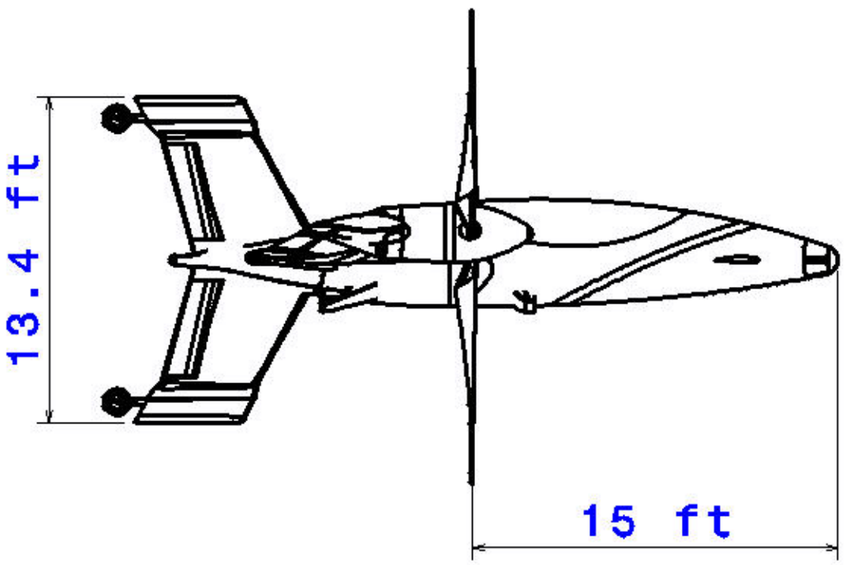

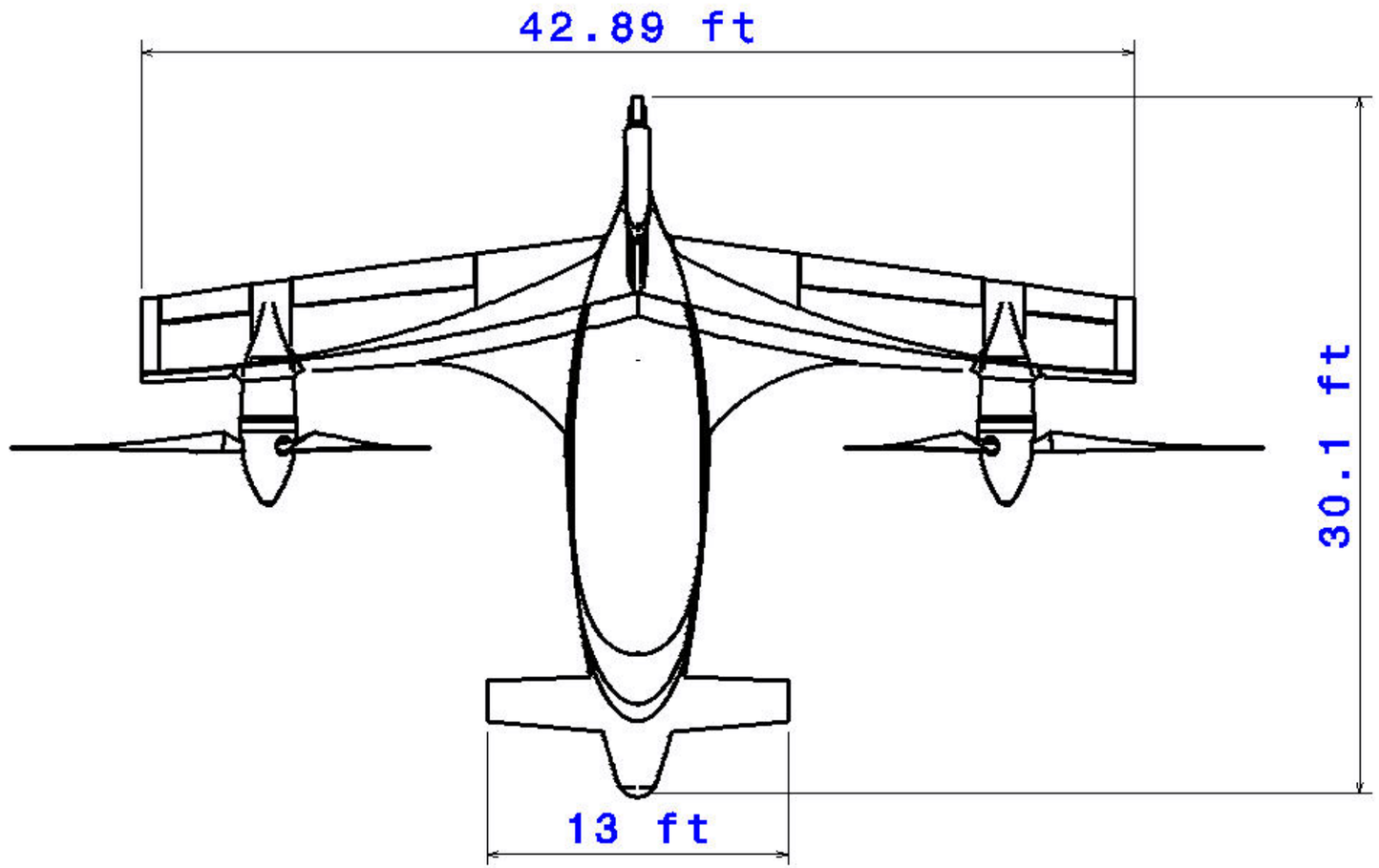

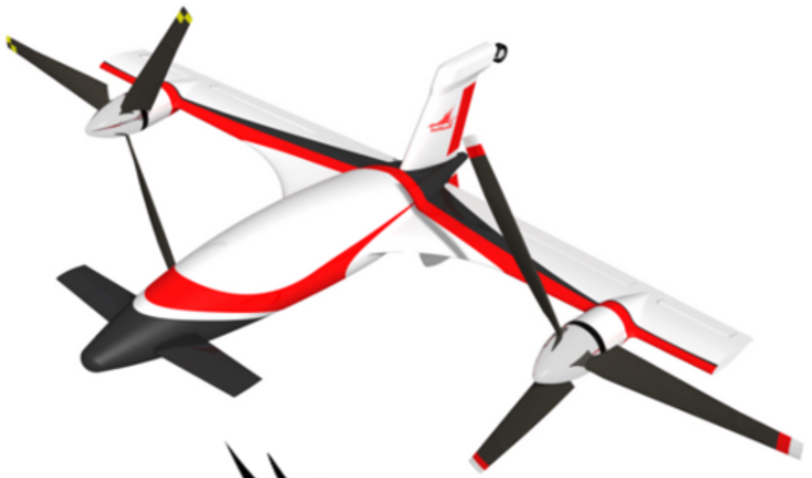

Kestrel

3 Performance Overview

Main Rotor Specifications		Performance	
Diameter	10.75 ft	Cruise Speed	200 kts
Number of Blades	3	Maximum Cruise Speed	350 kts
Chord	1.40 ft	Maximum Endurance speed	125 kts
Solidity	0.125	Maximum Acceleration	0.5 g
Disk Loading	15.15 lb ft^{-2}	Maximum Vertical Load Factor	3.5 g
Inboard Blade Twist	4.5° ft^{-1}	Maximum Endurance	10.78 hr
Outboard Blade Twist	Hyperbolic	Maximum Ferry Range	1618 nm
Blade Taper Ratio	2	Maximum Mission Radius	809 nm
Rotor Speed	555 rpm		
Root Cutout	20%		
Inboard Airfoil Section	RC(4)-10		
Outboard Airfoil Section	RC(3)-08		

Vehicle Dimensions		Engine Specification	
Total Length	13.40 ft	Number of Engines	2
Total Height	30.15 ft	Maximum Rated Power	4,794 hp
Fuselage Height	4.41 ft	Maximum Continuous Power	4,454 hp
Fuselage Width	6.12 ft	Operating rpm	6,000
Fuselage Height	4.39 ft		

Wing Specification		Canard Specification	
Span	43 ft	Span	13.08 ft
Chord	4.3 ft	Chord	2.04 ft
Aspect Ratio	10	Aspect Ratio	6.4
$C_{L,MAX}$	2.1	$C_{L,MAX}$	1.55
Taper Ratio	0.7	Taper Ratio	0.7
Sweep	Forward 4°	Sweep	Aft 4°
Dihedral	4°	Dihedral	0°
Incidence	0°	Incidence	-6°
Airfoil Section	Eppler 549	Airfoil Section	Rutan AMSOIL
Maximum Load Factor	3.5		

Weights	
Maximum Take Off Gross Weight	11,000 lb
Empty Weight	7,975 lb
Useful Load Weight	4,400 lb

4 Proprotor Design

Fulfilling the requirements of the RFP presented a unique set of challenges to design a proprotor for the *Kestrel* that could operate efficiently in both hover and high speed forward flight. A balanced level of performance between the two flight modes was essential to design parameters such as the rotor radius, rotor speed, solidity, blade twist, and blade taper. The following sections describe the design objectives and methodology used for the proprotor design.

4.1 Design Goals

The RFP required an efficient VTOL aircraft with an unprecedented forward flight airspeed capability of 300–400 kts. The RFP did not state a requirement for the forward flight efficiency, however it was a design goal for the *Kestrel* to operate efficiently across its entire flight envelope. The hovering efficiency, as defined by the metric k, was provided by the RFP as a function of power loading PL, disk loading DL, and air density ρ, i.e.,

$$k = PL\left(\frac{2\rho}{DL}\right)^{-\frac{1}{2}} \tag{1}$$

The RFP required that the hovering efficiency must be within 25% of the ideal power loading for that rotor at MSL ISA. A large open rotor optimized for VTOL would satisfy the hover requirement, but would have poor efficiency in forward flight, and so was not considered. The *Kestrel* was designed to maximize the hovering efficiency as well maximize the propulsive efficiency, defined by η_P, given by

$$\eta_p = \frac{\text{Thrust x True Airspeed}}{\text{Power required}} = \frac{TV_\infty}{P_{\text{req}}} = \frac{C_T\mu}{C_P} \tag{2}$$

Modern propeller driven aircraft have propulsive efficiencies between 80–90%; a goal for the proprotor propulsive efficiency was to be within this range at or near the best range cruise airspeed.

4.2 Design Methodology

Each proprotor configuration evaluated the hover efficiency and propulsive efficiency using Blade Element Momentum Theory (BEMT) [9] with thrust, airspeed, and density altitude sweeps. The proprotor parameters (i.e., diameter, rotational speed, solidity, twist, and taper) were determined by a series of parametric sweeps, and then selected based on the obtained hovering and forward flight efficiency. The parametric study had initial input parameters that were stated in the RFP, such as the density altitude of MSL ISA and design maximum takeoff gross weight (MTOGW), of 10,942 lbs, and varied the remaining rotor parameters. A configuration that had unsatisfactory efficiencies at high-thrust, best range airspeed, or at maximum cruise speed was not considered. The process was repeated iteratively until a final proprotor configuration was reached that satisfied all of the requirements.

The initial benchmark of the proprotor system was determined by comparison with similar 10,000–12,000 lb MTOGW aircraft. Contemporary 10,000–12,000 lb tailsitter aircraft do not exist, so contemporary tiltrotors (i.e., the AW-609 and XV-15) without a wing download penalty were used as a benchmark. The goal of this study was to determine a proprotor configuration that could operate efficiently over the entire flight envelope, in addition to meeting the power loading efficiency and maximum cruise speed requirements stated in the RFP.

Figure 4.1 shows the hover efficiency evaluated at the design MTOGW versus the propulsive efficiency evaluated at a cruise speed of 350 kts for each of the rotor configurations considered in the parametric sweep. A Pareto analysis was used to make design decisions for competing design goals, such as maximizing the hover efficiency and forward flight propulsive efficiency (which make up the Pareto Frontier) and to determine qualities that are common among the optimum design points. For the *Kestrel's* Pareto analysis, the optimum configurations maximized the hover efficiency (power loading efficiency of at least 75%) and forward flight efficiency at maximum cruise.

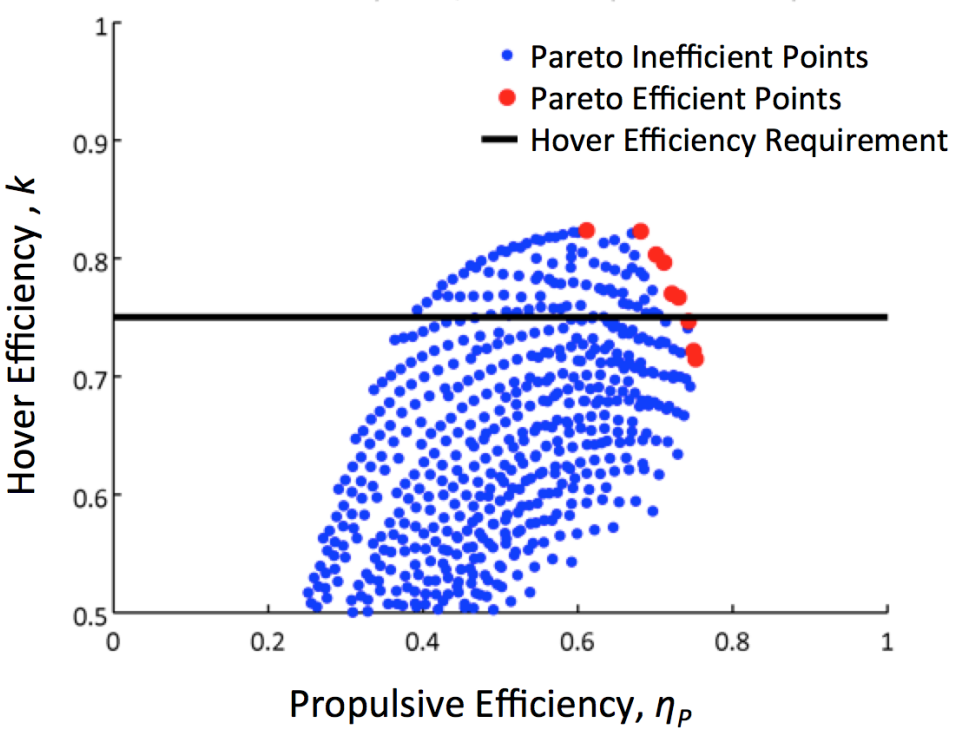

Figure 4.1: Pareto efficiency plot for all proprotor configurations evaluated.

4.3 Number of Rotors

The number of rotors was selected by assessing the performance benefits produced by each configuration in hover and forward flight. One large open rotor would be ideal to meet the efficient hover requirement. However, such a rotor would not be efficient in forward flight at high cruise speeds. The large diameter would lead to a high helical tip Mach number at the maximum cruise speed with the tip speeds needed to prevent proprotor stall.

Additional rotors provide an equivalent rotor disk area with a smaller rotor diameter for the same thrust. The smaller diameter reduces the tip speed for a given rotational velocity, forward speed, and helical Mach number. Reducing the helical Mach number will prevent encroaching on the Mach drag divergence number (M_{dd}) at the blade sections. However, this capability comes at the cost of an empty weight penalty and increased mechanical complexity from additional drive shafts and cross-shaft redundancies. From a practical standpoint, an increase in mechanical systems will increase the overall downtime for maintenance and inspection. An aircraft with additional rotors must also have additional spare parts and/or spare subsystems on site, which will increase the logistical footprint. Three or more rotors were considered but not selected because of the numerous deficiencies associated with these configurations. Two rotors were selected because it is the simplest configuration that satisfied the requirements of the RFP.

4.4 Blade Taper Ratio

Blade taper effects on the proprotor were investigated at a constant thrust weighted solidity. The taper ratio from tip to root was varied between 1.0 to 0.5. A tapered blade decreases the local blade lift coefficients at the root and increases the local lift coefficients at the tip, which will also reduce the profile power for a given amount of thrust and, therefore, give improved hover power loading efficiency. Upon closer examination of the Pareto chart, shown in Fig. 4.1, it was determined a majority of all configurations within the top right corner of the figure had a blade taper ratio of 0.5, which led to the selection of 0.5 taper ratio.

4.5 Rotor Disk Diameter and Rotor Speed

Selection of the proprotor diameter was a balance between achieving a high power loading efficiency in hover and maximizing the propulsive efficiency at the designed cruise. A rotor in hover with a relatively large radius and low disk loading is desired to have a higher power loading efficiency. A rotor with high disk loading could create downwash velocities capable of moving debris that could become hazardous to ground personnel. A proprotor in forward flight is more efficient when operated at a high disk loading because the smaller blade area reduces the profile losses while the induced losses are relatively small. In hover, a higher rotor speed would result in a lower blade loading coefficient C_T/σ but would lead to higher tip Mach numbers during forward flight. A higher rotor speed would prevent the proprotor from stalling which is required for the *Kestrel* to operate at the designed dash speed. Because of the foregoing discussion, a balance was struck between a proprotor that is efficient in hover and forward flight.

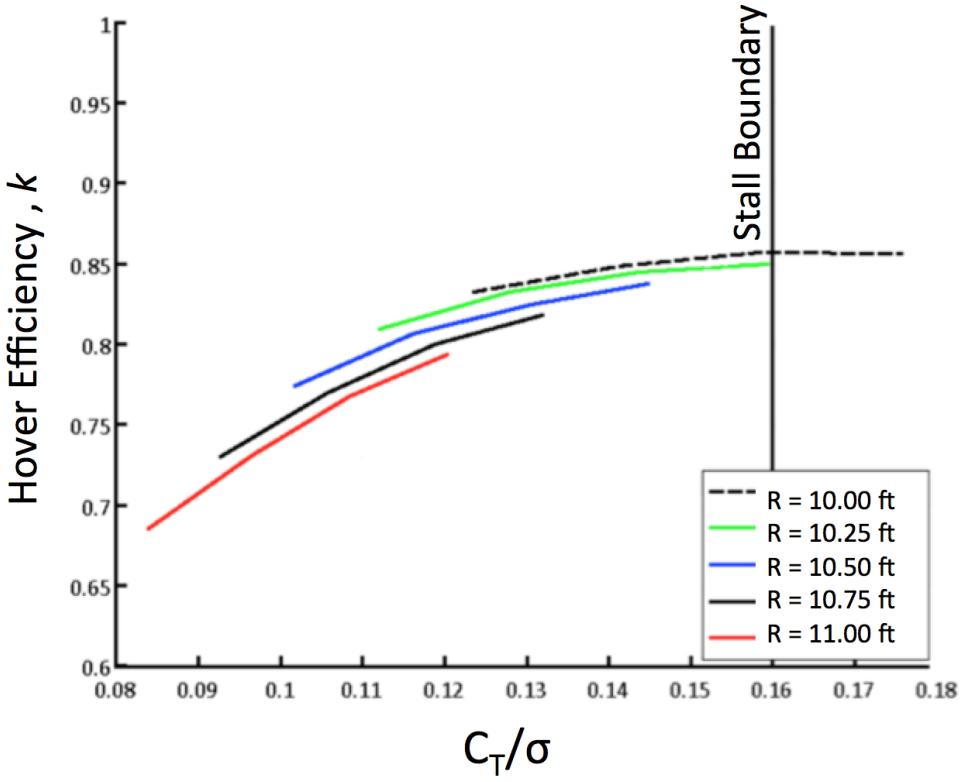

Figure 4.2: Hover power loading efficiency versus C_T/σ for varying radius.

Figure 4.2 shows the hover power loading efficiency against C_T/σ at a rotor solidity of 0.125, rotor speed of 550 rpm, blade taper of 2:1, and the final twist distribution selected in Section 4.7 for different radii. The range of C_T/σ shown in these figures are for a total thrust required of 7,250 lbs to 11,000 lbs at MSL ISA, where 11,000 lbs is the design MTOGW, and 7,250 lbs is the minimum allowed MTOGW without fuel. The fuel, as stated in the RFP, is 27.5% of the MTOGW. As shown in Fig. 4.2 the power loading efficiency would improve as radius was reduced, however, the rotor would approach the rotor stall boundary of $C_T/\sigma = 0.16$. A larger radius would offer a greater stall margin but would introduce disadvantages such as decrease the hover power loading efficiency, increase the empty weight, and increase the tip helical Mach number at the maximum cruise airspeed. The rotor radius selected to be 10.75 ft, which

was the smallest radius that provided adequate stall margins at the design MTOGW while meeting the other efficiency requirements. A variable diameter rotor was considered but was not selected due to the technology readiness level discussed in Section 4.11.

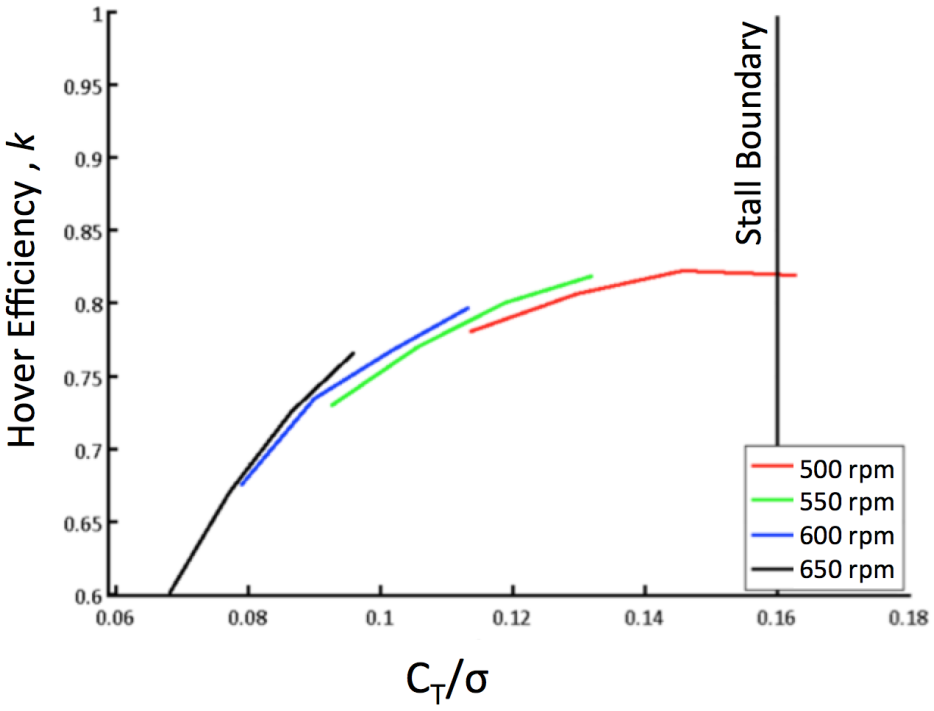

Figure 4.3: Hover power loading efficiency versus C_T/σ for varying rpm.

Figure 4.3 shows the effects of rotor rpm at a rotor solidity of 0.125, rotor radius of 10.75 ft, blade taper of 2:1, and the final twist distribution selected in Section 4.7. As rpm is reduced, the hover power loading efficiency improves but the proprotor approaches stall. The rotor radius and rpm were chosen (shown in Figs. 4.2 and 4.3) for the hover regime based on values that could satisfy the RFP hover requirements and allow for adequate stall margin, while also maximizing the propulsive efficiency in forward flight.

Figure 4.4 shows the propulsive efficiency against the helical Mach number at varying rotational speeds for a rotor solidity of 0.125, rotor radius of 10.75 ft, blade taper of 2:1, and the final twist distribution selected in Section 4.7. The maximum allowable helical Mach number for the rotor system was determined by the onset of drag divergence of the blade section. The drag divergence Mach number, M_{dd} of 0.89, for the NASA RC(3)-08 airfoil, is shown in Fig. 4.4 and is described in Section 4.8. A rotational speed of 550 rpm was evaluated to have a maximum propulsive efficiency of 72%. Although the rotor rpm was initially selected to operate at 550 rpm the final rotational speed was at 555 rpm because of transmission geometry issues discussed in Chapter 7.

4.6 Rotor Speed for Best Range Cruise

Figure 4.5 shows the propulsive efficiency against the true airspeed for the same rotor configuration as in Fig. 4.4. The results show that at 550 rpm the proprotor is far from optimal at the design best range cruise airspeed of 160 kts, which is discussed in Chapter 14. The propulsive efficiency dramatically increases with a reduction in rpm to 275 rpm

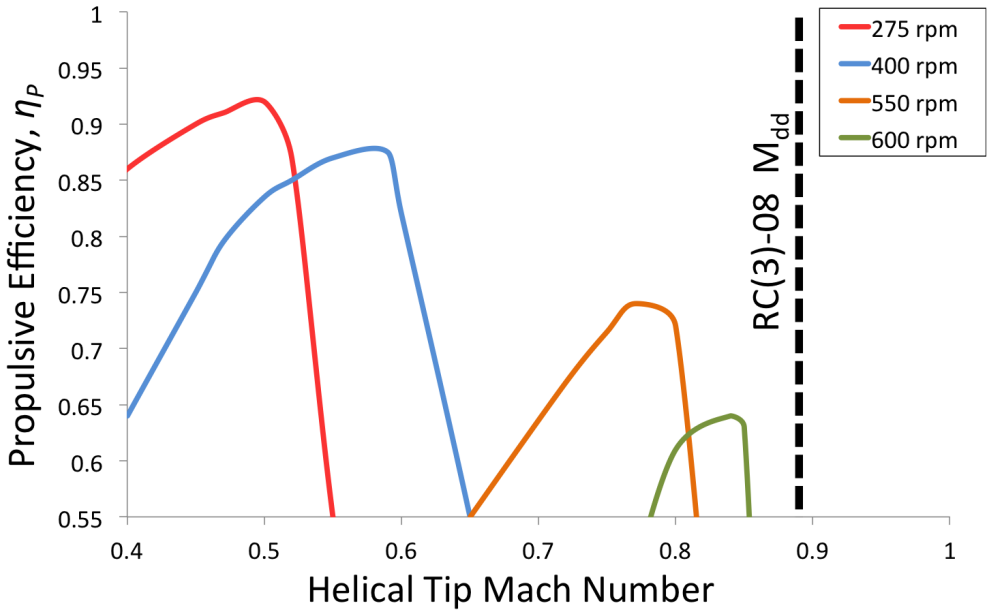

Figure 4.4: Propulsive efficiency versus helical Mach at different proprotor speeds.

with the proprotor efficiency above 80%. The potentially high proprotor efficiency was a motivating factor to pursue a variable rpm proprotor system. The ideal proprotor speed at the maximum cruise airspeed is twice the proprotor speed for the best range airspeed. The relationship between the two proprotor speeds drove the selection to a 2:1 rpm ratio between highest and lowest proprotor speed. The lower speed was initially selected as 275 rpm, but because of transmission geometry, 269 rpm was finally selected. Figure 4.4 and 4.5 show the forward flight efficiency benefits of using 275 rpm at the best range cruise and 550 rpm in hover and maximum cruise speed. The rpm scheduling within the flight envelope is given in Table 4.1 with the details of the transmission design discussed in Chapter 7.

Table 4.1: Scheduling of rpm with respect to airspeed

Airspeed (kts)	0	50	100	150	200	250	300	350
Rotor Speed (rpm)	555	555	555	269	269	269	555	555

4.7 Blade Twist

The inboard and outboard twist rates of the blade were varied to optimize aerodynamic efficiency between the hover and forward flight regime. The ideal twist for a rotor operating in hover or axial climb will be hyperbolic. The resultant uniform inflow will minimize the induced power required for a given C_T. The optimal hovering twist and corresponding taper would also result in the local airfoil angles of attack near to the maximum lift-to-drag ratio across the span.

In forward flight, the proprotor will experience axial inflow conditions, but the relative airspeed is greater than the induced inflow. The inflow angle at high forward flight speed is approximately linear so a twist compromise must be made between the two flight regimes. The inboard blade twist and outboard twist were varied, using a parametric sweep, to maximize the efficiencies in both hover and forward flight, as defined in Section 4.1. A bimodal twist was selected to compromise between the two flight regimes. The inboard twist was varied 4.5° ft^{-1} to the 70% span position. The outboard twist is a hyperbolic distribution. The 70%–80% spanwise region across the blades were then

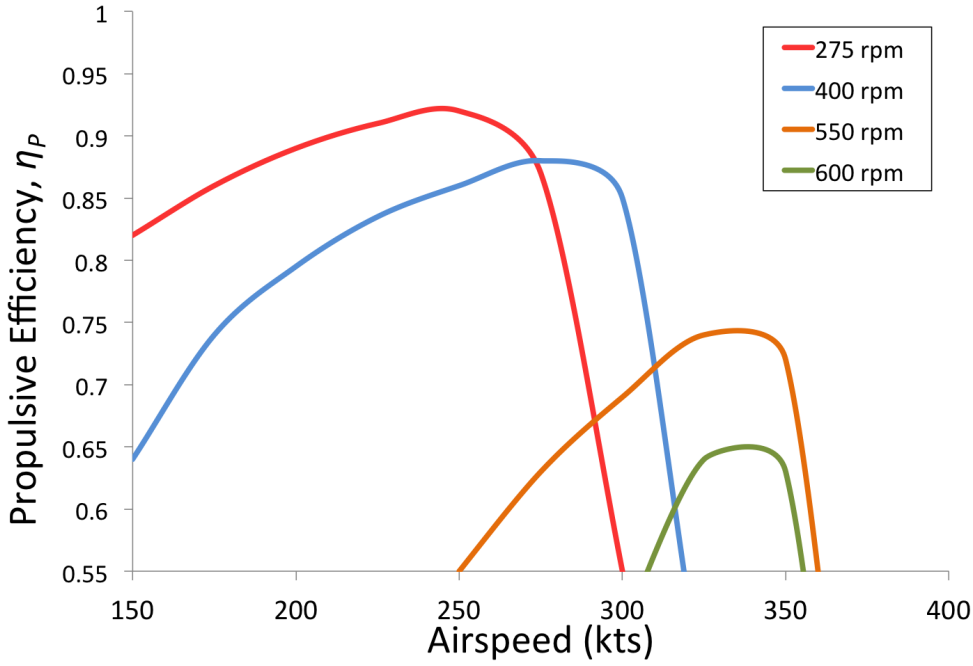

Figure 4.5: Propulsive efficiency vs airspeed (kts) for different proprotor speeds.

blended between the two modes of twist as shown in Fig. 4.6.

4.8 Airfoil Selection

The inboard airfoil selected for the proprotor was the NASA RC(4)-10. This airfoil provided a high maximum lift coefficient, of 1.6, which is required for the most extreme ends of the flight envelope. The airfoil also provided an exceptional L/D within its intended range of operation. The outboard airfoil selected was the NASA RC(3)-08. In addition to favorable L/D properties, the airfoil has an exceptionally high drag divergence Mach number of 0.89 [10]. The proprotor was designed for a peak helical Mach number of 0.8 at the maximum airspeed of the aircraft, as shown in Fig. 4.4. Compressibility tip relief was also incorporated in the power loss estimate [11], when using the blade element theory.

4.9 Rotor Solidity

A parametric sweep on the solidity (σ), was conducted to yield a more thorough understanding of the proprotor aerodynamics. The value of σ was varied between 0.07 – 0.14, and the proprotor was evaluated according to the hover and forward flight efficiency metrics, k and η_p, respectively. The solidity of the rotor was selected with sufficient stall margin in hover. By designing a proprotor with a lower blade loading coefficient (C_T/σ), (i.e. by increasing the rotor solidity) the *Kestrel* has the benefit of a having higher stall margin. A higher stall margin was desirable to enable easy transition from hover into forward flight, improve gust response, and allow operations at higher density altitudes. A higher solidity rotor provided a better stall margin in hover. However, a lower solidity gave a higher hover power loading efficiency over a greater range of gross weights, as shown in Fig. 4.7.

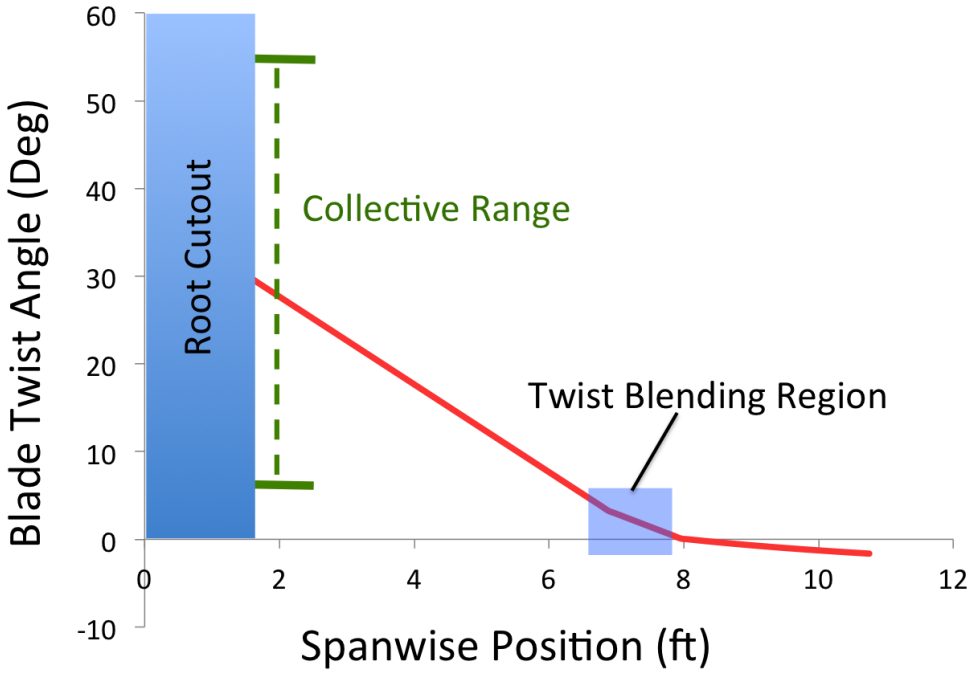

Figure 4.6: Spanwise twist distribution.

Figure 4.7 shows the hover power loading efficiency versus the blade loading coefficient at a rotor radius of 10.75 ft, rotor speed of 550 rpm, and the final twist distribution selected in Section 4.7. Figure 4.7 shows that as the C_T/σ decreases the lower solidity gives higher hover power loading efficiency. A solidity of 0.125 provided enough stall margin while delivering an acceptable hover power loading efficiency of 0.82.

4.10 Blade Structural Design

A hingeless rotor is used on the *Kestrel* to achieve the control moments required to transition from hover to forward flight. The blades are designed with the appropriate strength and fatigue life for the demanding transition maneuver. Continuous composite fiber placement connects the three primary structural sections of the rotor blade. The blade loads are transferred from the blade spar to the hub through the blade cuff.

4.10.1 Blade Composite Tailoring

Composite materials provide the appropriate stiffness and fatigue characteristics required for the blades on the *Kestrel*. The spar is composed of unidirectional S-glass/epoxy and encloses a Rohacell 75 foam D-spar mandrel. Similarly, the trailing edge block is also composed of uni-directional fiber glass/epoxy. Compared to a Graphite/epoxy layup, the S-glass/epoxy is much lighter and less expensive. The foam is cut to shape using hotwire and then compressed into a closed die mold. The inner skin of the blade is composed of $\pm 45^\circ$ Graphite/epoxy layup. There is an additional layer of extended copper mesh and a leading edge erosion strip.

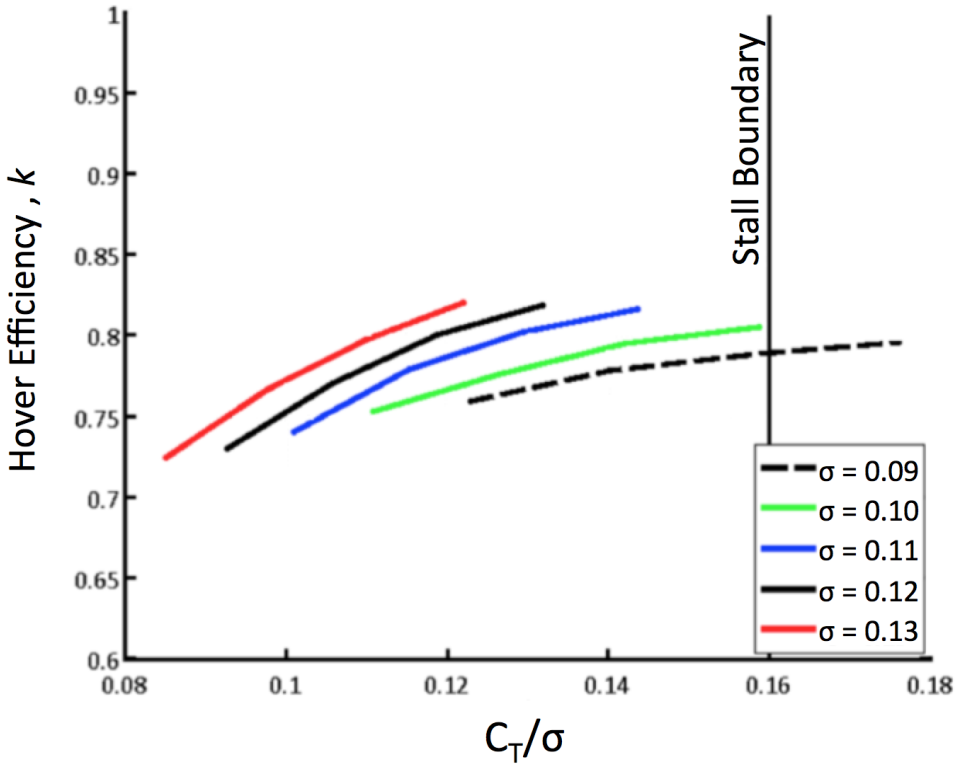

Figure 4.7: Hover power loading efficiency versus C_T/σ for varying rotor solidity.

4.11 Technology Readiness Design Considerations

A potential subsystem design choice for the *Kestrel* was a variable diameter rotor (VDR), but was not used because of the lower technical readiness level (TRL). The VDR would allow for an increased diameter in hover to decrease disk loading and improve the hover power loading efficiency. A VDR could also decrease the diameter when transitioning to forward flight to decrease the helical Mach number and reduce compressibility effects to improve propulsive efficiency. As attractive as these performance benefits were, the RFP called for a synergistic effort to bring together a combination of relatively technologically mature subsystems that would yield unprecedented levels of performance. The VDR is currently at a TRL of 4, which is considered too low to incorporate into an aircraft that is expected to be technologically mature by the end of Phase I of the competition. The 16 months allocated to Phase 1B, the Technology Maturation and Advanced Preliminary Design segment, was considered insufficient to complete an advanced preliminary design and to develop such a major subsystem that has had no previous application and limited wind tunnel success [12].

4.12 Summary of Proprotor Parameters

The rotor characteristics were selected using a BEMT methodology and parametric studies converged to a design with a total aircraft hover power loading efficiency of 0.82, propulsive efficiency of 0.87 at the best range airspeed, and propulsive efficiency of 0.72 at the maximum cruise speed. As shown by the Pareto analysis, the current design selection achieves efficiencies higher than any other potential configurations for the design space. The variable speed rotor is the enabling technology that allows for high aerodynamically efficiency in hover and forward flight. From the aforementioned sections, the summary of the proprotor parameters are shown in Table 4.2.

Table 4.2: Summary of Proprotor Parameters

Radius, R	10.75 ft
Taper, λ	2:1
Solidity, σ	0.125
Twist Change Spanwise Position	$0.7R$
Inboard Twist, $\theta_{TW,IB}$	4.5° ft^{-1}
Outboard Twist, $\theta_{TW,OB}$	Hyperbolic
Inboard Airfoil	NASA RC(4)-10
Outboard Airfoil	NASA RC(3)-08
Hover/Maximum Cruise Airspeed	555 rpm
Best Range Cruise Airspeed	269 rpm
Hover Power Loading Efficiency, k	0.82
Best Range Cruise Airspeed Propulsive Efficiency, η_P	0.87
Maximum Cruise Airspeed Propulsive Efficiency, η_P	0.72

Rotor and Hub

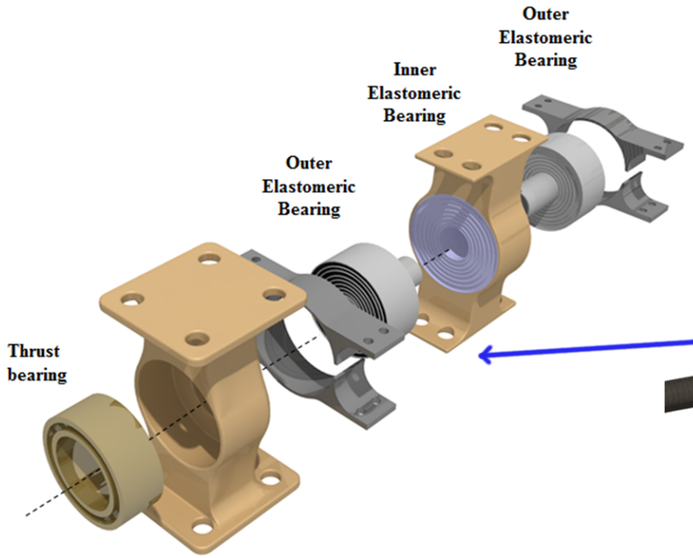

Bearing Pack Assembly

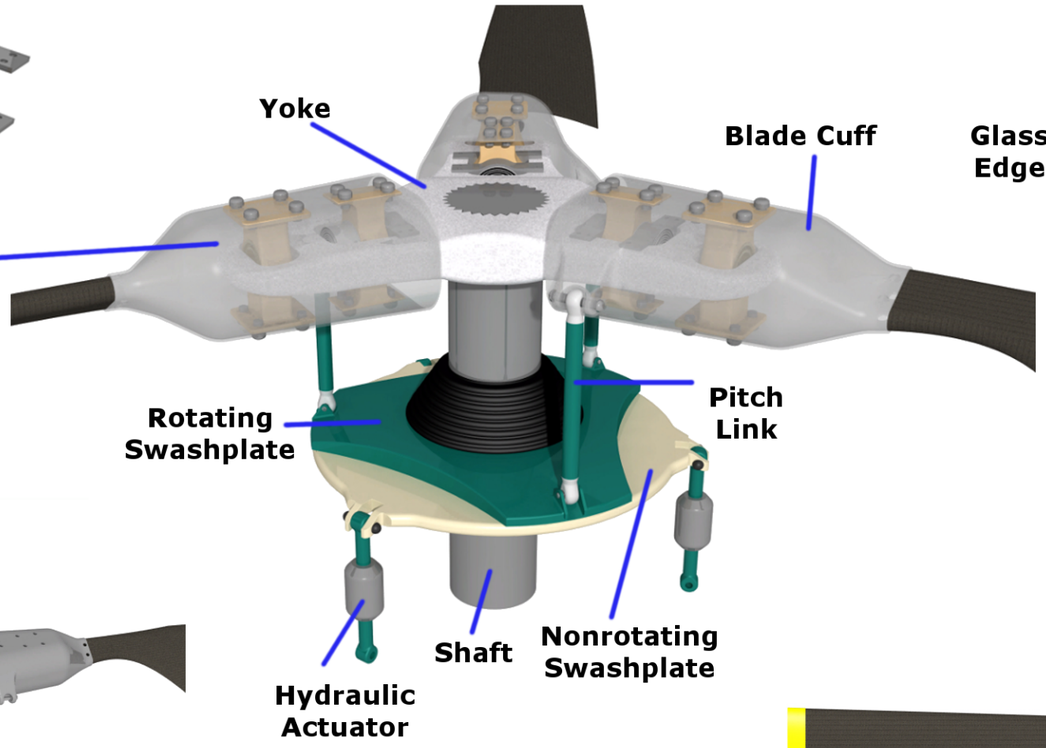

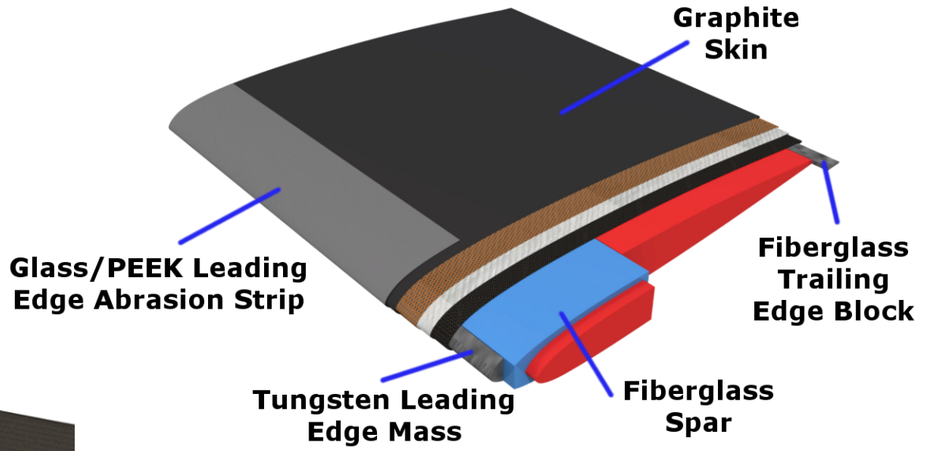

Blade Construction

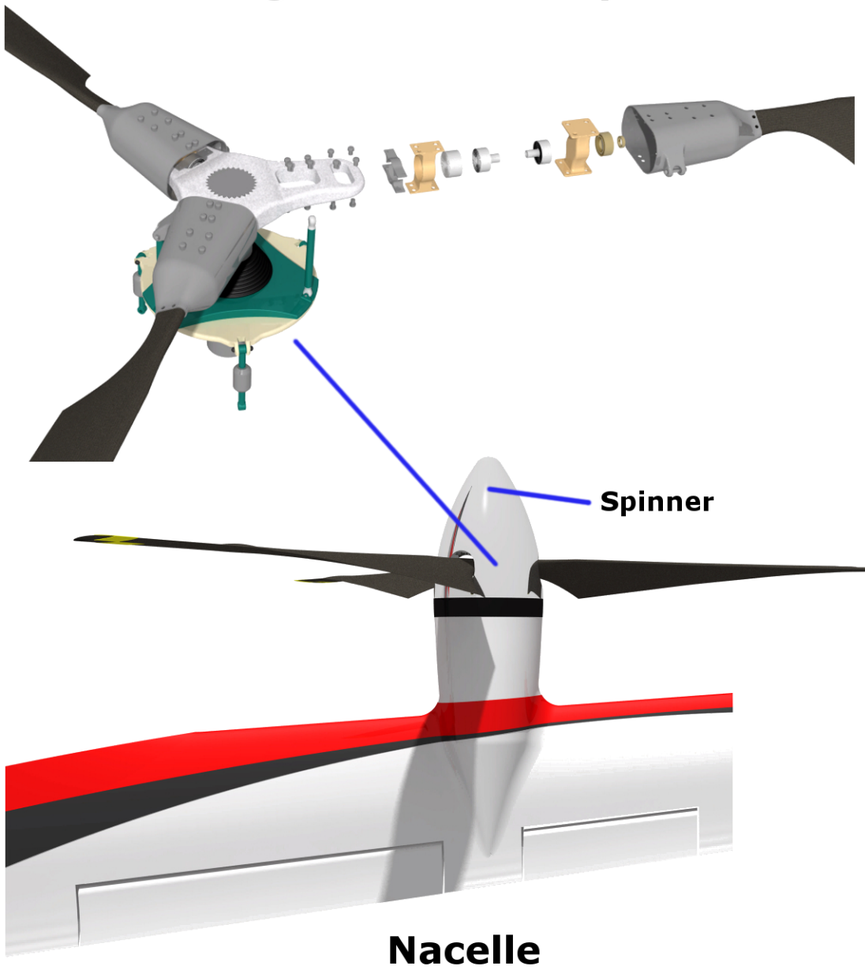

Nacelle

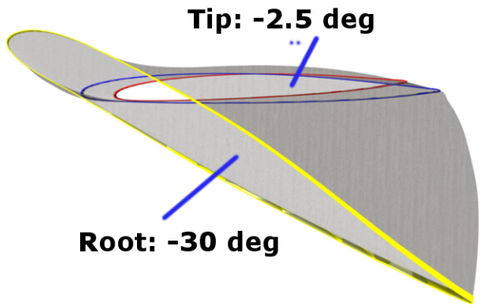

Blade Characteristics

2:1 Linear Taper Ratio

Inboard Twist: Linear 4.5 deg/ft

Outboard Twist: Hyperbolic

Inboard: NASA RC(4)-10

Outboard: NASA RC(3)-08

5 Proprotor Hub Design

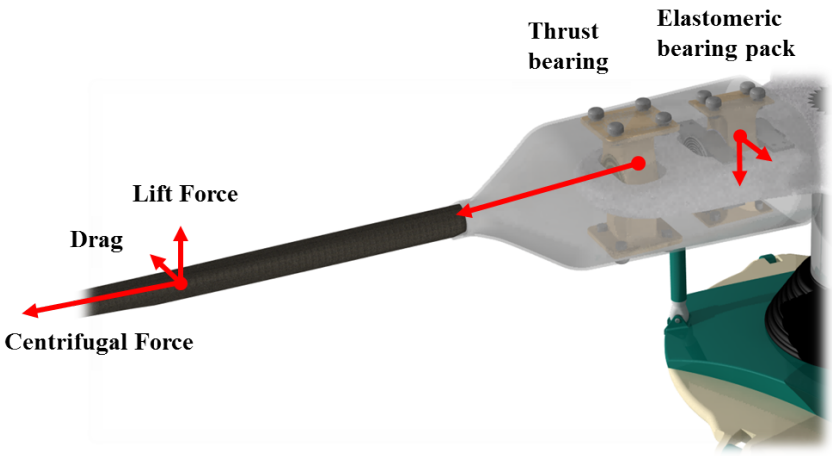

Figure 5.1: Reaction forces on the rotor hub bearings.

The hub design for the *Kestrel* was driven by the need to transition between hover and forward flight modes. The transition involves significant aircraft pitch rotations, necessitating large control moments. To support mission requirements, a hingeless rotor configuration that is stiff-in-plane was chosen over a gimbaled, articulated, or bearingless rotor hub.

The gimbaled and articulated rotor hub systems may not have enough authority to transfer hub moments to control for the aircraft and were therefore not considered for the *Kestrel*. As mentioned in Chapter 10, the *Kestrel* requires a 50° collective pitch range for propulsion in both hover and forward flight modes. A hingeless rotor system allows a larger collective pitch range compared with a bearingless configuration. Bearingless rotor hubs rely on the physical flexure of components constructed from layered composites, inherently limiting the torsion range that can be achieved. By using pitch bearings for blade twist, the hingeless hub chosen for the *Kestrel* can support the necessary collective pitch range.

A hingeless rotor system offers increased sensitivity to control inputs and high maneuvering capability. With a direct connection between blade and hub, an equivalent tip-path-plane tilt from a hingeless rotor produces larger hub moments, which can provide control in a transition mode.

A stiff-in-plane hub offers numerous advantages for a tail-sitter vehicle. By restricting blade motion in the lead/lag degree of freedom, stiff-in-plane rotors are inherently less sensitive to ground and air resonance instabilities that may be critical during operations in the vertical mode. A stiff-in-plane design eliminates the need for added mechanical lag dampers, resulting in a comparatively less complex hub design with fewer parts. Operationally, the stiff-in-plane hingeless rotor has lower maintenance requirements compared to a traditional articulated rotor.

One disadvantage of a hingeless, stiff-in-plane configuration is the increased vibratory loads that are experienced by the hub components. However, the majority of the mission is performed in axial flight, reducing the load requirements on the hub. The vehicle is in edgewise flight only at low forward airspeeds and transition, which accounts for a very small portion of the mission profile.

5.1 Bearing Assembly

The forces and moments acting on the blade are first transferred to the hub through a blade cuff attached to the blade spar. The overall height of the blade cuff and bearing housings were designed such that there is enough clearance for the bearing clamps to rotate up to 50°, as required by the collective pitch range throughout the flight envelope.

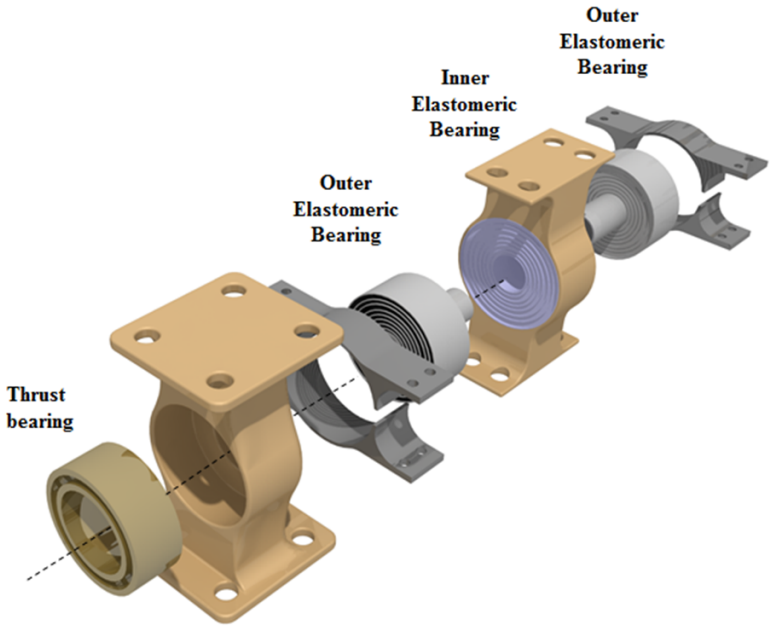

Figure 5.2: Location of thrust and elastomeric bearings.

Figure 5.1 shows the bearing assembly and the respective reaction forces acting on the bearings. Both of the bearing packs transmit the forces and moments to the shaft through a yoke. The pitch axis is fixed by the inboard and outboard bearings. The outboard bearing assembly contains a thrust bearing, which react to the centrifugal loads.

The inboard bearing assembly houses three radial elastomeric bearings connected in series and react to the resulting flap and lag forces. The bearings are on centering springs and require low force input from the pitch rods. The two outer elastomeric bearings are clamped to the yoke and are serially connected such that the center shaft of one bearing rotates on the shaft of the other bearing. The innermost bearing is connected to the blade cuff through a clamp, and is serially connected to the two outer bearing through the hollow shaft. The serial connection of the three elastomeric bearings allow for increased torsional motion.

5.2 Rotor Dynamics

Rotorcraft are susceptible to a number of different aeromechanical instabilities that require special attention in the design of a rotor system. *Kestrel's* stiff-in-plane rotor and its blade construction provides a safety margin from some of these instabilities. Aeromechanical instabilities such as as flap-lag flutter, pitch-flap flutter, pitch divergence and ground resonance (inplane hub/regressing lag) were calculated using simple analyses, and these were further verified using UMARC, the University of Maryland's comprehensive rotor analysis tool.

5.2.1 Pitch-Flap flutter and Pitch Divergence

Pitch-flap flutter is a dynamic instability caused by the coupling of the blade pitching motion with its flapping motion. Pitch divergence is a static instability that occurs when an air disturbance causes the rotor blade to elastically pitch until failure. Both of these instabilities are dependent on the offset of the c.g. from the aerodynamic center of the blade. The *Kestrel*'s blade c.g. spanwise location is placed at the quarter chord, coincedent with the aerodynamic center, and the torsional frequency of 4.78/rev remove all likelihood of both pitch-flap flutter and pitch divergence.

The pitch-flap and pitch divergence boundaries as plotted in Fig. 5.3, clearly show sufficient margin of stability.

5.2.2 Flap-Lag Flutter and Ground Resonance

Flap-lag flutter is an undesirable coupling of the flap and lag modes being caused from perturbations in aerodynamic and coriolis forces with limited inherent lag mode damping. For soft-in-plane rotors, lag damping is augmented by adding a damper to each rotor blade. The *Kestrel's* stiff-in-plane rotor is inherently protected from this instability due to its high mechanical blade stiffness in the lag mode and therefore, does not require any mechanical damper. The flap-lag flutter eigenvalues are shown in Fig. 5.4.

Ground resonance is an explosive instability that arises from the coupling of the fuselage landing gear modes with the lag modes of the rotor. As with flap-lag flutter, a mechanical damper is typically added to soft-in-plane rotors to protect against ground resonance. Because the *Kestrel* has a stiff-in-plane rotor system, ground resonance is not a concern.

The *Kestrel*'s design has shown a sufficient margin of stability from all aeromechanical instabilities during all operating conditions.

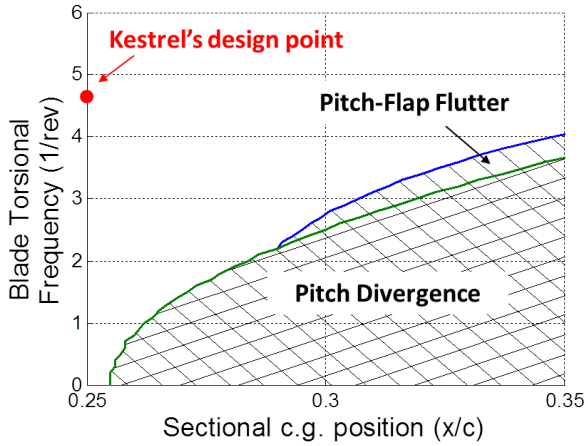

Figure 5.3: Pitch-flap flutter and pitch divergence boundaries.

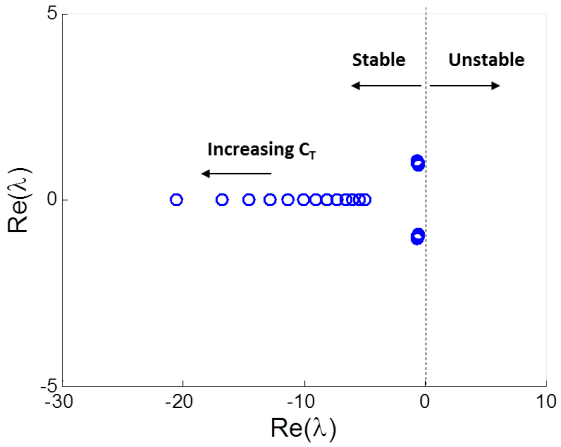

Figure 5.4: Flap-lag flutter eigenvalues.

6 Wing and Control Surfaces Design

The following section details the selection of the wing parameters such as the aspect ratio, dihedral, twist, taper, sweep, wing loading, and airfoil selection. This section also summarizes the main requirements for the wing design.

6.1 Selection of Wing Parameters

The main wing will provide the majority of the lift required during the end phase of the transition and forward flight. The wing must also help satisfy the RFP requirements to maintain or exceed a lift-to-drag (L/D) ratio of 10 at the best range speed. To meet these requirements, the *Kestrel* is outfitted with a high aspect ratio wing to reduce the induced drag and improve the lift-to-drag ratio. The high aspect ratio wing yields lower fuel consumption and improves the range of the aircraft. Moreover, high aspect ratio wings come at the cost of high root bending moments that result in heavier structural components. Design trade studies were required to balance the potential aerodynamic benefits with the empty weight increase.

The main wing sizing was based on the total aircraft L/D, wing loading (W/S), and clearance between the proprotor tips and fuselage. The initial wing loading of 65 lb ft^{-2}, was based on the Piaggio P180, a contemporary fixed-wing propeller-driven aircraft with a canard and is capable of flying 300–400 kts [13]. The initial aspect ratio (AR) of 10 was selected to meet a target lift-to-drag ratio of 12. With the wing loading and aspect ratio, the wing reference area (S), wingspan (b), and average chord length (c) were be determined to be 43 ft^2 and 4.3 ft respectively.

6.2 Lift Requirements

The lift requirements were driven by the design wing loading of 65 lb ft^{-2}, design stall speed, best range cruise speed, and maximum cruise speed. The C_L requirements based on the MGTOW, speed, and altitude are summarized in Table 6.1. The lift required for the aircraft could vary as much as 30% from other lift contributors such as lift sharing by the fuselage and canard. The lift sharing was taken into account when assessing the lift requirements for transition and the maximum cruise speed. The three-dimensionality of the wing which reduces the lift curve slope was also accounted for in the $C_{L,Required}$.

Table 6.1: C_L requirements for different flight conditions.

Airspeed (kts)	MSL ISA	5,000 ft ISA	10,000 ft ISA
100	1.92	2.23	2.60
125	1.23	1.43	1.66
150	0.85	0.99	1.16
200	0.48	0.56	0.65
250	0.31	0.36	0.42
300	0.21	0.25	0.29
350	0.16	0.18	0.21

6.3 Airfoil Selection

The airfoil selection for the wing was based on the following requirements:
1) The C_L requirements given in Table 6.1
2) A high sectional $C_{L_{MAX}}$ and gradual stall onset for transition
3) Low C_D at low C_L to reduce drag at higher airspeeds
4) Minimize the aerodynamic moment
5) High L/D ratio at $C_{L,required}$ for V_{br}

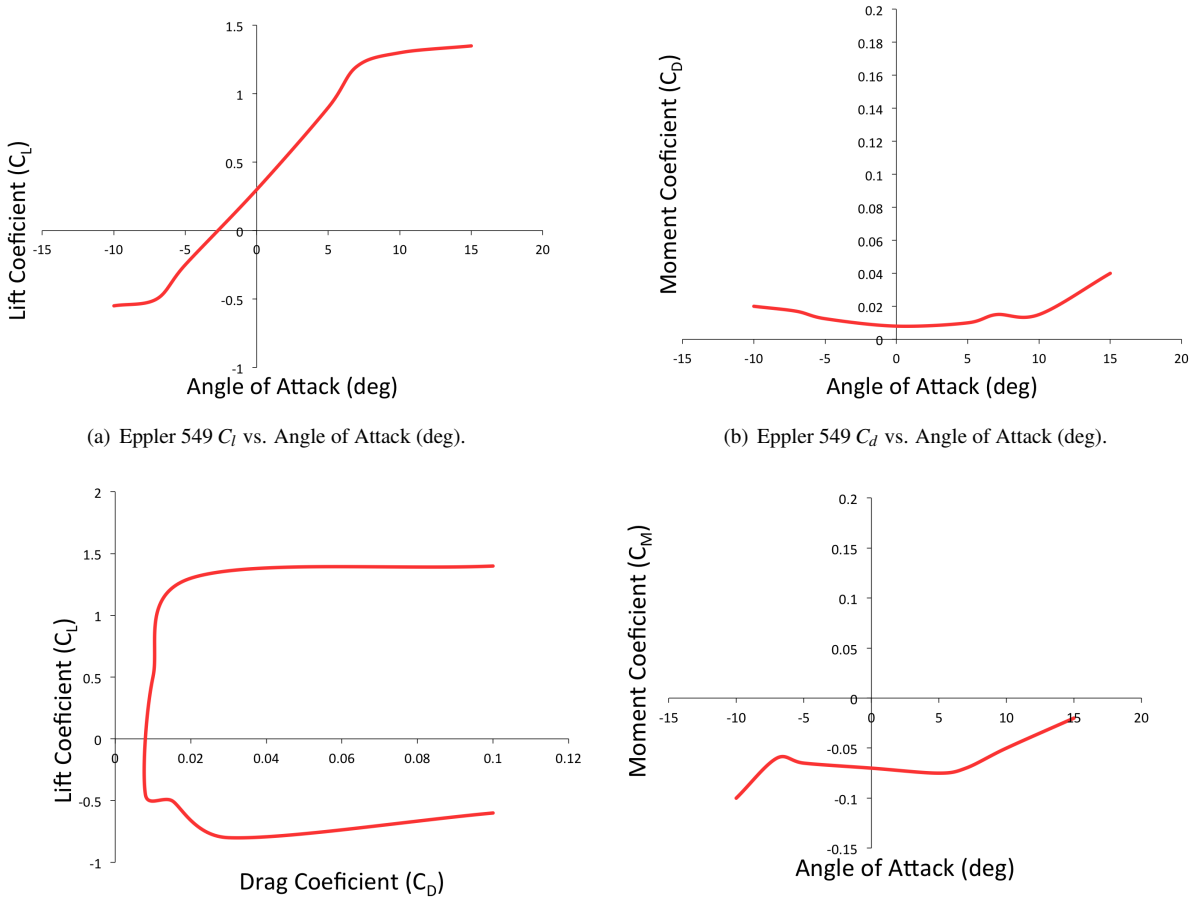

(a) Eppler 549 C_l vs. Angle of Attack (deg).

(b) Eppler 549 C_d vs. Angle of Attack (deg).

(c) Eppler 549 C_l vs. C_d.

(d) Eppler 549 C_m vs. Angle of Attack (deg).

Figure 6.1: Wing airfoil characteristics.

6) Relatively high thickness-to-chord (t/c) ratio (15–20%) for torsional stiffness and prevent whirl flutter instabilities

The Eppler 549 airfoil section best satisfied all of the selection criteria highlighted for the design. This airfoil section maintains a considerably high L/D over the operational range of the airfoil. The lift and drag polars are shown in Fig. 6.1.

6.4 Selection Other Wing Parameters

The wing dihedral (Γ) increases the lateral stability control of the vehicle, however, any dihedral will reduce the component of lift generated by the wings. A compromise of 4° was selected because the roll stability is improved without significantly reducing the lift generated by the air vehicle.

The planform taper (λ) of the wing reduces lift generated bending moments and induced drag on the wing. A taper ratio of 0.7 was selected to reduce the induced drag of the wing with minimal impact of the stall characteristics of the aircraft.

The wing was forward swept at an angle of Λ to increase the clearance between the rotor tips and the wing. The wings

were swept forward 4° to also promote stall inboard and gives the aircraft better roll stability at stall [14]. Additionally, forward sweep promotes spanwise flow inboard where the fuselage acts as an aerodynamic fence to prevent early flow separation.

Twist (ϕ) on the wing was also used to reduce the outboard stall and to create a more elliptical lift distribution on the wing. The elliptical lift distribution will apply lift more evenly across the wingspan and reduce bending moments at the root which reduces the structural weight required to support the wing loading.

Setting the wing incidence angle (i_w) was driven by the maximum cruise speed. To minimize the power required at maximum cruise airspeed, the fuselage was set near to a zero angle of attack to reduce the parasitic drag of the aircraft. Based on the maximum cruise speed requirement, the wing incidence angle was selected as -1 degree. Table 6.2 summarizes the main wing parameters.

Table 6.2: Summary of major wing parameters.

W/S (lb ft^{-2})	AR	S (ft^2)	b (ft)	Γ (deg)	λ	Λ (deg)	ϕ (deg)	i_w (deg)
65	10	43.0	4.3	4.0	0.7	4.0	1.6	-1.0

6.5 Wing Download Penalty

The wing download penalty, *fv*, was calculated to be 0.6% of the total thrust required in hover. This low download is considered one of the many strengths of the tailsitter configuration, as convertible rotors with fixed wings can increase the thrust required by an additional 15% of the thrust required [43]. Eliminating the download penalty on the wings yielded a considerable hover efficiency gain.

6.6 Structural Design

Kestrel's wing is optimized for high torsional and bending stiffness during the maximum forward flight cruise segment. The wing is comprised of a tapered torque box spanning 80% of the wing up to the nacelle, with the front vertical web located at 10% and rear at 43% chord. In addition to providing the necessary stiffness, the torque box houses 50% of the fuel required for the mission. Figure 6.2 shows the torque box with ribs, internal fuel tank, and wing skin.

A structural analysis was conducted using Euler–Bernoulli beam theory to determine bending stresses and tip deflections. In addition, a torsional analysis using the St. Venant torsion theory was performed for the transition maneuver to limit the twist of the wing.

The dimensions of the torque box were initially sized to meet static structural requirements. All the aerodynamic and inertial forces of the wing and proprotor were represented by distributed loads and point forces for a first-order analysis of the shear and bending moments. The chordwise and beamwise stiffness were determined by the airloads at maximum cruise airspeed and the torsional stiffness of the wing was sized for transition flight.

Final sizing of the torque box was determined by the torsional stiffness required to prevent the onset of pylon whirl flutter [16]. The stiffness model was based on a uniform beam with a concentrated tip mass for the fuselage and nacelles, and with the wing clamped to the root. The stiffness was then fine-tuned in conjunction with the whirl flutter analysis to reduce structural weight of the wing while maintaining a margin for whirl flutter instability.

The front and rear webs were spaced 1.41 ft apart and has a thickness of 0.33 in, while the top and bottom layers have a thickness of 0.21 in. Typically, the top and bottom layers of the torque box are much thicker than the sides for tiltrotors because the rotor thrust forces are applied spanwise. However, the front and rear webs are thicker for the

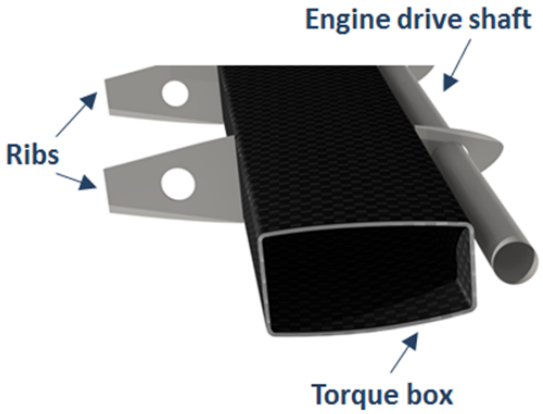

Figure 6.2: Structural composition of the wing.

Kestrel's torque box because the rotor thrust forces act chordwise.

6.7 Composite Tailoring

Increased whirl flutter stability is provided by composite tailoring. Therefore, the *Kestrel*'s torque box is aeroelastically tailored with structural bending-torsion coupling. The torque box is composed of unbalanced multi-layered graphite-epoxy laminate with a ply thickness of 0.005 in. Graphite-epoxy was selected for its light weight and high material stiffness compared to other composites. The lay-up of the front and rear webs is $[0_9/90_9/\pm 45_{15}]_S$. To incorporate bending-torsion coupling into the wing structure, the lay-up for top and bottom skin is a 70/30 ratio of [$\pm 45^\circ$] plies [17]. The lay-up fiber orientation was determined using Classical Laminate Plate Theory (CLPT) to ensure adequate stiffness and increase in the whirl flutter velocity. The wing skin provided primary torsional stiffness and used angular and cross plies composed of graphite-epoxy. The entire skin has a thickness of only 0.1 in. With the inclusion of tailored bending-torsion couplings, the whirl flutter stability increased significantly over using just balanced laminates.

6.8 Whirl Flutter Analysis

Because the *Kestrel* operates at high forward airspeeds, the proprotor nacelle mounted on the wing could potentially lead to pylon whirl flutter instability. Whirl flutter is a key concern for the *Kestrel* compared to conventional propeller-driven fixed wing aircraft because of large rotor flapping motion [17]. This instability is mitigated by ensuring the flap, lag, and torsional frequencies of the rotor blades do not coincide with the bending and torsional modes of the wing. A simplified finite-element model of the wing as a cantilevered beam with chordwise, beamwise, and torsional degrees of freedom was used to derive the damping ratios and frequencies of the various modes [17], [18].

The whirl flutter model assumes quasi-steady aerodynamics and a rigid-body structure with a coupled wing and proprotor dynamics. Figure 6.3 shows the chordwise, beamwise, and torsion modes of the wing at different airspeeds in fixed-wing mode. The maximum airspeed before whirl flutter is determined by the torsion mode instability at 470 knots. Because the *Kestrel* operates at a maximum cruise airspeed of 350 knots, there is an adequate margin of safety for whirl flutter instability.

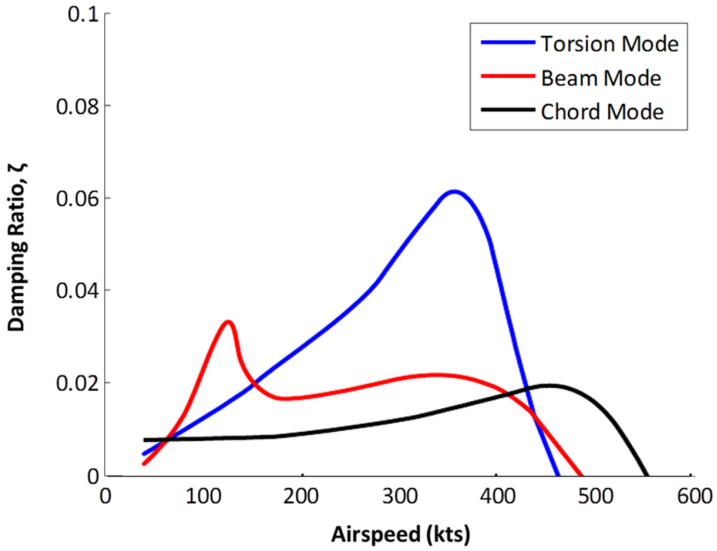

Figure 6.3: Wing damping ratio versus airspeed.

6.9 Canard

In forward flight, the pitch, roll, and yaw controls are provided by the canard, aileron, and rudder, respectively. The lift augmentation gained from deflecting the canard incidence angle is used to vary the pitch moment about the airframe c.g. Flaps generate a higher lift coefficient during transition to forward flight and also act as airbrakes when transitioning back into hover. All the control surfaces were carefully designed to provide adequate stability and control authority of the aircraft.

As a tailsitter, the *Kestrel* requires an aft center of gravity to improve stability in hover and to reduce gust sensitivity. With the c.g. located ahead of the wing's aerodynamic center, a canard was used to provide longitudinal static stability in forward flight instead of a traditional aft horizontal stabilizer.

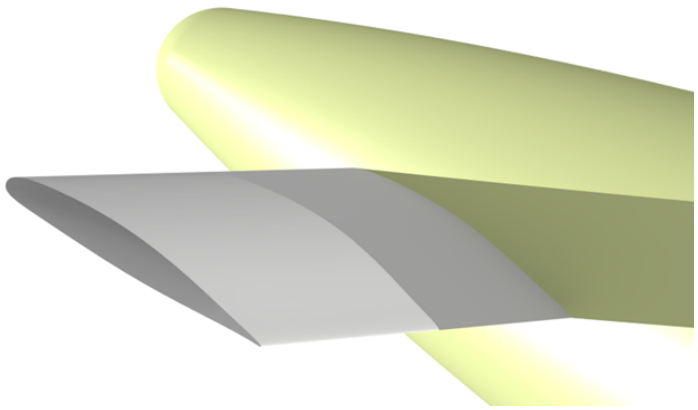

Figure 6.4: Rutan AMSOIL Racer canard airfoil.

With a canard designed to stall at a lower angle of attack than the main wing, the main wing can be prevented from entering a stall due to the stabilizing nose-down moment generated when the canard loses lift. A forward-mounted surface produces positive lift in trimmed flight and reduces the lift that needs to be produced by the main wing, allowing the aircraft to operate at lower angles of attack and therefore generate less induced drag. To reduce canard wake influence on the main wing during steady and level forward flight, the canard on the *Kestrel* is vertically displaced lower than the wing.

6.9.1 Longitudinal Static Stability

The aerodynamic design of the canard has to provide large pitching moment such that the aircraft is longitudinally stable in cruise. The typical canard design requires at least a 15% static margin and capability to trim the aircraft throughout the expected flight envelope [19]. The flight envelope of the *Kestrel* involves a wide range of angles of attack, such as those encountered during the transition maneuver, necessitating a large range of control surface movements. The *Kestrel* is therefore fitted with a variable incidence canard that can rotate $\pm 45^{\circ}$; by controlling incidence angle instead of by using a separate elevator, the canard can retain trim effectiveness over a very large range of flight attitudes.

6.9.2 Geometric Parameters of the Canard

The entire canard is a movable surface that provides pitch trim and maneuverability by deflecting the incidence angle. A low camber or symmetric airfoil is ideal to achieve a trimmed flight condition for a wide range of angles of attack. Another criteria is that the canard airfoil must stall at a lower angle of attack than the wing airfoil. Furthermore, a relatively low thickness-to-chord ratio (11–12%) is preferred to reduce drag at higher airspeeds (300-400 kts). Based on the requirements, the Rutan AMSOIL Racer canard airfoil was selected with its maximum thickness-to-chord ratio of 11.6% at 39% chord and zero lift angle at -2° (Fig. 6.4). The planform area was determined by the vertical and horizontal moment arm selected for longitudinal stability. All the geometric parameters of the canard are summarized in Table 6.3.

Table 6.3: Geometric parameters of canard.

Parameter	Tail-sitter
Airfoil	Rutan AMSOIL Racer
Planform area (ft^2)	31.1
Average chord (ft)	2.19
Span (ft)	14.2
Taper ratio	0.70
Sweep (deg)	4.00

6.10 High-Lift Devices

The flaps on the *Kestrel* occupy the inboard section of the wing. The entire control surface spans 8 ft and is equivalent to 30% of the wing chord. In forward flight, the flaps increase the maximum lift coefficient of the wing and reduces the stall speed to 100 kts. When transitioning from maximum cruise airspeed to hover, the flaps act as airbrakes and reduce the airspeed. The Fowler flap was selected because of its high contribution to the wing lift coefficient. The Fowler flap is mechanized by a hydraulic actuator that travels on a slotted track and depicted in Fig. 6.5.

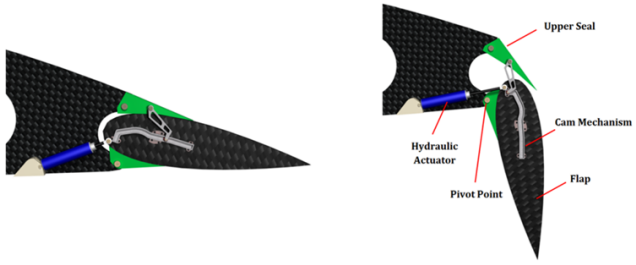

Figure 6.5: Fowler flap mechanism

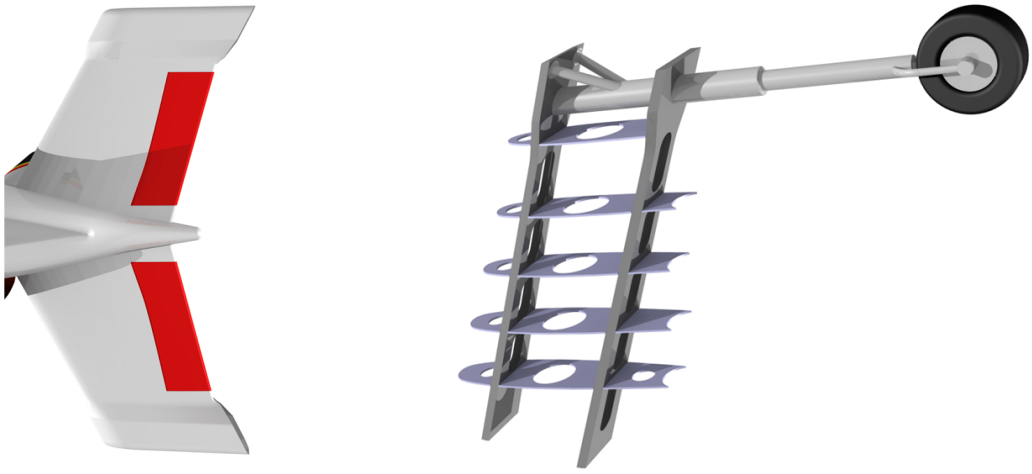

(a) Exterior (b) Structure

Figure 6.6: Vertical fin.

6.11 Vertical Tail

The vertical tail provides the directional and lateral stability such that perturbations from the trim position will create a restoring moment. Because the *Kestrel* has an aft c.g., there is a moment arm of 6 ft between the vertical tail and the c.g. Consequently, the vertical tail required surface area is 33 ft^2 per fin (Fig. 6(a)) to achieve control effectiveness. A NACA 0015 airfoil was selected for its thickness because the fixed landing gear is attached to the beams on the fin (Fig. 6(b)). The overall planform and geometric characteristics of the vertical fin is designed to accommodate the landing gear. All the parameters of the control surfaces are summarized in Table. 6.4.

Table 6.4: Control surface parameters.

Parameters	Vertical tail	Rudder	Aileron
Planform area (ft^2)	66.0	12.0	5.20
Average chord (ft)	2.19	1.33	1.29
Aspect ratio	2.00	3.38	3.89
Span (ft)	14.2	4.50	5.00
Taper ratio	0.70	1.00	1.00
Sweep (deg)	8.00	-	-

7 Transmission

The two-speed transmission of the *Kestrel* transmits a maximum total of 4,454 shp from the two turboshaft engines to the proprotors. For maximum efficiency in hover, at V_{BR}, and at V_{BE}, the nose gearbox speed of 6,000 $\pm$2% rpm is reduced to 555 and 269 rpm respectively. A proprotor speed of 555 rpm is utilized in max cruise airspeed and in hover, while a speed of 269 rpm is used for V_{BR}. A differential dual-drive gearset has been developed for use in the *Kestrel* to get this 52% change in proprotor speed for efficiency at V_{BR}. With a constant engine speed input, most multi-speed gearboxes will abruptly change rpm between two discrete output speed points. The Differential Dual-Drive gearset provides a smooth transition between two set proprotor output speeds, delivering continuous power to the proprotor with no driveline shock. The addition of the two-speed functionality for the *Kestrel* transmission only added about 250 lb to the weight of the drivetrain.

A simple four gearbox layout is employed for the transmission of the *Kestrel*. The first gearbox is centrally located in the fuselage between the two engines, and encases the differential dual-drive gearset that provides the two-speed functionality. The second gearbox is a single bevel gearset located in front of the torque box. The last two gearboxes are located in the nacelles, and provide the final speed reduction to the proprotor.

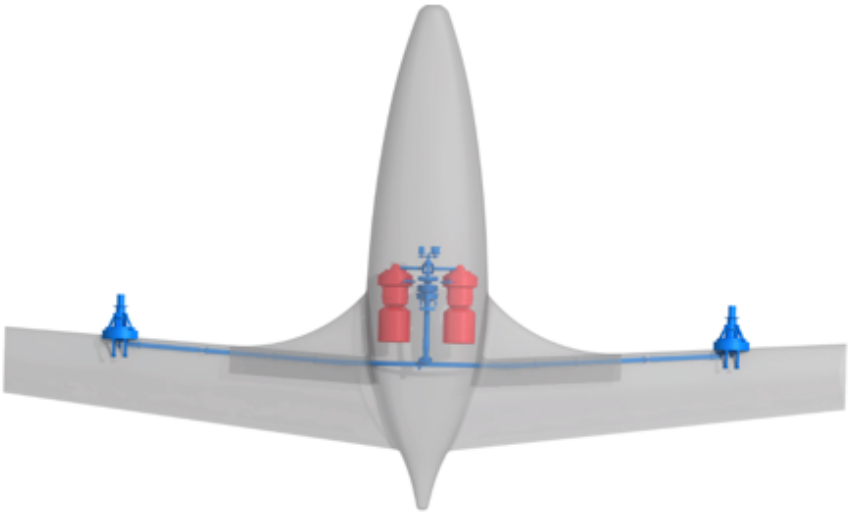

Figure 7.1: Transmission orientation

7.1 Transmission Overview

The proprotor of the *Kestrel* is subjected to substantially different thrust requirements in vertical, horizontal, and maximum cruise airspeed flight. While in helicopter mode the proprotor must provide thrust to overcome weight. In horizontal flight mode it provides forward thrust to overcome drag. The *Kestrel* has 150 knots between its cruise and maximum airspeeds, yet the aircraft can only be fully optimized for best efficiency in a single flight condition. To attain optimum efficiency in both regimes, it is desirable to be able to vary the rotational speed of the proprotor.

With the use of a turboshaft engine, varying the proprotor speed can be done by adjusting the throttle or by incorporating a variable speed transmission. Changing the output speed by adjusting the throttle, as done in the V-22, is a simple but lower efficiency option compared to a wide range of proprotor speeds. With this method, the engine never operates at its maximum efficiency but instead straddles this point with its hover and cruise rpm. Although throttling alone provides some increase in efficiency, the overall result is still a compromise in efficiency. For a proprotor speed range of under 10–15%, throttling may be most practical considering efficiency and weight. For higher rpm ranges

such as the 52% range of the *Kestrel*, engine throttling is inefficient. Therefore, to obtain the large speed variations of 52%, a variable speed transmission was developed. Reduction of the proprotor rpm while maintaining engine speed at its peak point of efficiency was the goal.

Drivetrain layout has a lot of influence on overall aircraft c.g. location, aerodynamics, and structural design. Effects on vertical and horizontal c.g. location were taken into account for gearbox placement. The wings have a smaller front cross sectional area and have lower induced drag with the first two gearboxes placed in the fuselage. Also, the bulk weight centered at the fuselage reduces the roll moment of the *Kestrel* lending to the stability and control of the aircraft.

The transmission provides an overall speed reduction ratio of 21.9:1 and 11:1 to reduce the engine nose gearbox output speed of 6,000 rpm (±2%) to 269 and 555 rpm for the low and high speed modes respectively as shown in Fig. 7.2. Highlighted in red and blue are the high and low speed modes respectively. Stages 2,3,and 4 represent the variable speed gearset (bolded box). The complete transmission system is rated at 4,454 shp and operates at 97% efficiency.

Stage	Gear Type	Number of Teeth	Gear Ratio	RPM (high/low)	Pitch Diameter (in.)	Diametral Pitch (teeth/in.)	Face Width (in.)	Helix Angle (degrees)	No. of Gears	Combined Weight (lb.)
1	Bevel	46	1.02:1	6120/5880	5.75	8.00	3.44	20	1	53.2
	Bevel	47		6000/5765	5.88	8.00	3.44		1	
2	Spur	24	1.75:1	6000/5880	6.86	3.50	2.74	20	1	81.9
		42		3429/0	12				1	
3	Spur	24	1.75:1	3429/0	6.86	3.50	4.39		1	131.0
		42		1959/0	12				1	
4 (Planetary)	Sun	25	2.02:1/4:1	6000/5765	4	6.25	3.20	0	1	120.0
	Planet	25		N/A	4				5	
	Ring	75		1959/0	12				1	
	Carrier	N/A		2970/1441	N/A					
5	Bevel	33	1.03:1	2970/1441	8.25	4.00	4.60	20	1	144.6
	Bevel	34		2884/1399	8.5				1	
6	Bevel	30	1.3:1	2884/1399	6.32	4.75	4.95		2	165.8
	Bevel	39		2218/1076	8.21				2	
7 (Planetary)	Sun	30	4:1	2218/1076	5.71	5.25	4.00	0	2	563.2
	Planet	30		N/A	5.71				10	
	Ring	90		0/0	17.14				2	
	Carrier	N/A		**555/269**	N/A					
*All pressure angles are 20°									**Total Weight=1259.7 lb.**	

Figure 7.2: Transmission gear sizing summary.

As seen in Fig. 7.3, the main gearbox contains the first four of seven gear stages including a 1.02:1 spiral bevel collector stage that combines the power from the two engines into one shaft. A simple 1:1 ratio was avoided in the bevel collector stage to ensure that different teeth would be meshing during each cycle to prevent uneven wear of gear pairs. The main gearbox also incorporates the two-speed gearset which provides a 4:1 or 2.02:1 reduction ratio depending on the desired proprotor speed. By consolidating the spiral bevel junction and the variable speed gearset into a single

gearbox, weight is saved in reduced gearbox casing volume. Weight was saved in reducing the casing volume by consolidating the spiral bevel junction and the variable speed gearset into a single gearbox weight. The lubrication system was also simplified by being centralized into a single unit.

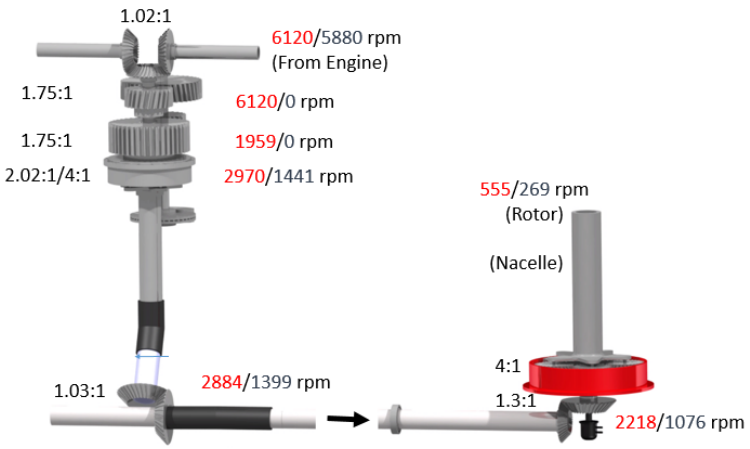

Figure 7.3: Drive system layout

The fifth stage of the transmission is a 1.03:1 bevel pair that redirects power from the central driveshaft to the perpendicular wing driveshaft. The entire central section of the transmission, including the gears of the first and second stages used a higher factor of safety to compensate for being the only part of the transmission that does not have redundancy.

The sixth and seventh stages of the transmission are located in the nacelles in each wing. The sixth stage is a 1.3:1 spiral bevel gear pair that redirects power towards the proprotor. The seventh stage is a 4:1 planetary gearset which outputs to the rotor hub. A planetary gearset enables the frontal area, and therefore the overall size of the nacelle, to be reduced when compared to a standard non-concentric split torque gearset. Despite a slight aerodynamic penalty by having the final reduction stage in the nacelle, weight savings are realized by having the sixth and seventh stages in the nacelles from decreased torque loading on preceding shaft sections. Wing mounted gearboxes also provide a structural bending moment relief while the aircraft is in horizontal and vertical orientations.

7.2 Variable Speed Transmission Analysis of Options

Continuously variable and discrete (two-speed) transmissions were compared. The transmission must provide smooth and continuous power during speed changes and to be lightweight, mechanically simple, and very reliable.

7.2.1 Continuously Variable Speed Transmission (CVT)

A continuously variable speed transmission is desirable because of its ability to transition smoothly between modes of operation and provide a large number of possible reduction ratios. One conventional CVT method is through a traction drive system. However, a traction drive system with any speed mismatch and internal slippage in high inertia applications such as in rotorcraft can generate an excessive amount of heat and wear. With the traction fluid properties of the system being compromised with increased heat, the traction can become unstable and deteriorate to the point of complete loss of power transfer [20]. Thermal control of a traction drive system requires additional hardware. Therefore, having complete power transfer through a traction type of CVT was not a viable option for the *Kestrel*.

A promising CVT option was a dual-input planetary differential system (Fig. 7.4). This differential planetary gearset concept provides variable gear ratios with the change of relative motion of its gears. A differential planetary gearset in which the input is the sun gear, output is the carrier, and the ring gear held stationary provide a set gear ratio (say 4:1). However, if the ring gear is not held stationary and rotates in the same direction as the sun gear, a reduced gear ratio is obtained. A 1:1 gear ratio is achieved with the ring gear rotating at the same speed as the sun gear. For the desired 52% reduction of the input speed (2:1 ratio), the ring gear must rotate at 1/3 of the input speed.

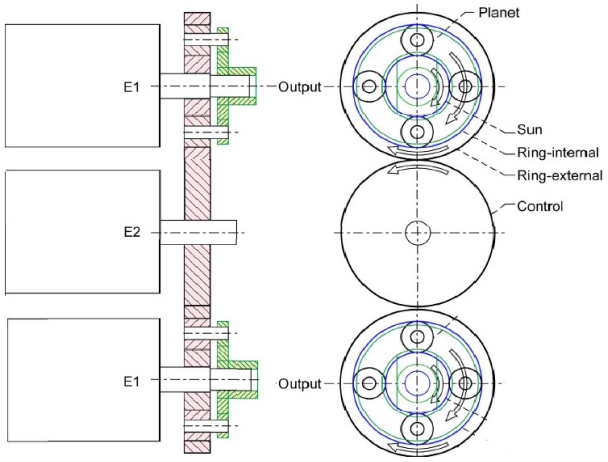

Figure 7.4: Differential planetary layout [20]

The differential planetary layout, as shown in Fig. 7.4, necessitates the use of a turboshaft engine input (E1) in conjunction with some form of controller (E2) that sets the speed of the ring gear. This controller can be internally driven by an additional CVT (traction type), or externally powered by an electric or reciprocating motor. The power required of the controller had to be determined prior to any further decisions on this concept were made. It was found that the total power load would be split between the turboshaft engine and the controller with relative magnitudes varying with the desired output ratio as shown in Fig. 7.5. Therefore, any power not provided directly from the engine to the differential planetary would have to be rerouted to the controller. For the *Kestrel*, with total output of 4,454 shp the controller would have to provide a large percentage of the total of power required. For a 4:1 ratio the ring gear would be locked and there would be no power required from the controller. For the desired 52% speed reduction of a 2:1 ratio, the total power would be split evenly between the engines and the controller. For a gear ratio of 1:1 the controller would need to provide about 3,400 shp of the total 4,454 shp required output.

For a smaller reduction ratio from a 4:1 ratio differential planetary, Fig. 7.5 shows that the required power from the variable speed controller is a significant percentage of the total required output. At these power levels, reliability, weight, and complexity become an issue for existing CVT options. At this power level, an internally driven traction type CVT to drive the controller was eliminated for the same reasons it was eliminated as a standalone CVT option. Using an external power source such as an electric motor or reciprocating engine was not desirable either because of the weight it would add to the aircraft. Utilizing a reciprocating engine controller would not only induce a large weight penalty, but excess power from the turboshaft engines (up to 2,227 shp) would be wasted. The overall additional weight and fuel consumption would negate the benefits of the variable speed transmission.

The dual-input differential planetary concept appeared to be attractive because of its inherent simplicity and variable speed capability, but the large amount of power required for the controllers means that this concept is not practical.

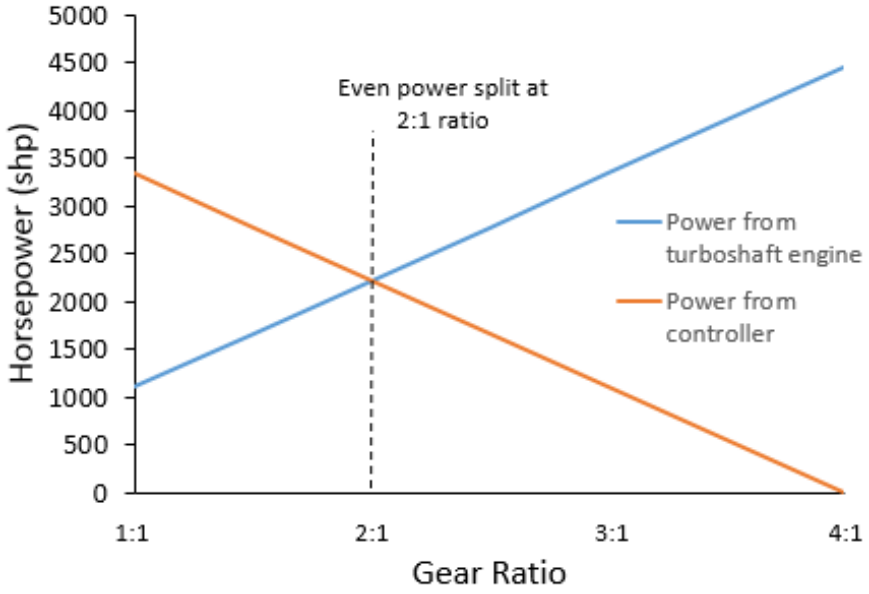

Figure 7.5: Differential planetary power split. Figure shows that there is a balance of power at a 2:1 ratio.

7.2.2 Discrete Two-Speed Transmission

A challenge of operating a discrete speed transmission is the synchronization of both the engine and rotor speeds during gear changes. Because undesirable driveline shock will be induced if the rotor and engine are not synchronized, these gear changes can be especially dangerous in emergency situations. The Bell XV-3 was able to accomplish shifts with a two-speed gearbox through the gradual application of a heavy friction clutch [21]. With a wide margin to match the speed of the rotor with the engine necessary, the clutch had to withstand high stress and wear that made it heavy and unreliable. With higher power applications (the Bell XV-3 only had 450 shp), the clutch would weigh much more and would need to withstand large amounts of sliding friction and heat buildup.

A two-speed transmission proved to be a viable option only with a reliable method of smoothly changing gears and delivering uninterrupted power delivery. This could not be done through techniques that include high wear and stress rates on transmission components such as the method used by the Bell XV-3.

7.2.3 Differential Dual-Drive Concept

It was evident that a transmission design that was purely discrete or continuously variable would not be a viable option for the *Kestrel*, yet each design had its own benefits. The goal was to be able to utilize the continuously variable nature of the differential planetary without the required power input of a controller. A design study by NASA and ARL developed the framework for a Differential Dual-Drive concept that has two discrete speeds and can shift in a smooth manner like a continuously variable transmission [20].

Instead of using an external controller as in the two-input differential planetary system, the Differential Dual-Drive concept, shown in Fig. 7.6, uses an intermediate gearset linked to the input shaft that can initiate split-power between the sun and ring gears of the planetary gearset [20]. Intermediate gearset (red) is engaged/disengaged from the input shaft (yellow) by the centrifugal clutch (green). The intermediate gearset drives the ring gear of the planetary gearset to control output shaft (blue) speed. This power split is realized through the intermediate gearset with the application of a centrifugal clutch and brake. In final form, this transmission is effectively a two-speed gearbox that is able to provide smooth shifting capability.

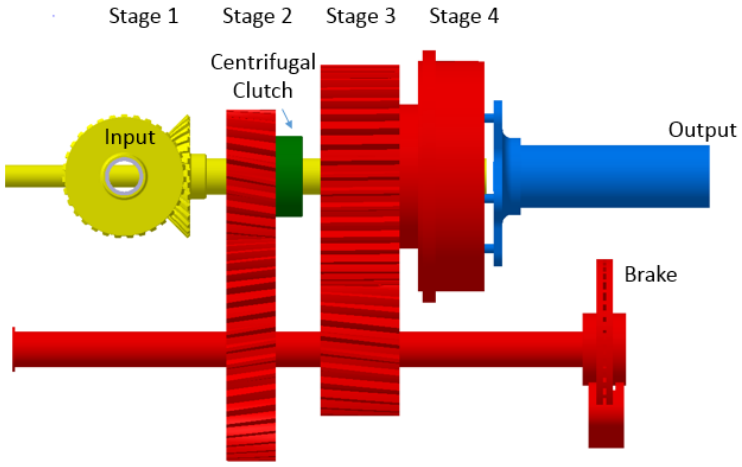

Figure 7.6: Differential dual-drive transmission.

The centrifugal clutch provides the system with a shifting mechanism that initiates power split and relative motion between the sun gear (input) and ring gear as shown in Fig. 7.7. With the centrifugal clutch disengaged from the input shaft, the intermediate gearset and ring gear are stationary providing a set reduction ratio for the planetary gearset. With the clutch engaged to the input shaft, a percentage of the power is diverted through the intermediate gearset which powers the ring gear as shown in Fig. 7.5. The intermediate gearset is geared to turn the ring gear at 1/3 of the speed of the input shaft to get the desired 52% speed reduction from the differential planetary.

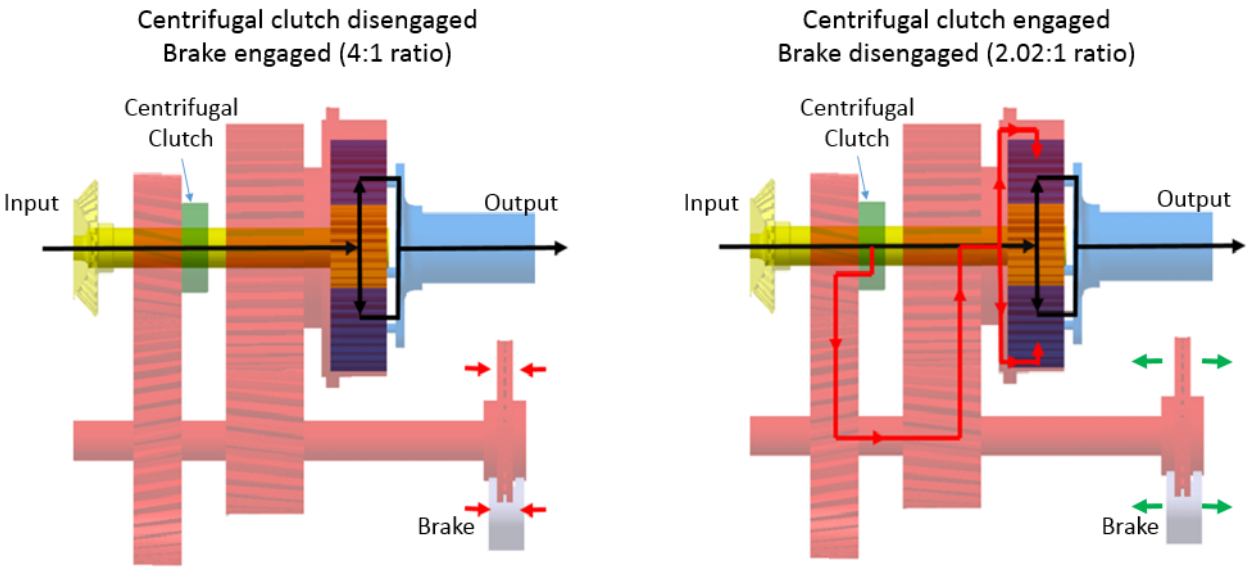

Figure 7.7: Power flow for high and low reduction modes.

The centrifugal clutch shown in Fig. 7.8 is actuated by fluctuating the gearbox's input shaft speed coming from the engine. The nose gearbox has a set output of 6,000 rpm at an intermediate throttle position and an engine throttling range of 5,880–6,120 rpm ($\pm$2%) to control centrifugal clutch engagement. The inner race of the centrifugal clutch is

attached to the gearbox input shaft and the clutch outer race is attached to the intermediate gearset [22]. The centrifugal clutch is designed to have an engagement speed of 6,000 rpm with engagement occurring within the $\pm 2\%$ margin. Therefore, the engine is throttled down to 5,880 rpm to fully disengage the centrifugal clutch and have all power sent directly to the sun gear. Similarly, the engine is throttled up to 6,120 rpm to fully engage the centrifugal clutch to the input shaft and to initiate split-power between the sun and ring gears.

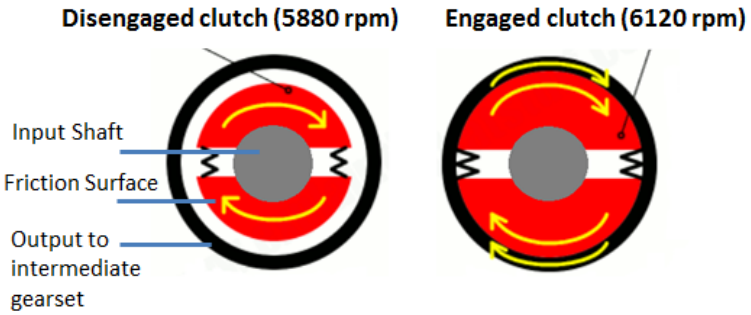

Figure 7.8: Centrifugal clutch engagement.

The brake enables the planetary ring of the differential planetary to be smoothly slowed down to a stop or to be gradually accelerated to a set speed during the engagement and disengagement action of the centrifugal clutch. The brake is fully engaged and holds the ring gear stationary for the low-speed mode. For the high-speed mode, the brake is completely disengaged allowing the ring gear to rotate freely under power.

For the *Kestrel*, the low-output speed is utilized for V_{BR}, while the high-output speed is used in hover and V_{BE}. To get to cruise rpm, the *Kestrel* downshifts to low-output speed; for V_{BE} or for hover, the aircraft upshifts back to the high-output speed.

Transitioning from hover or maximum cruise velocity to best range airspeed requires a decrease in input speed and then application of the brake to slowly bring the ring gear to a stop. Transitioning from cruise to hover or maximum cruise airspeed requires a slow release of the brake and simultaneous increase in input speed to engage the centrifugal clutch, initiating split power flow as shown in Fig. 7.9. The centrifugal clutch does not instantaneously engage, but gradually gets up to input speed in a few seconds enabling the transition to be smooth while releasing the brake.

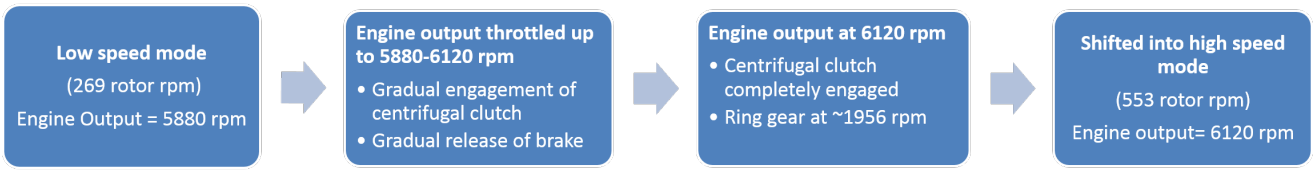

Figure 7.9: Dual speed transmission upshifting methodology.

The simultaneous engagement/disengagement of the centrifugal clutch and the release/application of the brake, respectively, must be carefully controlled to execute a smooth and continuous shift. Therefore, throttle adjustment with concurrent brake application will be a computer controlled operation.

Further development of this transmission concept must be done to realize the most effective rate of engine throttle variation to change speeds in regards to smoothness and wear of the clutch. In addition, the application of trapped roller, sprag, or other forms of clutches that have a critical speed initiated engagement mechanism could be tested for their effective engagement speed, smoothness, and wear properties.

7.3 Gearset Options

Gearset geometries were chosen for minimal weight and volume. For helicopter applications, the two general types of gearsets for reduction stages are split torque and planetary gearsets.

7.3.1 Split Torque Gearset

Split torque gearset configurations divide torque into multiple pinions opposed to having a single pinion gear mesh as shown in Fig. 7.10. Therefore, split torque configurations provide a simple system that can handle more torque than a standard gear and pinion assembly. They also provide lower energy loss, reduced weight, and increased safety and reliability by having separate drive paths. With the torque on the pinion usually being the limiting factor for size and gear strength, having multiple pinions divides the torque load and reduces the force on each pinion. Therefore, a split torque gearset enables a reduced pinion size, or an increase in overall stage ratio.

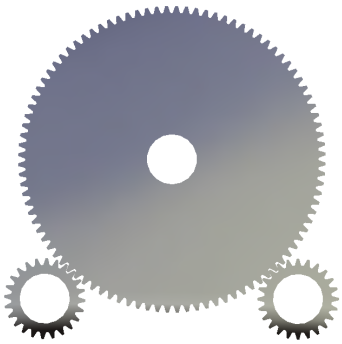

Figure 7.10: 4:1 gear ratio split torque gearset.

7.3.2 Planetary Gearset

Planetary gearsets are a subset of split torque systems that provide a compact and low weight design with a favorable torque capacity per a given volume as shown in Fig. 7.11. The input and output of a planetary gearset are collinear providing a low profile gearset that does not alter the torque axis. Therefore, planetary gearsets provide a clean and linear design that is strong because of its relative symmetry and concentricity, and easy to implement in tight spaces. Bearing forces are applied evenly with all radial forces reacted as a hoop stress in the ring gear. The size of the gears are reduced by increasing the number of planets in the gearset. Torque is able to be split between the planet gears to reduce transmitted loads. For a planetary gearset with a non-rotating ring gear, the ring gear can also serve as the outer casing.

A parametric study was done to determine the lowest weight and volume gear ratio for a planetary gearset in this transmission application. It was found that a 4:1 planetary is optimal for both weight and space. This ratio has the unique attribute of having the sun and planet gears equal in diameter. The same trend was observed regardless of position and application conditions of the planetary gearset within the transmission as shown in Fig. 7.12. Therefore,

Figure 7.11: Five planet, 4:1 gear ratio planetary gearset.

a 4:1 ratio was used for the planetaries used in the differential dual-drive gearset and the nacelle gearbox.

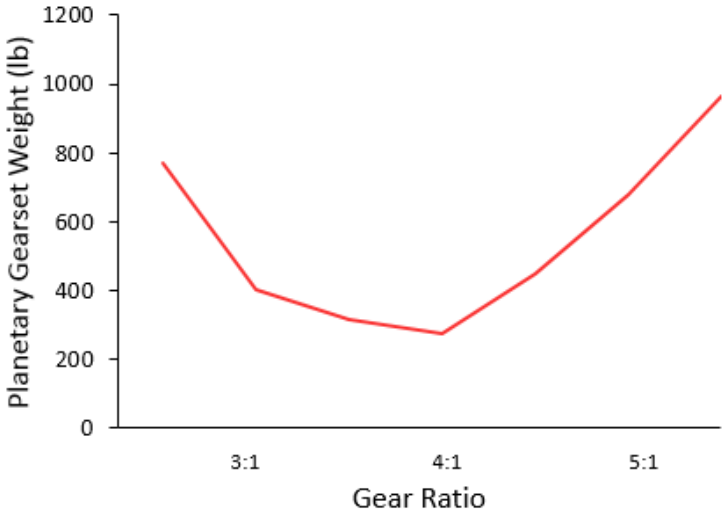

Figure 7.12: Nacelle gearbox weight versus planetary gear ratio.

Weight and volume savings were also realized by having a single main gearbox instead of a separate main gearbox for each engine. By having a single main gearbox, the total power rating could be reduced by 376 shp. With the overall reduction of 376 shp running through this section, weight savings of about 120 lb were achieved. The volume of the main gearbox section was also reduced by 40% by consolidating two possible gearboxes into one.

7.3.3 Gear Standards

Gear sizes were determined by the AGMA 2001-C 95 and AGMA 2003-B97 standards, with special applications to helicopter transmissions from AGMA 911-A94 and AGMA 908-B89. All gears were formulated to resist the three main failure modes of gears: compressive (Hertzian) stress, bending stress/fatigue, scuffing/scoring resistance. Dimensions of the gears, including pitch diameter and face width were formulated off the strength of gear geometries to resist compressive (Hertzian) stresses [23]. Diametral pitch and the number of teeth on each gear were maximized

through the maximum allowable bending stress to enable the highest attainable contact ratios. Scoring resistance comes with the implementation of appropriate and suitable gearbox cooling. With sufficient cooling, the breakdown of the viscosity of the oil will not occur, preventing metal-to-metal contact of the gear teeth that results in scoring.

The gears are manufactured from high strength AISI 9310 case-hardened steel which has desirable contact stress, bending stress, hardness, and density characteristics. Simple, well-guided cylindrical roller bearings are used in the transmission because of their reliability and efficiency in most transmission applications.

7.4 Subsystems

Subsystems of the transmission were analyzed for best fit with the differential dual-speed gearbox as well for the *Kestrel* as a whole.

7.4.1 Casing

The gearbox casing is to be manufactured from aluminum. Although a magnesium casing would be appreciably lighter in weight, it is subject to corrosion. Aluminum is also stronger and has a lower coefficient of thermal expansion compared to magnesium. Lower expansion coefficients reduce stresses and help maintain joint alignment through temperature cycles. Thermal conductivity for aluminum is 30% greater than that of magnesium, increasing heat flux and convective cooling of the gearbox.

7.4.2 Lubrication and Cooling

The lubrication system has the dual role of providing the gears a cushion of lubrication and removing excess heat. Dependability of the lubrication system is critical to the health, reliability, and longevity of the gearbox. The tailsitter configuration presents the unique challenge of consistent operation required in both horizontal and vertical orientations. Because of the required functionality through different flight modes, a wet sump layout with oil splash on the gears is not practical. A dry sump configuration will be utilized that can withstand not only multiple orientations, but also high G-loading while supplying continuous oil flow to gears.

Therefore, the dry sump utilized provides consistent oil pressure with multiple scavenge line inlets placed strategically where oil will flow at respective transmission orientations. A natural gravitational flow path is provided for vertical and horizontal orientations with the use of ribs and webs to guide oil flow on the internal surfaces of the casing.

Close fitting shrouds around gears and return lines from cavities between bearings and shaft seals provide effective means of preventing oil entrapment and excessive churning in the gearbox. Careful consideration was taken in the design to prevent traps around rotating components that could create vortices and trap and suspend oil against the housing causing undesirable heat and oil buildup. A minimum clearance of 0.5 in was given around all gears to enable the free flow of oil around the gears [25]. Spray bars along the face of the gears provide lubrication and cooling. Lubrication is provided to the gears through in-mesh jets, while out-of-mesh oil jets provide cooling. Sufficient oil flow is important for cooling, but is controlled to prevent churning and excessive flow to gears and bearings that can cause heat generation.

Loss of lubrication to the gearbox is a common cause of transmission failure. For traditional dry sump setups, weak points including external oil pipes, fittings, oil coolers and filters can cause rapid oil loss. The entire dry sump system for the *Kestrel* will therefore be fully encased and internal to the gearbox casing reducing the chances of catastrophic oil loss due to the failure of any of the lubrication system components.

The gearbox has been designed at 3,000 hours between overhaul and to last 30 minutes after the loss of oil flow and lubrication. Cells and oil dams in the casing allow oil to pool up after the loss of oil flow in horizontal or vertical flight. Super-finished low roughness gear surfaces as well as gears with lower sliding velocity with maximized number of teeth reduces friction between gears. Layout and placement of the gearbox casing has also been maximized for

convective cooling. A chip detector is located in the oil system to help identify any internal damage and is connected to the Health and Usage Monitoring System (HUMS).

7.4.3 Shafting

Titanium forging is utilized for all driveshafts. Each shaft is segmented to allow for misalignment of connected drive-train elements from motion such as wing bending. Shaft lengths were determined to keep all shafts in the sub-critical range in high and low speed transmission modes. This eliminates the need to provide additional damping for the shafts to pass through their respective natural frequencies. Bending of the shafting system is allowed through couplings that connect shaft sections. Hangers utilize grease-packed bearings to support the shafts at all sections of the driveline. Shafts are also capped with splines at the ends to allow for expansion of the shafts in the axial direction. Constant velocity joints are utilized where the shafts need to change direction without the use of gearing.

7.4.4 Differential Dual-Drive: Shifting Clutch

The Differential Dual-Drive transmission requires a clutch for engagement and disengagement of the intermediate gearset that powers the ring gear. It is required that the clutch engages over a span of a few seconds (opposed to instantaneously) which allows for gradual application/release of power and braking force to enable smooth shifts. Also required is a centrifugal element that provides engagement/disengagement at a prescribed shaft speed. This device enables shifting of the transmission to be determined by the variation of engine input rpm between two speeds.

Clutches such as sprag, trapped roller, and centrifugal types were analyzed for these attributes. The centrifugal clutch was the only type of clutch found to provide both centrifugal and gradual engagement. The application of a centrifugal clutch does require attention in maintenance procedures for its wear characteristics, but its ability to provide desirable shifting attributes is worth the wear monitoring required by this clutch.

7.4.5 Differential Dual-Drive: Intermediate Gearset Brake

A brake system that has characteristics of low wear and reliability is desirable for application in the Differential Dual-Drive system. The brake is required to maintain constant applied force to keep the ring gear static in low-speed mode. It must also provide smooth and predictable release or application of braking force to the ring gear during shifting. Application of braking force during shifting will be the main source of heat and wear and brake components. Friction type brakes such as disk and drum brakes were considered because of their proven abilities in applying braking force. Disk brakes were more desirable in their ability to dissipate heat and provide high braking forces in high performance applications.

Carbon ceramic disk brakes are utilized because of their superior durability and consistency in providing braking force. The ability of carbon ceramic brakes to shed heat and their low thermal expansion properties provide reliable and consistent braking ability. Therefore, multiple gear changes over a short period of time requiring braking for ring gear control will not affect the brakes performance.

7.5 Transmission Summary

Aerodynamic considerations established a need for a two-speed gearbox. The Differential Dual-Drive two-speed gearbox concept has the ability to change proprotor speed smoothly without drivetrain shock or disruption of power. Because of the use of existing technologies, the team is confident that this two-speed drivetrain will be a successful design.

Drivetrain

3 4 Nacelle Gearbox

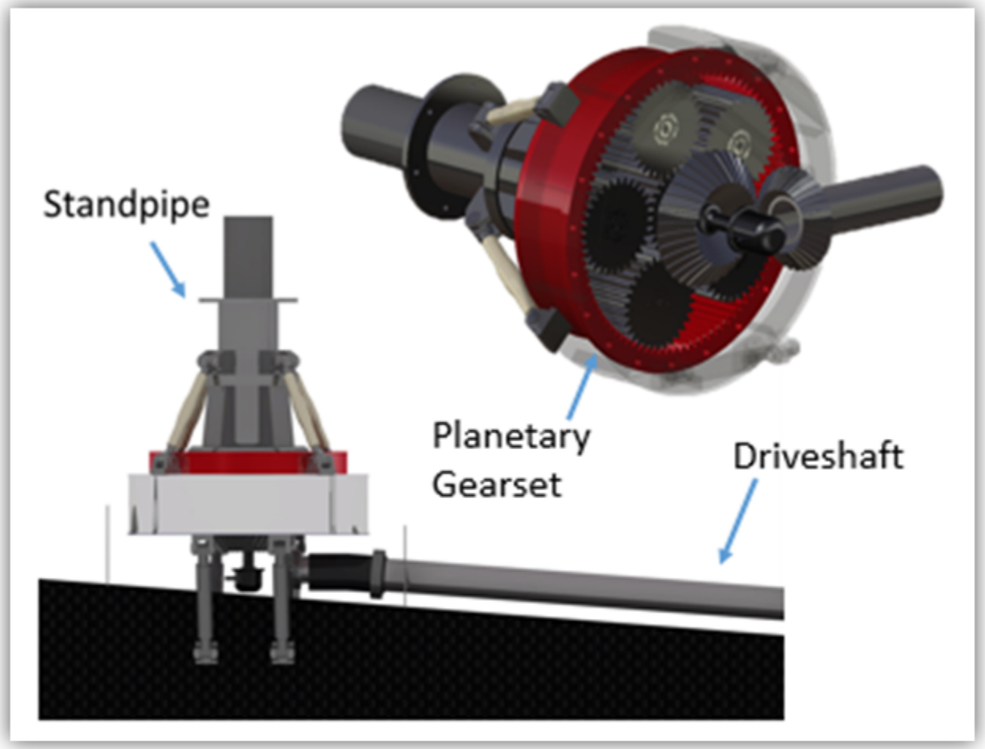

1 Variable Speed Gearbox

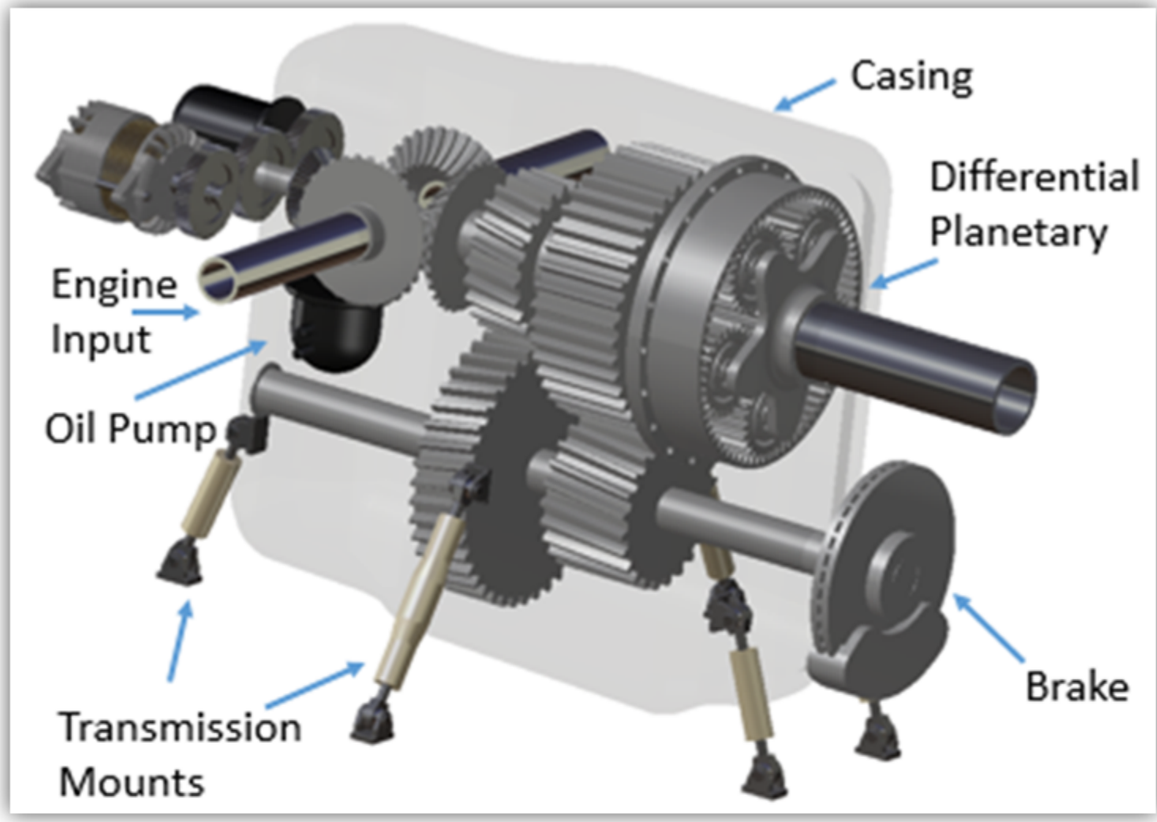

2 Bevel Gearbox

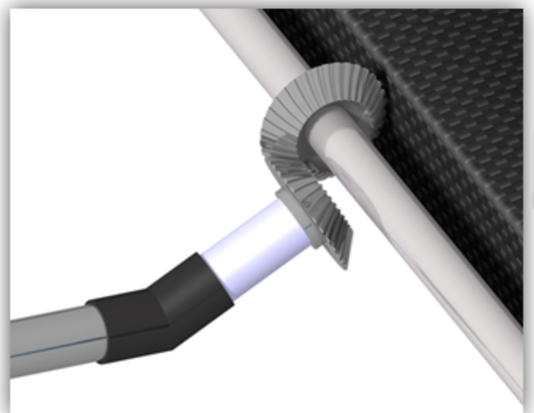

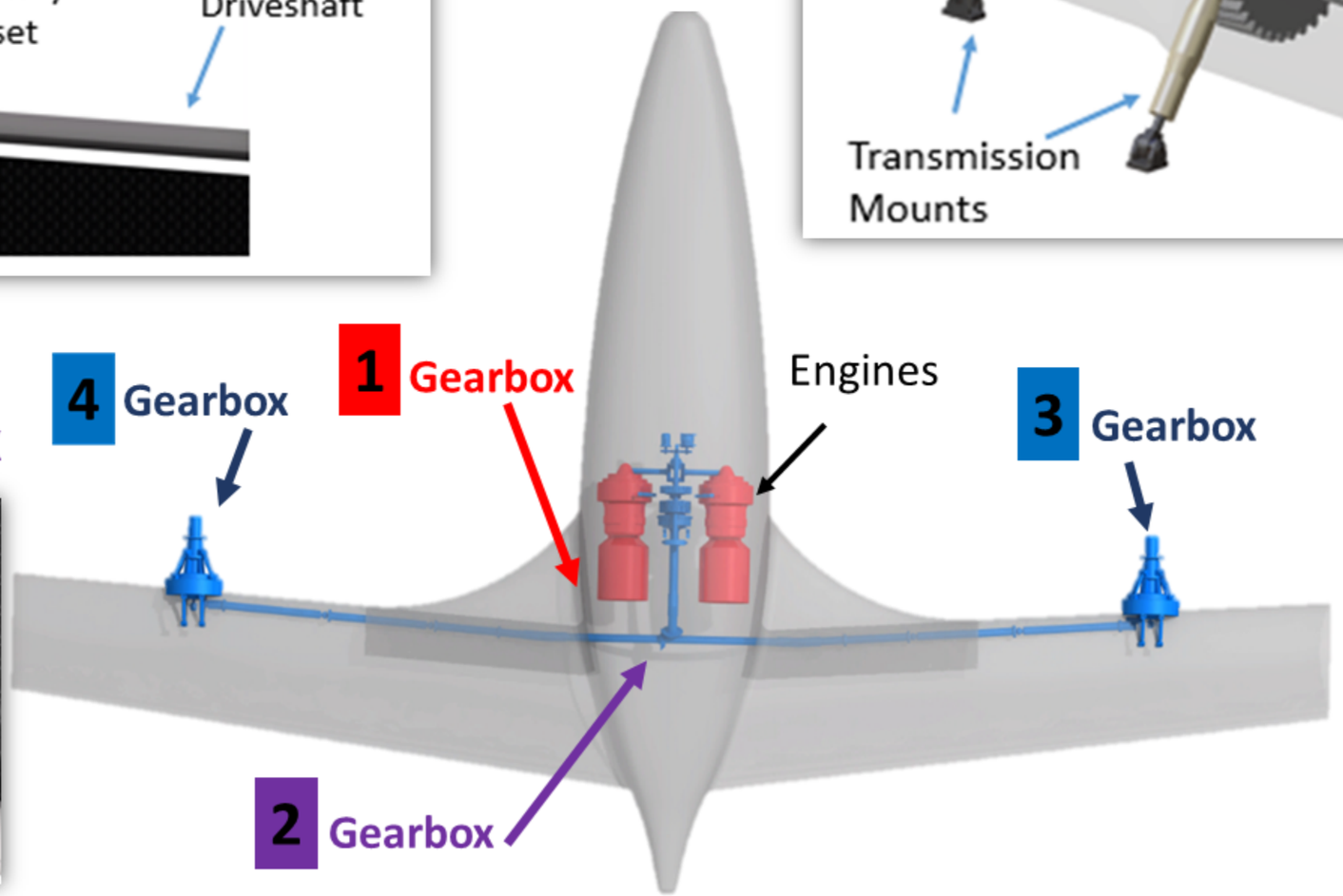

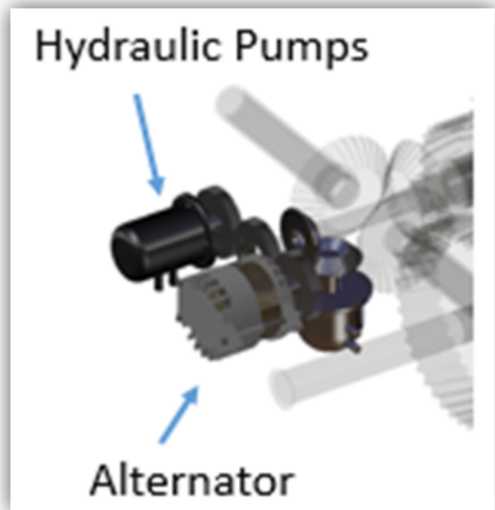

8 Airframe

The airframe of the *Kestrel* is designed to be robust and have an aerodynamically streamlined body that enables efficient high speed operation. The aircraft structure is a semi-monocoque design comprised of a load-bearing composite skin and aluminum frame. A modular internal layout was developed to establish positioning of components and provide flexibility for future layout modifications to adapt to variable mission capabilities. Transmission and engine positioning was also governed by structural demands to have a low drag impedance on the aircraft. Additional structural design considerations include insertion of a controlled and accessible cargo area, retractable landing gear, and implementation of unmanned and optional manned piloting options. The *Kestrel* can be divided into four distinct sections. The front of the aircraft encases avionics, cargo, and the canard, while the back locates the fuel, drivetrain, wing, and four landing gears. All of the aircraft's components were positioned to achieve short load paths and a c.g. location in close proximity to the front of the torque box.

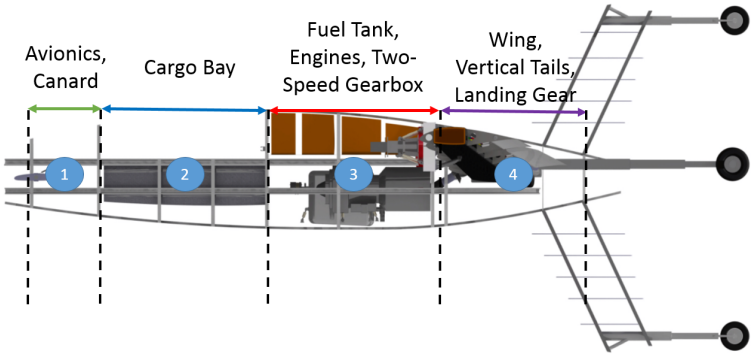

Figure 8.1: The four sections of the fuselage that the main bulkheads support

8.1 Load Paths

With its unique tailsitter geometry, the *Kestrel* structure must handle distinctly different load paths in horizontal and vertical orientations. While in flight, the thrust load from the rotors is transmitted to the wing torque box that is mounted centrally in the fuselage. In vertical flight, the load on the torque box is primarily in the direction of thrust. Rotor thrust is carried by thrust bearings in the rotor standpipe. From the standpipe, the load is transmitted by means of support rods that diffuse the load around the gearbox and on to two ribs and the torque box. In horizontal flight, the predominant load is from the lift produced by the wings and canard. All loads on the torque box are disseminated at the fuselage via the wing box that is strategically placed between two bulkheads.

When on the ground, the *Kestrel* exhibits very different load paths. The load path is distributed evenly between the four landing gear that are positioned on each wing and on the tips of the vertical tails. For the two landing gear mounted to the wing, the load transferred to the torque box produces a force vector in the same direction as the thrust vector. This unified load direction in conjunction with a shorter moment arm to the base of the wing mean that no additional structural strength was required to support the landing gear load. The landing gear in the vertical tails required additional strength of the vertical tail structure. The load is transferred to two angled vertical spars that transfer loads directly to longitudinal spars in the fuselage. Overall, there is a smooth and direct load path from each landing gear to the fuselage where the force is then dispersed.

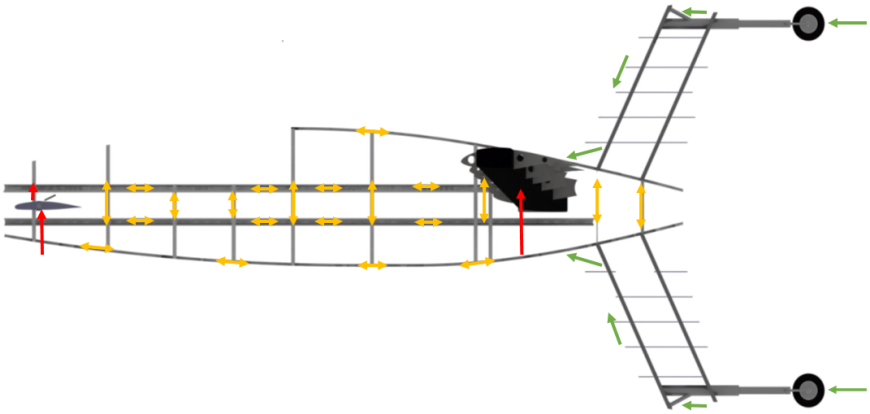

Figure 8.2: Load path diagram. Green arrows are ground forces. Red arrows are lift forces. Yellow arrows are internal structure forces.

8.2 Fuselage Structure

The *Kestrel* utilizes strategically placed aluminum stringers, longitudinal beams, and bulkheads to carry loads throughout the fuselage. A static load analysis helped in determining the placement of the bulkheads. Primary bulkheads are placed to bookend each of the four main sections as shown in Fig. 8.1.

All of the bulkheads utilize a simple I-beam profile to support radial loads. The first set of primary bulkheads are on each end of the canard to support the load on the canard as well as the avionics positioned in the vicinity. The second set of primary bulkheads are on each end of the second cargo area. Additional longitudinal and vertical support is provided around the opening of the cargo bay door. The third section of the fuselage has bulkheads on each side to support the weight of the engine, gearboxes, and fuel tanks. The last two primary bulkheads bookend the wing box to support all loads transmitted to the fuselage from the wings.

All of the longitudinal beams utilize a top hat beam profile for its inherent bending strength along both longitudinal and vertical axes. This ensures the beams resist bending in horizontal flight, and also resist buckling while supporting vertical loads in hover. Primary longitudinal beams are placed along the fuselage and are in line with the vertical tails and wing. This enables the loads from the landing gear to run smoothly into the fuselage where they will be dissipated. Similarly, some of the lift load on the wing is smoothly transferred from the torque box to the bulkheads and longitudinal beams.

8.3 Drivetrain

The engines and two of the three gearboxes are placed in the fuselage directly in front of the wing box. The intake of the engines is positioned on the bottom of the fuselage to ensure a steady source of air flow to the engine through transitions from vertical and horizontal flight. With up to 79% of speed reduction occurring in the fuselage gearboxes, the weight of the wing driveshafts is increased by 88 lbs when compared to having 0% of the speed reduction in the fuselage. This increase in weight is more than compensated for with the many advantages it provides. With most of the weight of the drivetrain in the fuselage, the wing strength is reduced with less weight on the wing. The central location of the weight in the fuselage also reduces the roll moment aiding in the agility and stability of the aircraft. The low drag profile was achieved partially by having engine and gearbox in the fuselage reducing the front view cross-sectional area of the nacelle.

8.4 Cargo Bay

The internal payload bay, as seen in Fig. 8.3, provides operational flexibility to incorporate a diverse range of payload shapes and sizes. The cargo bay is about 45 ft^3 in size. With adjustable modular partitioning, the cargo bay can be arranged to adapt towards properly supporting the load that is being carried. An alignment and retention system that utilizes L-track rails on every surface within the cargo bay in conjunction with tie-down straps ensures that payload is supported on all sides and will not shift during transitions between vertical and horizontal flight. The payload bay can also accommodate a variety of components for operational flexibility such as fuel, sensors, and communications modules to meet a diverse range of mission profiles.

Figure 8.3: Cargo bay.

The payload location aids in achieving a desirable c.g. position for the aircraft no matter what the weight of the payload is. Despite the seemingly high positioned payload bay, simple structural arrangements are made to make access easy. A forklift with a simple and safe loading surface is utilized to place payload to the level of the bay. A single clamshell style door is positioned on the top of the fuselage. This provides a wide area of opening to easily access the bay for cargo. Having the doors at the top of the fuselage also ensures that the payload will not rest on the cargo doors. The doors have the capability to open automatically ensuring ease of access for grounds crew members at initial approach. For air dropping payload, the *Kestrel* can simply invert its flight orientation to have the cargo bay doors open downward.

8.5 Landing Gear

The *Kestrel* has a total of four oleo-pneumatic landing gears. Two of the landing gears are mounted to the wing while the other two are mounted at the tips of the vertical tail. The landing gears mounted to each wing are fully retractable into the wing and fuselage to minimize drag in forward flight. The vertical tail landing gears are non-retractable, but are faired to maintain a smooth aerodynamic profile. There is insufficient volume for retraction of the vertical tip landing gear or aft fuselage. Wheeled retractable and fared landing gears are used because of their reduced flat plate drag area when compared to a fixed skid design. Wheeled landing gears also provide easier ground maneuverability than skids. The fore and aft vertical tail landing gear are castered in order to be steerable. Steering control is implemented using a push pull system which also includes a shimmy damper. Maximum turning angle of each wheel is 60° and disc brakes are installed in both the front and aft wheels for ground parking.

The four landing gear configuration was selected for complete ground stability. This configuration provides ground

stability through the range of the c.g. location to ensure that the vehicle will not tip over. The *Kestrel* has a wheel track and wheel base of 12 ft with all four landing gear evenly spaced from one another. The minimum roll over angle of 30° is satisfied between the four landing gears [24]. The wing mounted landing gears also have a clearance angle of 30° for the wing in order to avoid hitting the wing on canted surfaces or on angled approaches. The landing gear provides a minimum of 18 in of clearance between the ground and the tips of the vertical tails.

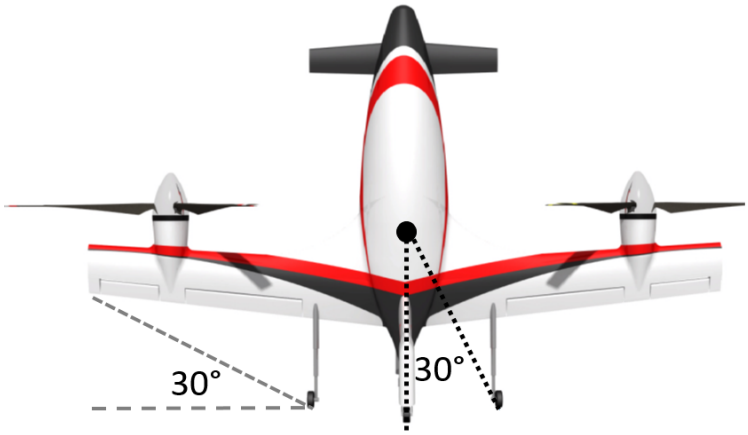

Figure 8.4: Roll over and wing clearance angles

The landing gears were sized for a gross weight of up to 12,500 lb. A dynamic load factor of 2.2, rotor lift factor of 2/3, and safety factor of 1.5 were also accounted for [24]. The landing gears were sized for multiple landing conditions, which included landing on one landing gear first, drift landing with roll velocity of 0.25 rad/s roll at 75% limit sinking velocity, landing with roll displacement of 5° roll attitude and 75% limit sinking velocity, landing on a 15° slope and four-point purely vertical landing [24]. An onboard LIDAR and camera system evaluates the ground terrain to control the aircraft to a smooth landing.

8.5.1 Tire Sizing

Three part tires were chosen as most operations of the *Kestrel* technology demonstrator vehicle will be from prepared runways. The inflation pressure of three part tires is higher and allows for a smaller overall size. All four landing gears were installed with identical tires, the Goodyear three-part tire, 13x5.0-4. The tire has 14 plies, a maximum bottoming load of 9,300 lb and rated inflation pressure of 143 psi.

8.5.2 Oleo-Pneumatic Strut Sizing

Single cantilever oleo-pneumatic shock absorbers were used for all four landing gears. Each landing gear strut was designed [25] for a drop velocity of 10 ft/s and drop height of 1.6 ft. Assuming a tire stroke of 3 in, tire and gear efficiency of 45% and 85% respectively, gear load factor of 4.0, the total stroke of the oleo-pneumatic strut was 10.6 in. The length of the cantilever strut was 3 ft with an external oleo housing diameter of 4 in and external piston diameter of 2.8 in. The 15° slope landing sized the wall thickness of the oleo housing and piston as 0.206 in and 0.184 in respectively. The oleo struts were also checked for buckling and crippling failures. An internal pressure of 1,800 psi was chosen for the oleo to allow for servicing with standard compressors.

8.5.3 Retraction Mechanism

The retraction mechanism for the wing mounted landing gear of the *Kestrel* rotates 90° between stowed and retracted landing gear positions just as most other aircraft. With the tailsitter configuration, the *Kestrel* rotates the landing gear into the vertical plane of the wing requiring clearance from the trailing edge of the wing and control surfaces. Additionally, with a low profile wing design and large torque box, room for the landing gear retraction mechanism behind the torque box is constrained to a 15 by 5 in cross section to remain within the skin of the wing.

The operation of the landing gear for the *Kestrel* acts as a very simple hinge mechanism as shown in Fig. 8.5. A stationary mounted cylinder acts as an axle to serve as an axis of rotation for the landing gear strut. With the retraction mechanism angled at about 5.5° to match the forward sweep of the wing, the landing gear strut is attached to a cylinder that is concentric to the axle at an angle of 42.25° (Fig. 8.5). This ensures that the landing gear deploys to an orientation that is perpendicular to the ground despite the forward sweep of the wing.

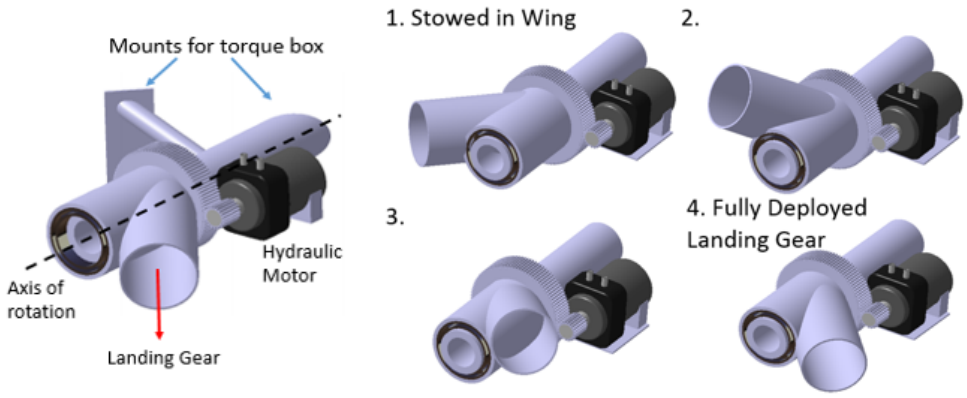

Figure 8.5: Landing gear rotation mechanism (180° rotation)

The mounted axle of the landing gear strut must be firmly mounted to the trailing edge end of the torque box. With a landing gear that is 8 ft 11 in long, lateral forces on the wheel can induce a large moment at the attachment point to the wing. This high torque load is controlled by a sturdy base mounted to the retraction mechanism. A triangular beam configuration from the axle is fastened to plates at the torque box that are rooted within the fiber weave of the torque box. Therefore, no holes are drilled sacrificing the integrity of the torque box.

The rotating arm motion is controlled by a hydraulic motor through a simple spur 6:1 ratio gearset. With a hydraulic motor speed of 45 rpm, the landing gear is rotated to either position in four seconds. With skin panels opening in two seconds, the landing gear can be fully retracted or stowed in about six seconds. The hydraulic motor has the ability to restrict any motion of the landing gear when desired in the retracted or stowed orientation. A simple solenoid clamp is utilized to clamp the landing gear strut in the stowed orientation, limiting any movement and vibration and offloading the motor and gears. The solenoid is spring loaded to release the strut in the event of a cutoff of power.

Although the required length of the landing gear of the Kestrel is 8 ft 11 in, there is only a length of 6 ft 10 in between the point of rotation and the center of the fuselage. Therefore, the originally sized strut is mounted to a hydraulically telescoping cylinder. In the stowed position, the strut of the landing gear telescopes into the outer cylinder. While the assembly is rotating to the retracted position, the strut is also telescoped out from the outer cylinder giving the landing gear its full length.

When the landing gear is retracted, portions of the skin of the wing must be moved or opened to provide clearance for retraction. The skin of the wing is hinged to open with a dual action hydraulic actuator in three locations for the

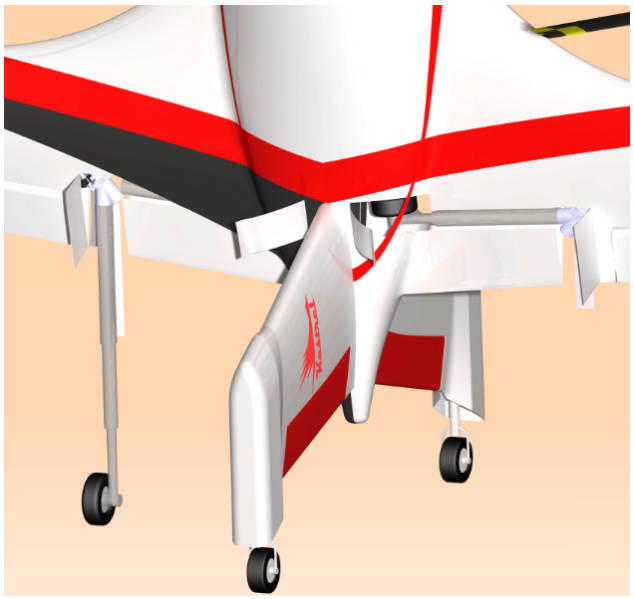

Figure 8.6: Retracted (left) and stowed (right) landing gear.

landing gear on each wing. The skin of the wing is opened at the top and bottom of the airfoil at the point of rotation to enable the landing gear to extend directly downwards and perpendicular to the ground. The skin also opens at the fuselage with clearance for the wheel. The middle section of the skin that needs to be removed is directly attached to the strut. Therefore additional actuator or hinging is not needed. All hinged doors for the landing gear were designed to open perpendicular to the rotor plane reducing down force on the doors in hover.

8.6 Material Selection

The *Kestrel* demands a sleek and strong airframe that is lightweight for maximum efficiency and speed. The aircraft is composed of a carbon fiber skin with aluminum internal structural elements. Carbon fiber-epoxy skin provides a smooth outer surface that is lightweight and has a low skin friction coefficient. Large continuous carbon fiber panels provide large smooth surfaces while limiting drag interferences at panel joints such as rivets. Continuous panels also contribute to airframe stiffness and crashworthiness while reducing the number of fasteners and support structures needed to attach the skin to the primary structure. The carbon fiber skin of the fuselage and wings consist of layers of $\pm 45^{\circ}$ and $0/90^{\circ}$ carbon fiber laminae. The skin panels are constructed using out of autoclave (OOA) pre-pregs. Traditional composite manufacturing techniques require expensive tooling. The use of OOA manufacturing requires the use of less costly tooling, savings that are critical for limited production aircraft. OOA manufacturing allows for larger panels that would otherwise be limited by autoclave size restrictions. Caution has to be taken with OOA manufacturing for the potential of air bubbles in the composite.
Aluminum used for the main structural elements provides high reliability and low manufacturing cost. Aluminum is also simple to fabricate under traditional manufacturing techniques. Aluminum-Lithium alloy 2099 is utilized for the internal structural elements [26]. This aluminum alloy is used for its low density and high stiffness as well as for its resistance to corrosion and fatigue when compared to other aluminum alloys.

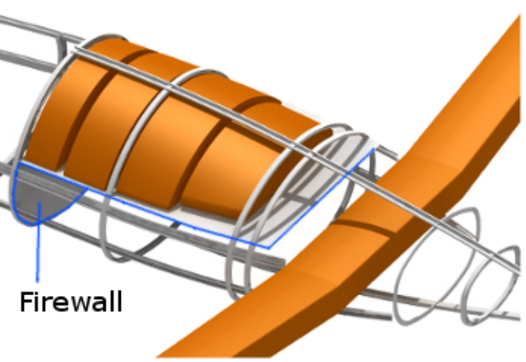

Compartmentalized Self-sealing Fuel Tanks

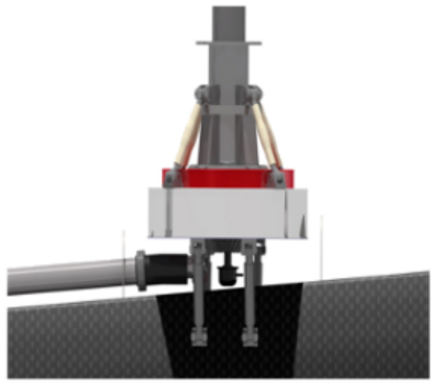

Nacelle Gearbox Mounted to Torque Box

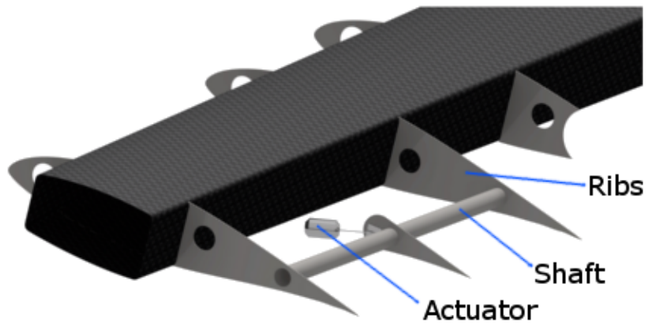

Aileron Structure

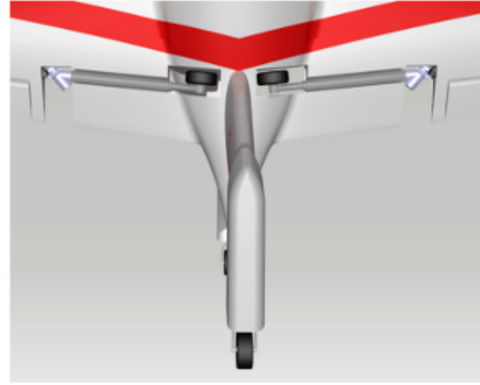

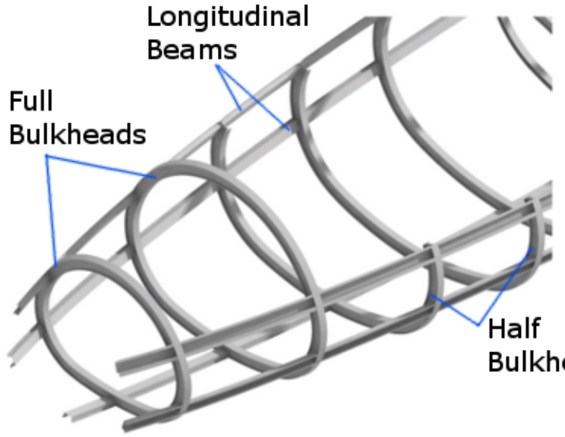

Fuselage Structure

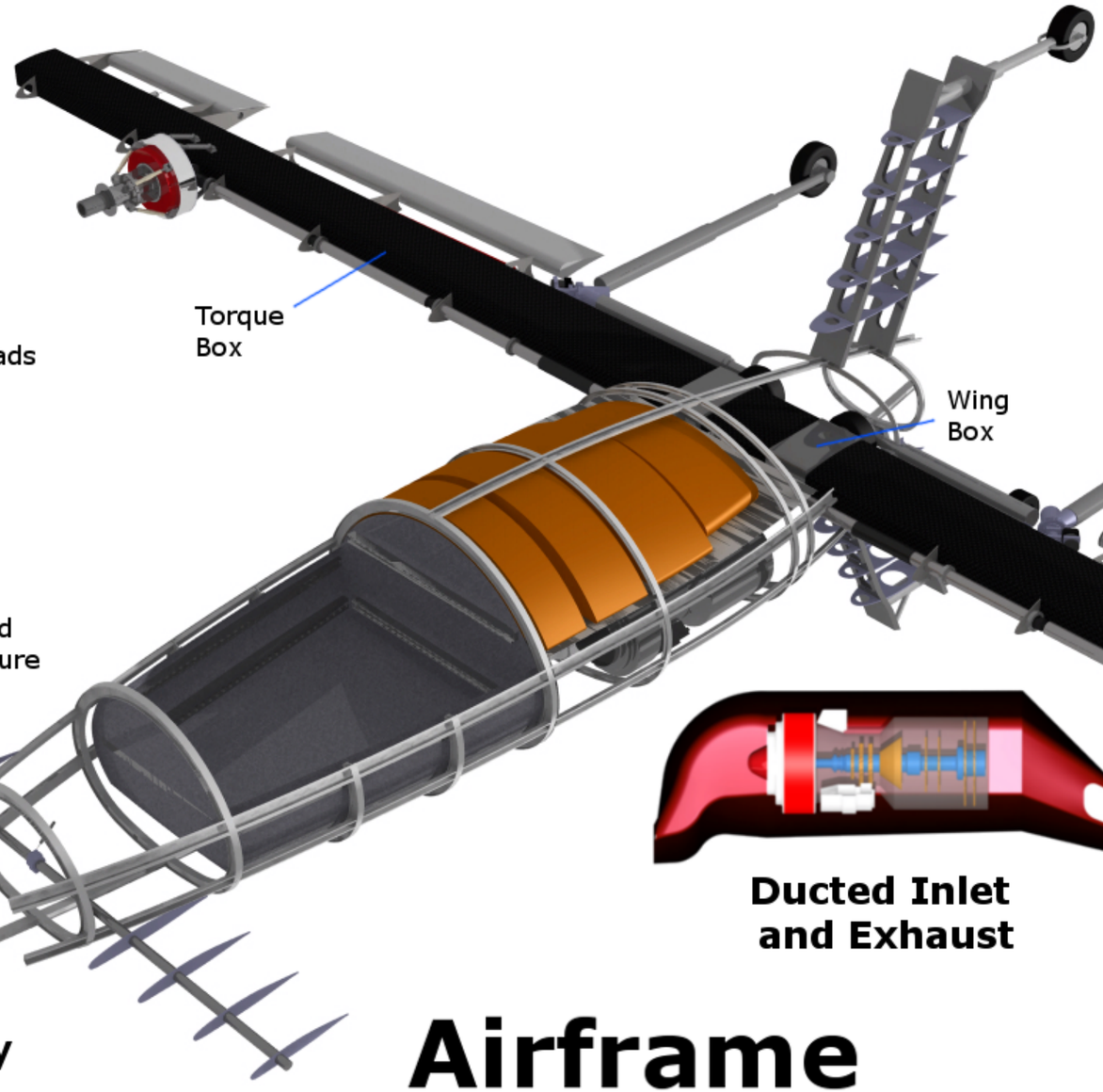

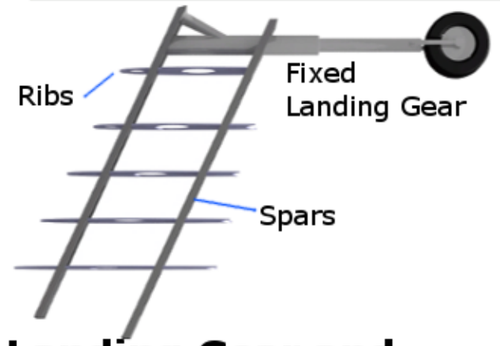

Landing Gear and Empennage Structure

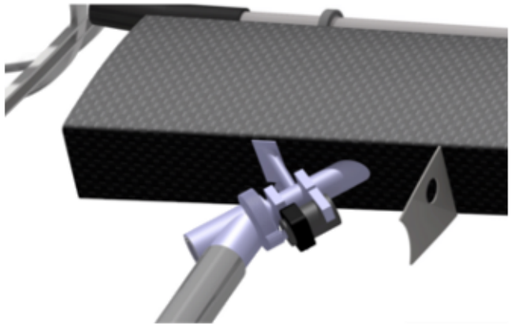

Landing Gear Retraction Mechanism Mounted to Torque Box

Ducted Inlet and Exhaust

Modular Cargo Bay

Airframe

9 Weight Analysis

The weight breakdown of the *Kestrel* is shown in Table 9.1. The weights were estimated using the Tischenko, NDARC, and other weight approximations, as described in Chapter 2.

Table 9.1: *Kestrel* weight estimates.

	Component description	Weight (lb)	% Gross Takeoff Weight	x_{cg} (ft)	z_{cg} (ft)
1	Wing group	826.2	7.6 %	21.0	2.00
2	Rotor group	619.7	5.7 %	19.50	2.00
3	Fuselage group	1,181.0	10.9 %	18.00	0.80
4	Landing gear group	361.2	3.3 %	26.00	0.00
5	Engine group	1,036.2	9.5 %	17.00	-1.00
6	Fuel system group	279.8	2.6 %	16.00	1.00
7	Drive system group	1,007.8	9.3 %	20.00	-0.50
8	Flight control group	260.6	2.4 %	23.00	0.00
9	Hydraulic group	136.4	1.3 %	24.0	2.00
10	Oil system group	83.2	0.7 %	17.00	-2.00
11	Electrical group	311.6	2.9 %	15.00	1.00
12	Avionics group	164.0	1.5 %	5.00	0.00
	Empty weight	**6,267.7**	**57.6 %**	**18.8**	**0.15**
	Payload	1,356.7	12.5 %	10.0	1.00
	Fuel	3,249.3	29.9 %	7.85	3.30
	Gross weight	**10,873.7**		**16.6**	**0.37**

A c.g. analysis was conducted to assess the c.g. travel for all possible payload and fuel configurations. As fuel is burned during flight, the c.g. of the aircraft will shift rearward as the fuel is burned from the forward-most fuel tanks first. Longitudinal stability is maintained by ensuring that the c.g. will not move outside of the boundaries determined by the restoring moment of the canard and the aerodynamic center of pressure. These boundaries are represented by the blue area in Fig. 9.1 which shows the c.g. locations of the total aircraft and its subsystems. The subsystem components were placed to ensure that the c.g. does not cross these boundaries for all combinations of payload weight and fuel weight.

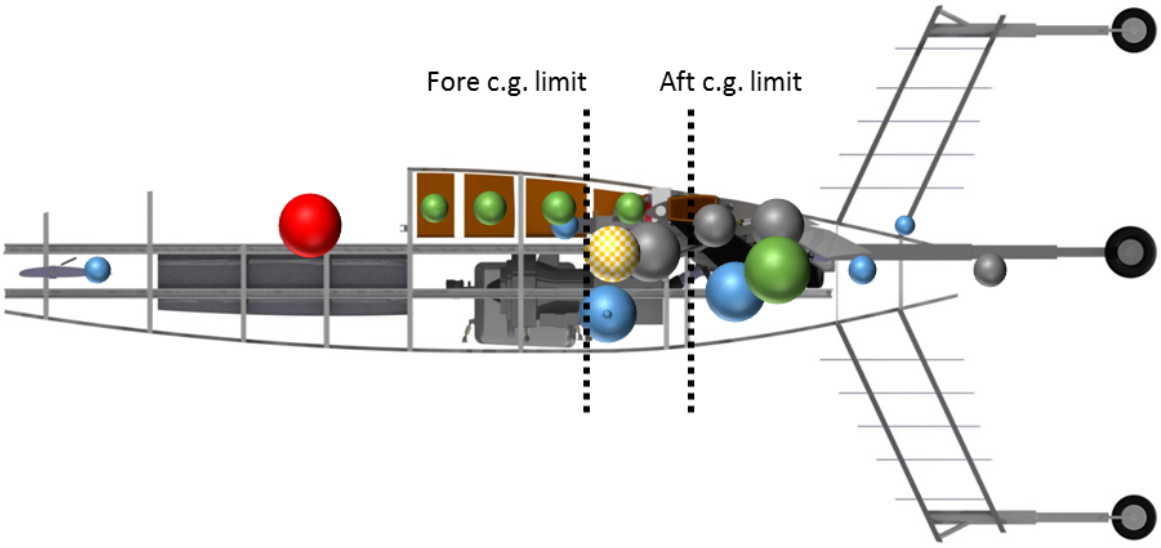

Figure 9.1: Center of gravity location and allowable travel.

10 Flight Control System

The Kestrel is an unmanned vehicle configured to fly autonomously or with a remote pilot from the Mobile Ground Control Station (MGCS). The vehicle is equipped with redundant subsystems, such as flight sensors and flight modules, as well as multiple redundant systems to ensure flight safety.

10.1 Autopilot Functionality

The Kestrel is equipped with three flight modules. Each flight module serves as a flight computer, Stability Augmentation System (SAS), and navigational autopilot. The flight computer and SAS are always active in flight while the autopilot can be selectively activated during the remotely piloted mode.

When the *Kestrel* is in helicopter mode, the autopilot is capable of VTOL, hover in ground effect (HIGE), hover out of ground effect (HOGE), lateral and forward flight, altitude changes, as well as transient maneuvers such as roll, pitch, and yaw. In airplane mode, the autopilot is capable of forward flight, altitude change, altitude and velocity hold, loiter, and waypoint navigation.

In remotely piloted mode, the pilot has full control of the vehicle at all times except during the fully automated VTOL and transition phase for enhanced safety. All three phases are initiated individually when the pilot triggers the corresponding switches. The transition is fully automated because of the complexity of the flight maneuvers. As for VTOL maneuvers, the vehicle should be autonomous for most flights except in landing conditions outside the normal landing parameters, such as a strong crosswind. The autopilot will execute Precision Approach To a Coupled Hover (PATCH) at a predetermined waypoint and altitude, to which the pilot can then guide the vehicle to a safe landing. For other flight conditions, the pilot can either choose to fly the vehicle or engage the autopilot.

10.2 Control Strategies

A tailsitter requires different control strategies for hover and forward flight. The control strategies for both hover and forward flight are shown in Fig. 10.1.

In hover, the *Kestrel* relies on the collective and cyclic controls from the proprotor instead of its aerodynamic surfaces. Differential collective generates a thrust differential between the port and starboard proprotors, rolling the vehicle. Longitudinal cyclic inputs on both proprotors pitch the aircraft fore and aft while differential longitudinal cyclic generates yaw moments. This type of control strategy for roll results in roll-yaw coupling because of unbalanced torque from increasing collective. For example, a positive roll input (increase left rotor collective and decrease right rotor), results in a counterclockwise yaw. Therefore, mixing between roll-yaw dynamics is incorporated into the controller such that all the degrees of freedom are decoupled.

In forward flight, the proprotor cyclic controls are locked and the aerodynamic surfaces provide control moments as on a conventional fixed-wing aircraft. The rudder is used to yaw the vehicle, variable incidence canard is used for pitch control, and differential aileron inputs are used for roll control. The collective setting on both proprotors are adjusted to provide the necessary propulsive thrust.

10.3 Proprotor Collective Pitch and Transmission Speed Scheduling

To obtain maximum power efficiency in hover and maximum cruise airspeed, the transmission operates at 555 rpm, whereas at the speed for best range, the transmission operates efficiently at 269 rpm. As shown in Fig.10.2, as the *Kestrel* transitions from hover to forward flight, the rotor rpm is decreased to 269 rpm and the proprotor collective angle increases linearly up to 58° at 230 kts. There is a sharp decline in the collective angle when approaching maximum cruise airspeed because the proprotor rpm is increased back to 555 rpm. From hover to maximum cruise airspeed, the total required range of collective angle is 50°. Both the change in proprotor collective pitch and transmission speed

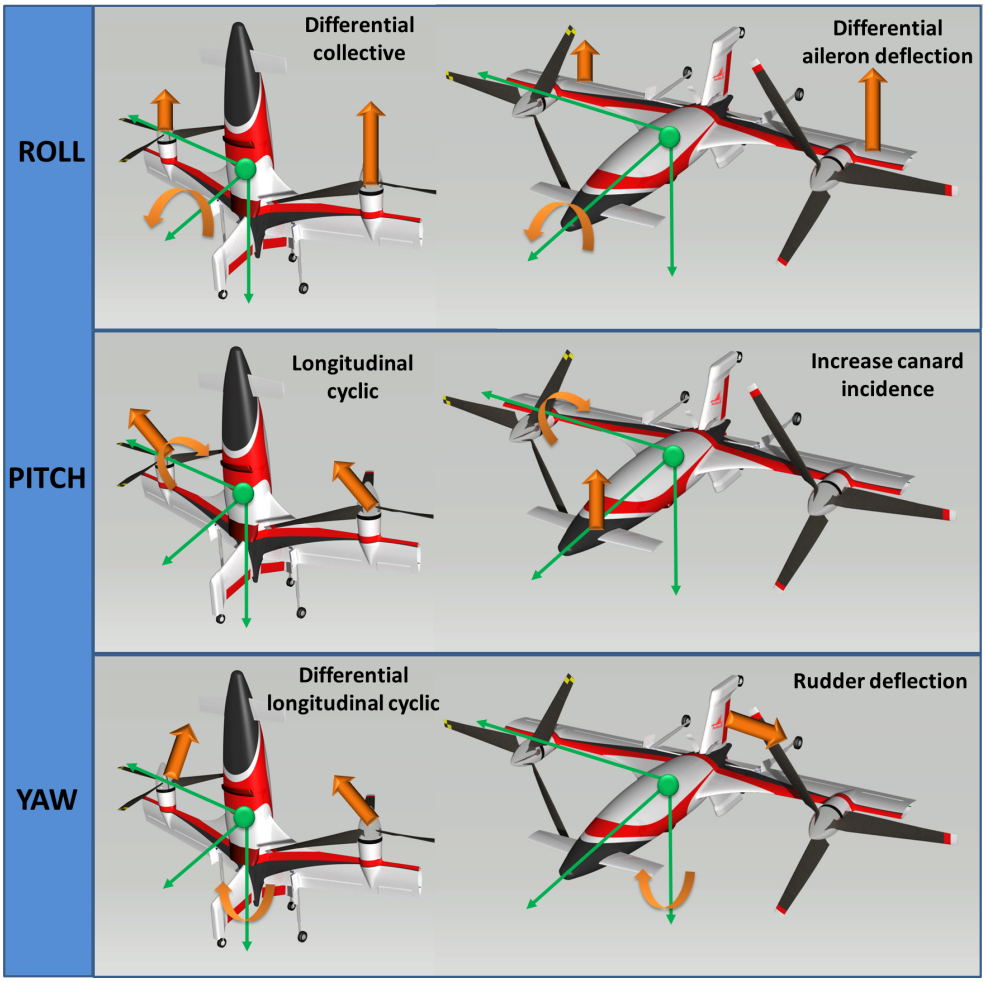

Figure 10.1: Flight control strategies in hover (left) and forward flight (right).

are regulated by the flight module for optimal power efficiency and to reduce pilot workload.

10.4 Control Laws

The flight module control laws are primarily robust controllers such as H_∞ dynamic observer, H_∞ mixed sensitivity tracking, and H_∞ loop shaping approach. One of the main reasons behind choosing robust controllers is the fact that the tailsitter concept is a relatively novel controls problem which brings with it vehicle model uncertainty. Likewise, the autonomous and remotely piloted flights must be robust towards disturbances and noise in order to guarantee flight performance. Hence, these robust controllers were selected based on fault tolerance, robust stability to additive uncertainties at high frequencies, and guaranteed controller stability in complex and new environments. Other advantages include attenuation of low frequency disturbances at plant output to ensure good tracking of low frequency remote pilot commands, attenuation of high frequency measurement noise, and minimization of control energy to avoid actuator saturation.

As shown in Fig.10.3, the H_∞ mixed sensitivity tracking controller is used to track the states of the vehicle in helicopter mode and stabilize the vehicle by minimizing the state errors. Fig.10.4 shows the H_∞ loop shaping controller employed as a multivariable lateral wing leveler in airplane mode to hold the aircraft wings level, while providing yaw

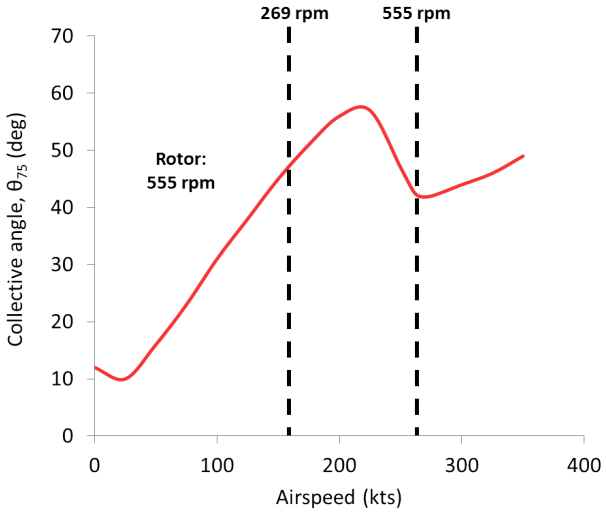

Figure 10.2: Optimal collective input for power efficiency throughout the flight envelope

damping by holding washed-out yaw rate r_w at zero [27]. The H_∞ dynamic observers are implemented to estimate the unmeasured states of the vehicle, such as sideslip angle, which are then fed back to the controllers.

10.5 Remotely Piloted Vehicle Controls

As shown in Fig. 10.5, the controls in helicopter mode consist of collective stick, sidestick, and foot pedals. The controls in airplane mode consist of throttle, sidestick, and foot pedals. To avoid Pilot Caused Control Reversal (PCCR), the collective stick and throttle are physically separated. Figure 10.5 shows the collective stick installed on the left armrest of the RPV pilot's seat, whereas the throttle is installed on the left side of the pilot's desk. This physically separate configuration layout allows the pilot to visually acknowledge whether the vehicle is in helicopter or airplane mode. Besides that, the vehicle mode will be clearly displayed at Line of Sight (LOS) as a constant reminder, with transition mode notification flashing constantly.

10.6 Transition Switch

In autonomous mode, the vehicle transitions from hover to forward flight when the vehicle achieves sufficient rate of climb. For transitioning from forward flight to hover, the vehicle has to slow to certain airspeed before the transition maneuver is carried out. In RPV mode, the pilot has to activate a transition switch located at the thumb position of the throttle and collective stick. The vehicle flight module then takes over the transition phase from the pilot until the vehicle has entirely changed flight mode. After the transition, the pilot assumes full control of the vehicle again upon contact with the throttle in airplane mode and collective stick in helicopter mode, which is implemented by tactile sensor feedback when the pilot grips the appropriate controller.

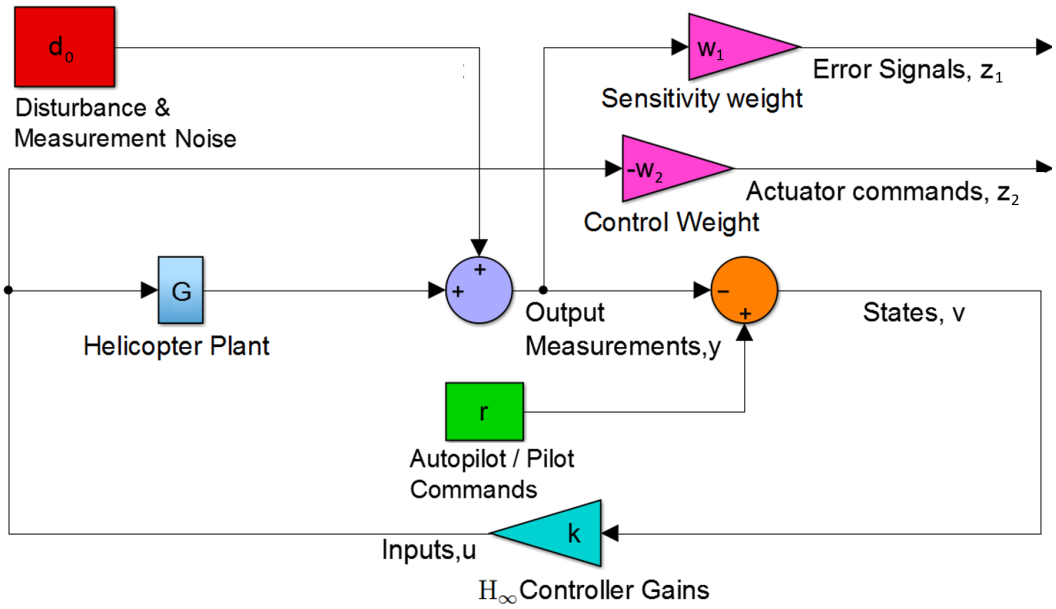

Figure 10.3: Hover tracking controller using H_∞ mixed synthesis in helicopter mode.

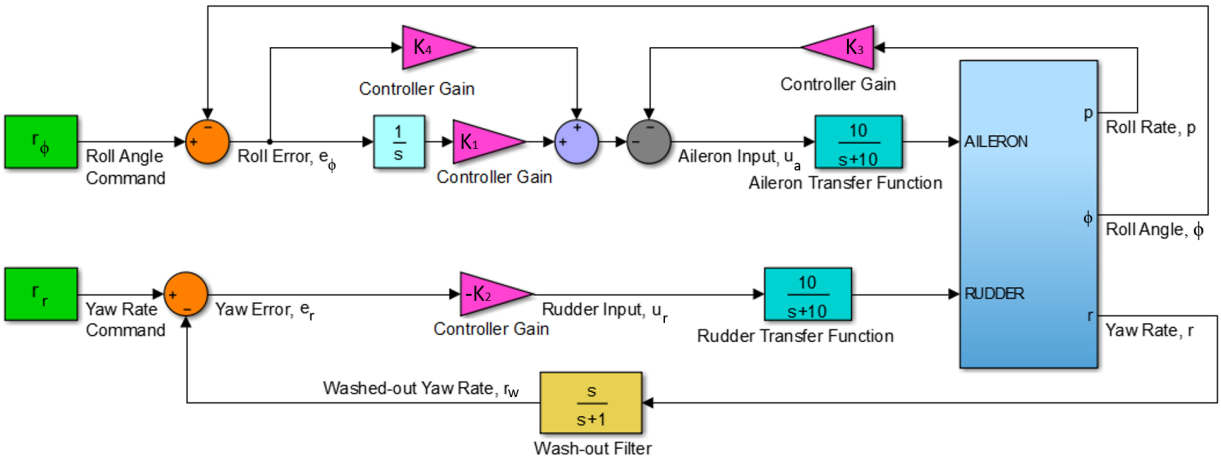

Figure 10.4: Lateral wing-leveler controller structure using H_∞ loop shaping approach in airplane mode.

10.7 Unmanned Aerial System (UAS) Architecture

The *Kestrel* is an unmanned aerial vehicle that is capable of autonomous flight, its encrypted communications and mission planning are facilitated by the MGCS. Together, these subsystems form the Unmanned Aerial System (UAS). As shown in Fig. 10.6, the *Kestrel* aircraft is configured the same for autonomous and remotely piloted mode from a systems standpoint. However, when a pilot is in the loop, the pilot control inputs need to be incorporated in the

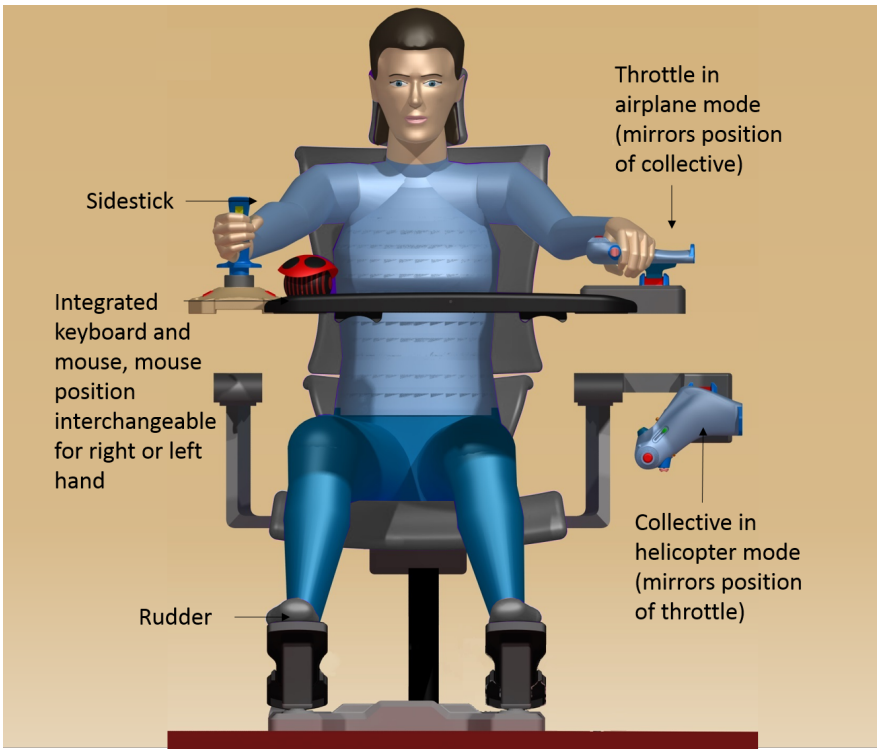

Figure 10.5: Remote pilot controls.

MGCS. The vehicle sensor data streams are first processed with sensor fusion and recursive Kalman filtering. The filtered attitude sensor data are then fused with the GPS data to estimate vehicle states. The vehicle states, along with the Full Authority Digital Engine Control (FADEC), control surface deflection, and optional HUMS data are then fed back to the flight module, which integrates these data to form a coherent output stream. The vehicle system architecture is shown in detailed in Fig.10.7. The communications module consists of antennas, receivers and transmitters, which streams the data to and from the MGCS. The MGCS interacts with the antenna and transceiver of the vehicle through both LOS and beyond-LOS communication. These data are then processed by the control module. Relevant flight data is displayed, and commands can be relayed via the Control Display Unit (CDU) consisting of a keyboard, mouse, curved screen display, and flat touchscreen display.

10.7.1 Failure Mode and Effects Analysis (FMEA)

In the unlikely event that the vehicle loses the datalink with the MGCS, it will hold its current flight mode while attempting to reinitiate communications with the MGCS, which include both LOS and beyond-LOS communications, as well as toggle between different communication channels and frequencies. The vehicle will attempt to hold its current flight mode upon loss of the datalink unless it is in a non-benign maneuver, such as a sharp bank or rapid descent, at which point, the vehicle will attempt to return to loiter in airplane mode or hover in VTOL mode. If it is unable to reestablish datalink within five minutes, the vehicle will return to base autonomously.

In the event of both MGCS and Global Positioning System (GPS) datalink loss, the *Kestrel* will fall back on its secondary and tertiary navigational equipment to navigate back to base. The base is preprogrammed as either the takeoff site or any landing site desired. In the event that it reestablishes datalink, it will prompt the MGCS regarding its current flight plan and allow the MGCS to reprogram it to continue its mission or return to base (RTB). If the *Kestrel* cannot reestablish datalink with the MGCS even when it is within close vicinity of base, it will loiter around a preprogrammed

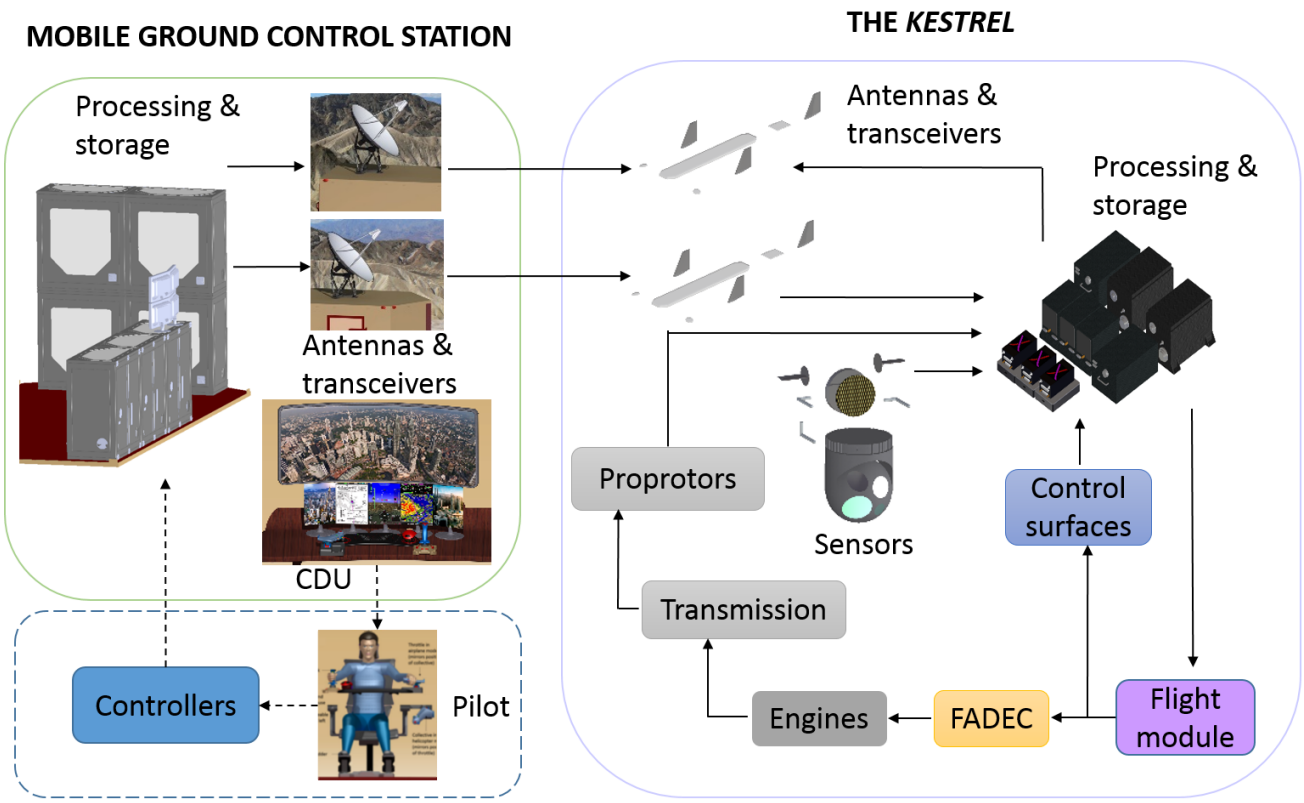

Figure 10.6: Unmanned Aerial System (UAS) architecture.

landing site which is close to base and sparsely populated. It will autonomously transition and finally land at this site when fuel reserves are low.

10.7.2 System Redundancy

Lightweight Microelectromechanical Systems (MEMS) sensors, such as accelerometers, gyroscope, magnetometers, and barometric pressure sensor are deployed as much as possible. With the usage of MEMS technology, triple redundancies are employed for most sensors, flight modules, and data storage units, with minimal weight penalties. Multi-system redundancy is incorporated to increase safety of flight, as shown in Fig.10.8. Even though only autonomous waypoint navigation and vertical landing are elaborated upon, system redundancies are prevalent throughout all flight maneuvers.

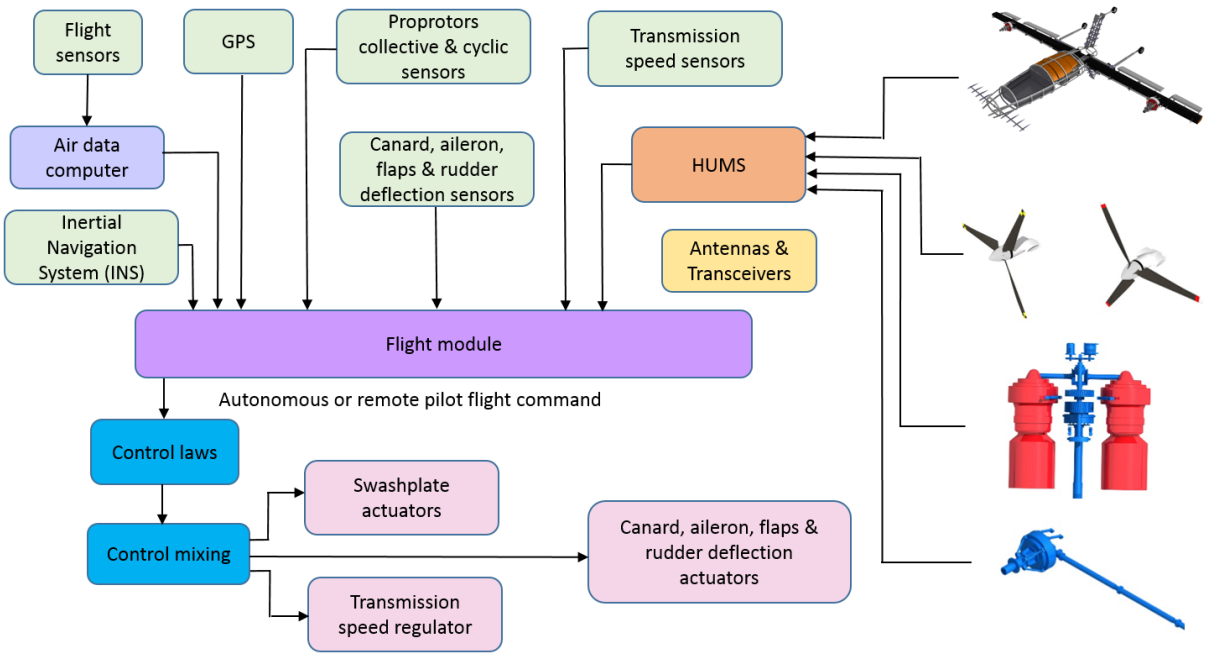

Figure 10.7: Vehicle system architecture.

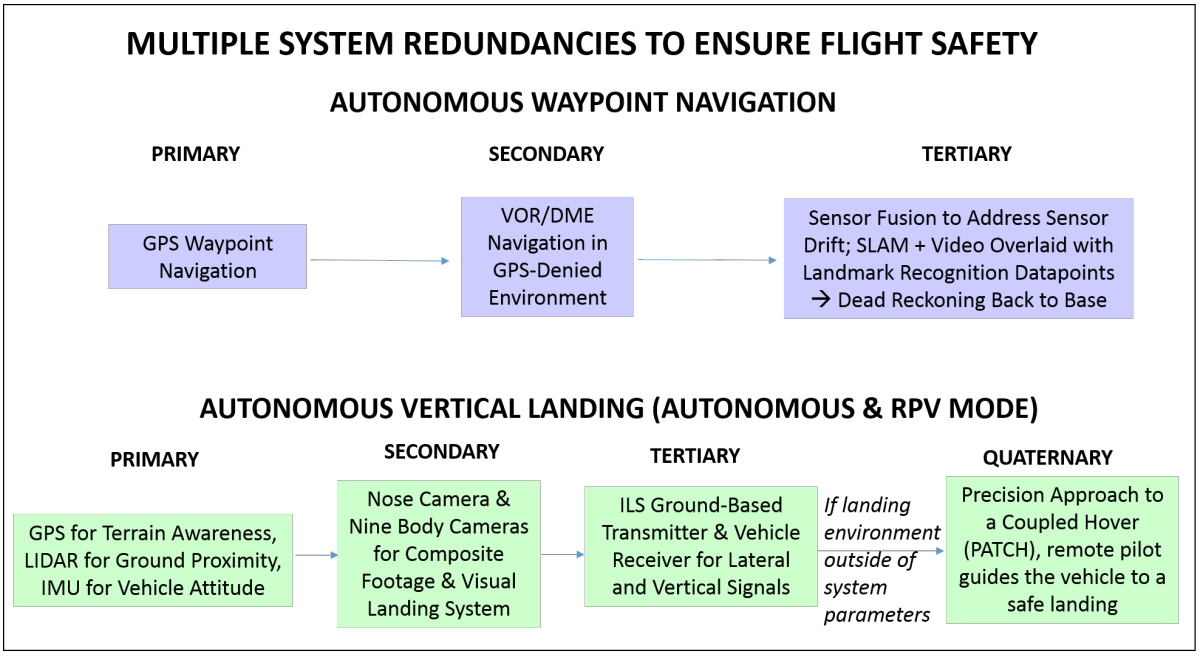

Figure 10.8: Flight control system redundancies.

11 Transition Maneuvers

The most critical phase of a tailsitter flight profile is the transition between hover and forward flight modes. At large fuselage pitch attitudes that are typical during edgewise flight, the aerodynamic surfaces may operate in deep stall conditions. Therefore, the lift coefficients vary in a nonlinear manner with respect to the angle of attack. The nonlinearity in aerodynamic forces makes it challenging to achieve steady flight conditions. Therefore the *Kestrel* is designed with an integrated aerodynamic sensing package to support safe and controlled transition from hover to cruise and vice versa.

11.1 Inertial and Aerodynamics-Based Feedback Control

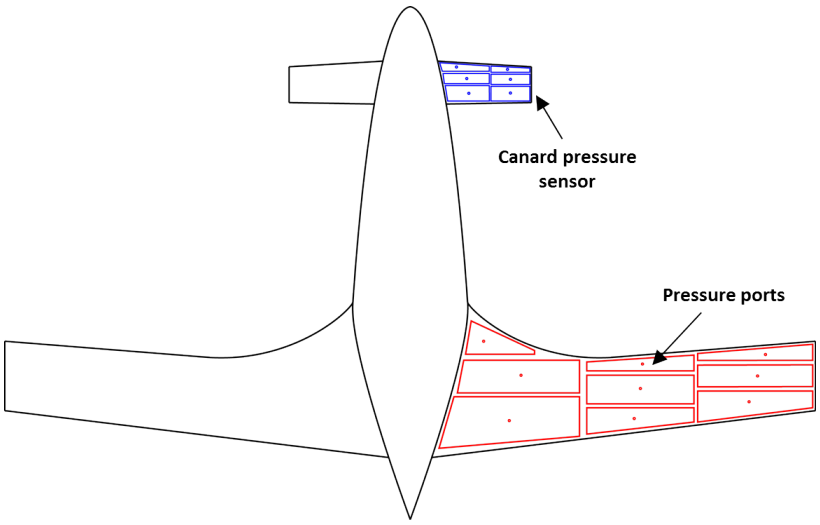

Figure 11.1: Aerodynamic surface discretization scheme and sensor locations.

Transition between hover and forward flight can be performed fully autonomously through a feedback control system using inertial measurements augmented with aerodynamic state information provided by an integrated flowfield sensing system. An array of embedded differential pressure sensors are distributed across the wing and canard, shown in Fig. 11.1. These sensors provide measurement of the pressure difference between the top and bottom surface of the wing at each spanwise location.

11.2 Lift Estimation and Stall Prediction

During hover-to-cruise transition, estimates of wing aerodynamic loads allow a guidance law to continuously tailor the control algorithm to match flight conditions, or to drive the decision of switching between different flight modes [29]. The aerodynamic sensing system provides estimates of the forces acting normal to the aerodynamic surfaces through a direct integration scheme [30]. With aerodynamic feedback, the autopilot on the *Kestrel* can track the flow field over the wings as airspeed increases throughout the transition to cruise mode. These measurements allow the control system to adapt control mixing ratios or change control modes depending on actual flight conditions.

When transitioning between the cruise and hover modes, an aircraft switches between the wing lift and rotor generated thrust to compensate for the weight of the vehicle. The intuitive approach is to balance the two forces by increasing airspeed and decreasing angle of attack. Traditional autopilots that rely solely on inertial measurements are incapable of handling such control sequences because the vehicle encounters flow separation and nonlinear aerodynamics.

To determine when the main wing begins to generate sufficient lift, and when control surfaces gain acceptable control authority active during the transition, a series of pressure ports are embedded on the wing and canard surfaces at three spanwise positions across the wing. One pressure port is located at the leading edge of the aircraft to measure the stagnation pressure, and three other ports are located at 35%, 55%, and 75% of the chord. The locations are constrained by structural design limitations because the landing gear, flap, and aileron mechanisms take up significant portion of the wing from the trailing edge.

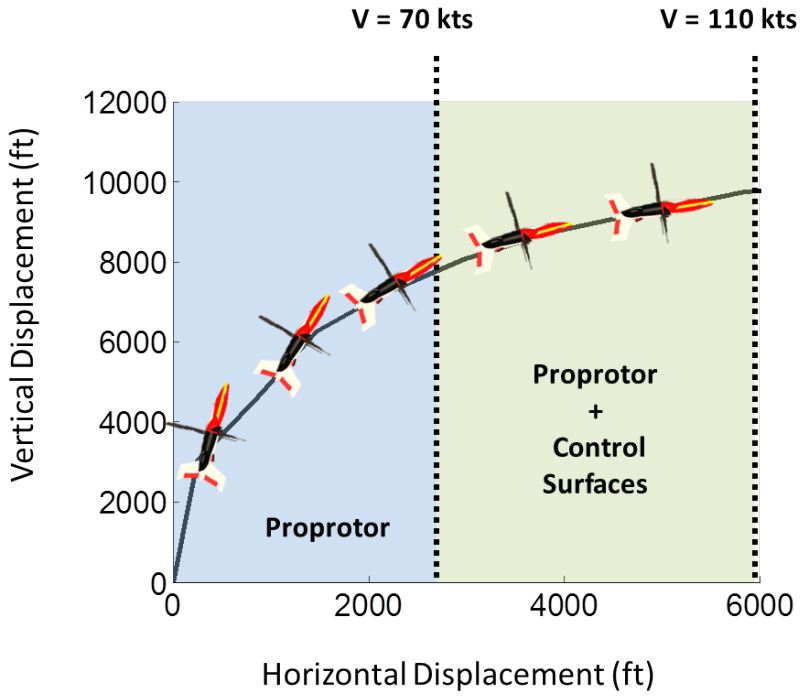

Figure 11.2: Control mixing schemes.

11.3 Transition Control Strategy

An effective transition strategy is critical to the operational performance of a tailsitter vehicle. Both the proprotor and control surfaces are used during transition to allow for maximum control authority of the vehicle. The aerodynamic control surfaces become effective at 70 kts and are used in combination with the proprotor controls until the vehicle has fully transitioned to forward flight.

The control mixing scheme is shown in Fig. 11.2. The proprotors must provide full control of the vehicle from hover up to 70 kts. The control surfaces become effective very early into transition because of the extra power available from the engines. The engines on the *Kestrel* are sized to achieve the maximum cruise airspeed and therefore in hover, the maximum achievable rate of climb is 45 kts at MSL. The excellent stall margin and excess power is used during transition to smoothly transfer primary controls to the aerodynamic surfaces.

11.4 Control Mixing

An important consideration during the transition is that the roll and yaw controls for the proprotor are interchanged between hover and forward flight. As seen in Fig. 11.3, at some flight path angle, differential collective will have a

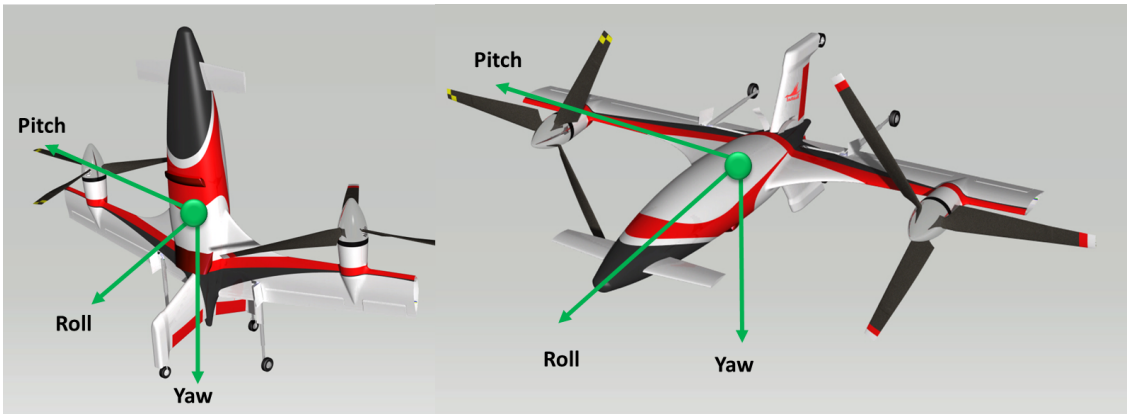

Figure 11.3: Inertial frames of reference in hover and forward flight.

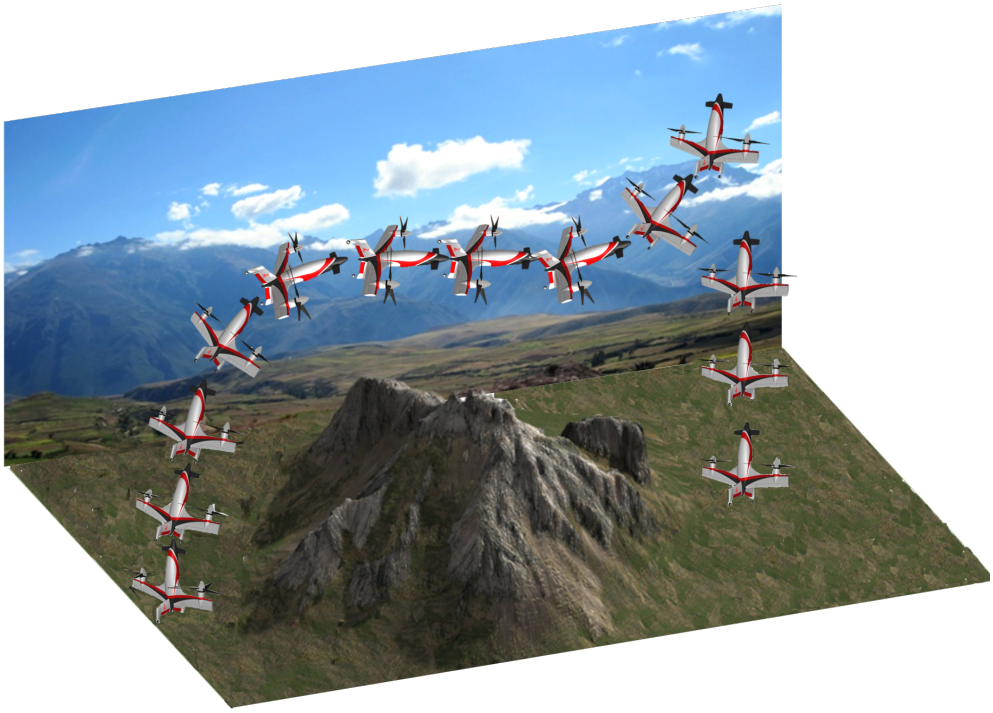

Figure 11.4: Transition maneuver flight path.

greater effect on the vehicle's yaw attitude instead of roll in helicopter mode. Therefore, the roll and yaw inputs will have to be appropriately mixed during the transition as a function of the flight path angle and airspeed. The control mixing is implemented in the flight controller as a function of the flight path angle until the vehicle reaches 110 kts. In airplane mode, control surfaces fully take over. This type of mixing has been successfully accomplished on UAV-scale tailsitters such as in [31], [32].

11.5 Climb to Forward Flight

A climb-to-cruise trajectory for the *Kestrel* was developed using a transition simulator that considers rotor, wing, and engine performance throughout the envelope. It leverages the *Kestrel*'s high thrust-to-weight ratio to rapidly reach cruise altitude and speed by balancing proprotor thrust and main-wing lift. Feedback throughout the transition is provided by both inertial and aerodynamic sensors.

A series of three flight control modes have been developed, along with a series of aerodynamic conditions throughout the transition. The autopilot advances through these states, lowering the flight path angle as conditions are matched at each attitude. In contrast to inertial-only transition guidance strategies, the aerodynamics driven feedback improves disturbance rejection and ambient flow fields, guaranteeing that the aerodynamic forces provided by the wing are sufficient for the transition to continue. This guidance strategy is shown in Fig. 11.5.

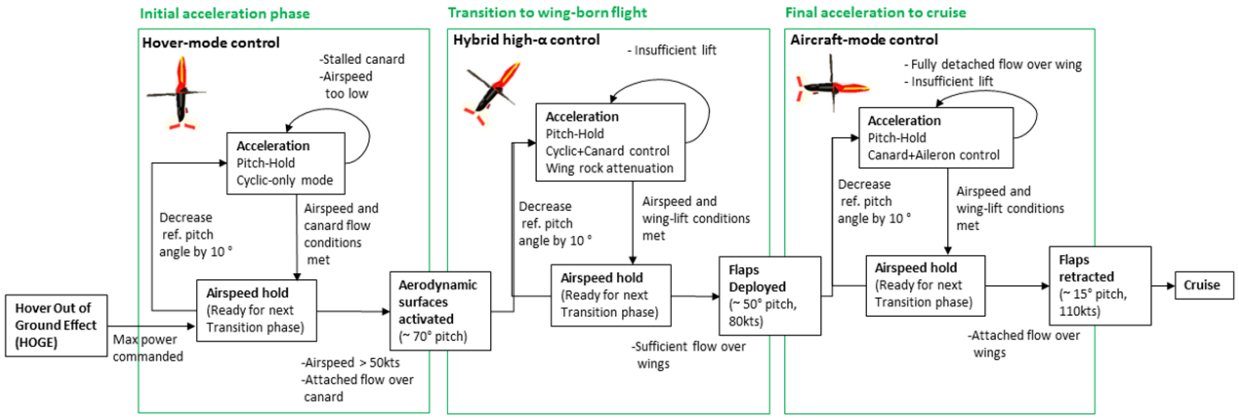

Figure 11.5: Transition guidance law.

The *Kestrel* initiates the transition by entering a vertical climb with full power. Longitudinal cyclic is applied to achieve an inertial pitch angle of approximately 70°. In this attitude, the *Kestrel* accelerates until the canard becomes effective and is used for pitch trim. The inertial pitch angle is lowered in 10° decrements until the wings begin to generate lift at an inertial pitch angle of 50°. The autopilot deploys the flaps as the wings begin to generate lift. Once attached flow conditions and high lift generation is detected over the main wing by the pressure sensors, the flaps are retracted and the aircraft enters cruise. The flight path is shown in Fig. 11.4. The altitude represented is the best range altitude, but the *Kestrel* would be able to transition without gaining significant altitude.

11.6 Cruise to Hover

A similar three-phase strategy is used for transitioning the aircraft from airplane mode to helicopter mode. Instead of a high speed climb to a vertical orientation, the aerodynamic feedback system supports an initial airspeed-bleed phase which terminates once imminent wing stall is predicted. The strategy is shown in Fig. 11.6.

The flaps are deployed and the nose of the aircraft is slowly raised to maintain level flight as the throttle is reduced. This allows the kinetic energy from high speed forward flight to be expended without the need for a significant altitude excursion. When imminent stall conditions are detected by the pressure sensors, the autopilot retracts the flaps and advances to the next phase. Proprotor collective is raised to accommodate the loss of lift from the wings and cyclic pitch controls are reactivated. The vehicle pitch attitude is increased and airspeed continues to decrease until a loss of control authority of the canard is detected, indicating that the *Kestrel* has transitioned to a helicopter mode. The canard is deactivated and the autopilot establishes a stable hover using the proprotor collective and cyclic inputs.

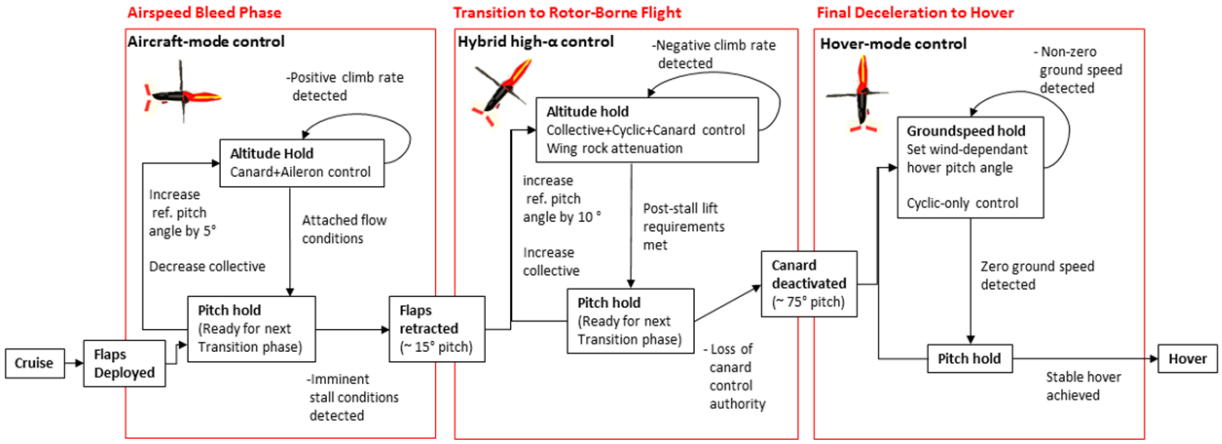

Figure 11.6: Aerodynamics-in-the-loop transition guidance law from cruise to hover.

12 Avionics and Mobile Ground Control Station

The *Kestrel* was designed to be an unmanned vehicle with a remotely piloted option, because of the challenging maneuver required to transition from vertical to horizontal flight. The remotely piloted option is available using a Mobile Ground Control Station (MGCS), which transmits real time data from the vehicle. The remotely piloted option was included to increase situational awareness of the aircraft, and to act as an additional redundancy in the event of sensors or autonomous system malfunction. In accordance with the Federal Aviation Regulation (FAR) Title 14 Code of Federal Regulations (CFR) 91.205(b), the vehicle is equipped with a Day Visual Flight Rule (VFR) Minimum Equipment List (MEl) avionics suite.

12.1 Unmanned Vehicle Equipment: Autonomous and Remotely Piloted

The Day VFR MEL was modified for the *Kestrel* by eliminating avionics unnecessary for an unmanned vehicle. The regular Day VFR MEL can be categorized into cockpit instruments and safety equipment. The non-exhaustive list of cockpit instruments includes the airspeed indicator (ASI), tachometer for the engine, and landing gear position indicators. The required safety equipment includes flotation gear, at least one pyrotechnic signaling device for flight over water, safety belt and shoulder harnesses for each seat, an emergency locator transmitter, as well as aviation red or white anti-collision light system. Onboard flight displays and gauges were omitted from the cockpit instruments with the corresponding flight sensors left intact and suitable safety equipment selected. Tasks implicitly executed by the pilot of a manned vehicle were accounted for in the avionics such as communication, stabilization, navigation, and control (SNC). There is a negligible weight penalty for the avionics between the autonomous and remotely piloted mode because similar servos, actuators and communication systems are required for both. The GCS for remote piloting will be equipped with the required flight data indicators.

Table 12.1: Avionics equipment weights and power requirements.

Equipment	Quantity	Unit weight (lb)	Unit power (hp)	Manufacturer & model
Nose camera	1	37.00	0.1502	L3 Wescam MX-10
Mid-fuselage camera	8	0.88	0.0028	Brandebury BTC-101 Retract
LIDAR	3	0.26	0.0027	FLIR MLR-4K
Barometric pressure sensor	3	2.43	0.0054	Setra 470
Emergency locator transmitter	1	1.80	0.0001	Kannad 121 AF-H
TCAS II	1	29.50	0.1475	Honeywell CAS 100
Ku-band satellite antenna & transceiver	1	45.00	0.4694	Honeywell Wavestorm DBS
GPS Antenna & Receiver	2	0.93	0.0081	Trimble Force 524D
Inertial Navigational System	2	10.20	0.0469	Kearfott KN-4072A
Flight Module	3	0.48	0.0054	Cloud Cap Technology Piccolo II
SSHD Storage Drive	3	2.00	0.0090	Seagate ST2000DX001
LiPo Battery Assembly	1	6.14	30mins @ 1.34hp	EEMB Co.
TOTAL		**164**	**0.9671**	

12.1.1 Day VFR Minimum Equipment List (MEL)

The flight sensors for Day VFR flight include sideslip angle probe, pitot-static and AoA probe, temperature sensor, barometric pressure sensor, inertial measurement unit (IMU) consisting of accelerometers, gyroscopes and magnetometers, control surface position sensors, landing gear position sensors, fuel level sensors, nose camera, three

retractable mid-fuselage cameras that swivel to provide composite footage of forward flight and landing, three mid-fuselage obstacle proximity LIDARs [33] for precision VTOL and FADEC for each engine. For safety, the vehicle will be equipped with an emergency locator transmitter (ELT) and aviation anti-collision light system. A traffic collision and avoidance system (TCAS II), which includes a transponder, TCAS II processor unit and antenna, is included for enhanced situational awareness even without a pilot in-the-loop.

The encrypted communication equipment includes LOS communication devices such as a very high frequency (VHF) antenna and transceiver, ultra-high frequency (UHF) antenna and transceiver, C-band antenna and transceiver as well as beyond-LOS Satellite Communication (SATCOM) devices such as Ku-band satellite antenna and transceiver. Processing, storage and SNC equipment include two GPS antennas, inertial navigation system (INS), flight module, air data computer, solid state hybrid drive (SSHD) data storage unit, video encoder, avionics temperature monitoring systems, electrical generator, and Lithium-Polymer (LiPo) battery assembly. As shown in Table 20.1, the avionics suite weighs a total of 164 lbs.

12.1.2 Sensor and Avionics Placement

The nose camera is located at the bottom fore section of the fuselage. The mid-fuselage cameras and LIDARs are located to provide optimal visibility especially during VTOL. Footage and data from the multiple cameras and LIDAR are merged through software to create a composite video. This technique is similar to the Sierra Nevada Gorgon Stare [34] and BAE Systems ARGUS [35] to create a composite view of the vehicle with respect to the ground and obstacles during helicopter mode, or of the surrounding environment during other flight modes.

12.1.3 Battery Backup

Thirty minutes of backup power is supplied by the high energy density LiPo battery assembly in a power-out case. The battery assembly provides full power to the sensors, flight modules, data storage units, control surface actuators, and communication equipment. The battery assembly is contained within a titanium housing to isolate it in the unlikely event of a battery pack fire.

12.1.4 Electromagnetic Interference (EMI) and Vibration Suppression

Multiple solutions were pursued for EMI suppression, which included avionics enclosure and shielding. Fiber optic cables were also deployed as they are immune to EMI since signals are transmitted optically as opposed to using electrical current. Integration of the avionics suite was carried out in accordance with MIL-STD-461, MIL-STD-464, DO-160 and ADS-37A-PRF4 [36]. Static dischargers were installed at the wing tips of the *Kestrel* to regulate corona discharge from the aircraft fuselage into the environment as static charge builds up. This equipment isolates static noise and prevents interference with the avionics. Vibration suppression were employed through passive absorber equipment as well as through active spring-damper systems.

12.1.5 IFR Equipment

The *Kestrel* is equipped with FAA Instrument Flight Rule IFR flight equipment, in accordance with FAR Title 14 CFR 91.205(d) and FAR 27 Appendix B. The additional equipment include thunderstorm lights, ice detector and de-icing unit, flight sensor anti-ice provisions, multiple static grounds, overvoltage disconnect circuit and battery charge disconnect circuits, VHF omnidirectional range/ distance measuring equipment (VOR/DME), Terrain Awareness and Warning System (TAWS), and weather radar system. Night and degraded environment visibility is provided by an electro-optical / infrared sensor (EO-IR) camera.

12.1.6 Health and Usage Monitoring System (HUMS)

The reliability and safety of the vehicle is enhanced by the addition of an integrated Health and Usage Monitoring System (HUMS) for global monitoring of performance, usage data, critical loads and identification of incipient failure. Other benefits include increased safety, which leads to lower insurance and maintenance costs along with shorter downtime from unscheduled maintenance. These benefits lead to overall decreases in the direct operating costs for the vehicle.

For the proprotor, track and balance records are obtained from the Goodrich Integrated Mechanical Diagnosis HUMS [37] which deviates from the conventional infrared camera tracker mounted on the fore fuselage section to track blade tip path. Instead, the lighter Goodrich system parses cabin accelerometer data to infer when the proprotors are out of track because they can be a significant source of increased cabin vibrations. FADEC data is also used to monitor the engine torque, oil temperature and fault monitoring. Fans, air vents, and temperature probes are installed in the fore and aft-fuselage avionics bay of the *Kestrel* to ensure the avionics are operating within their nominal temperature range.

12.1.7 Avionics Assisted Strictly Vertical Landing

The *Kestrel* is capable of four-point vertical landing due to its onboard sensing and processing capabilities. The onboard LIDAR and cameras evaluate the landing site terrain, the GPS and LIDAR provide relative distance to the ground, and the IMUs measure the vehicles attitude. All these data are processed by the onboard flight module in order to direct the vehicle flight controls to implement a four-point landing.

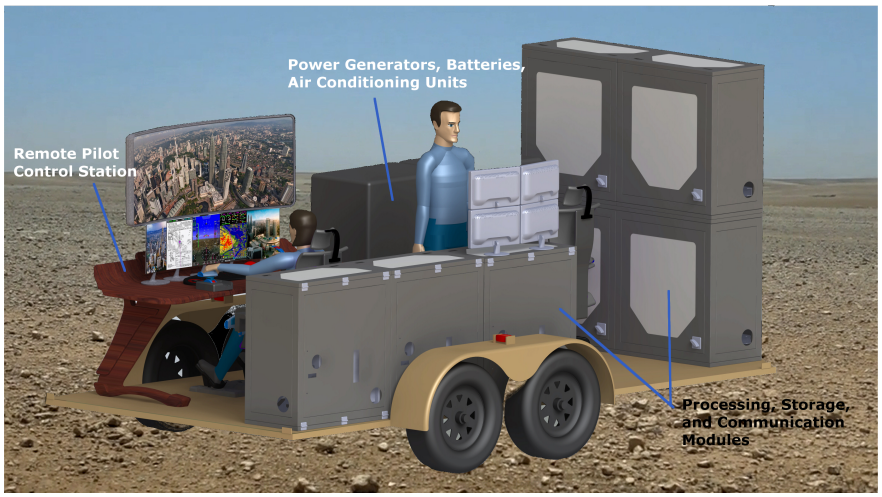

Figure 12.1: Autonomous and remotely piloted MGCS layout.

12.2 Autonomous Platform

The autonomous platform of the MGCS is equipped with a minimum of triple redundancies for every system as weight is not as heavily penalized as the airborne vehicle (Fig. 12.1). The communications module consists of Ku-band satellite, C-band, VHF and UHF antennas as well as transceivers. High definition video footage streams through Ku-band, while datalink is established via the other channels. The processing and storage modules consist of control modules, SSHD storage units and video decoder. Finally, all data are transmitted to the uplink vehicle and relayed to the airborne tailsitter to close the control loop.

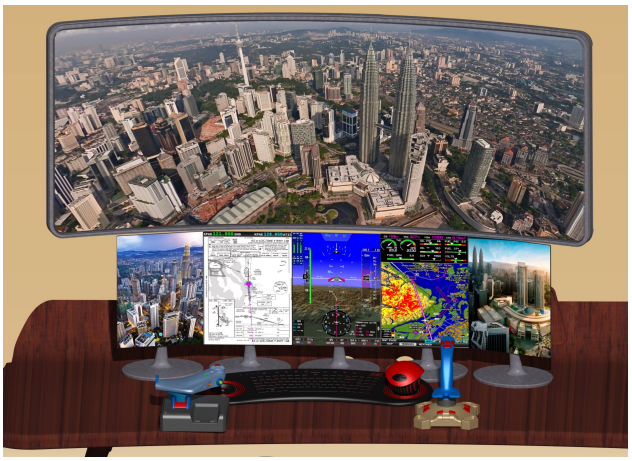

Figure 12.2: Control Display Unit (CDU).

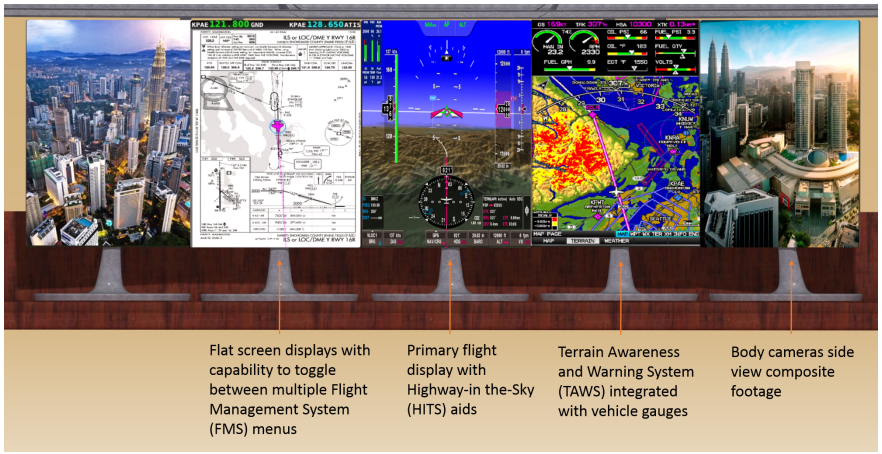

Figure 12.3: Control Display Unit (CDU) lower displays.

12.3 Remotely Piloted Platform

The remotely piloted MGCS is configured with the goal to minimize pilot fatigue through the display of concise flight data and consists of the pilot's displays, pilot seat, and controls. The cockpit view is displayed on the top curved displays from the vehicle's nose camera, while the surrounding topological view is overlaid from the composite footage of the mid-fuselage cameras to the bottom left and right display panels, as shown in Fig.12.3. As the vehicle transitions from helicopter to airplane mode, the nose camera will track the horizon automatically. Head movement of the pilot is monitored with use of the NaturalPoint TrackerIR 5 [38] head tracker which is mounted in front of the pilot. As the pilot's head moves, the vehicle body cameras will pan or tilt in unison while the nose camera continues to point forward. A heads-up display (HUD) is also available at the pilot's line-of-sight on the top curved displays to overlay critical information such as airspeed, altitude and heading.

Flight Controls

Airplane Mode

Roll: Ailerons

Pitch: Canard

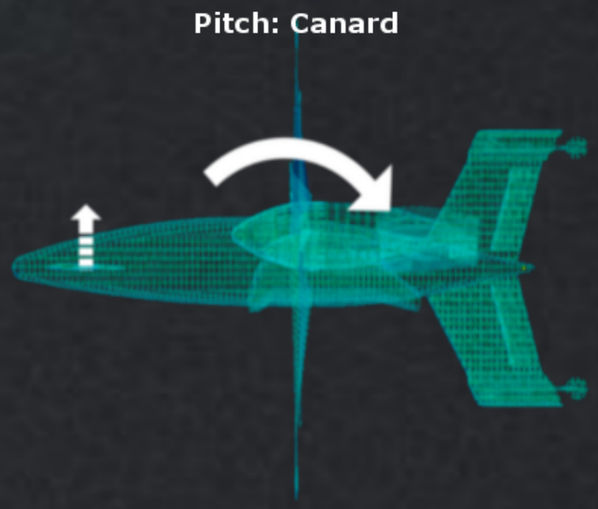

Yaw: Rudder

Hover Mode

Roll: Differential Collective

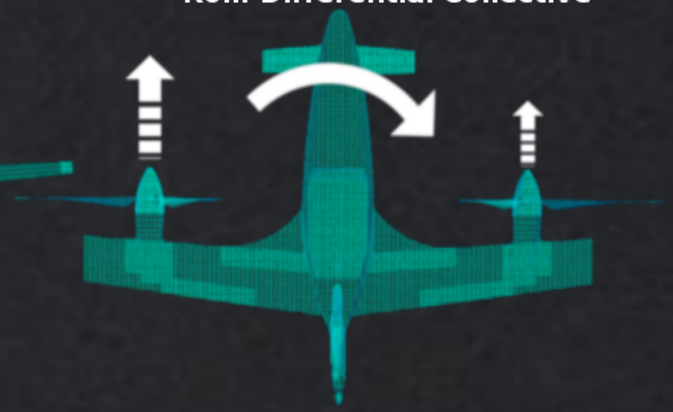

Pitch: Longitudinal Cyclic

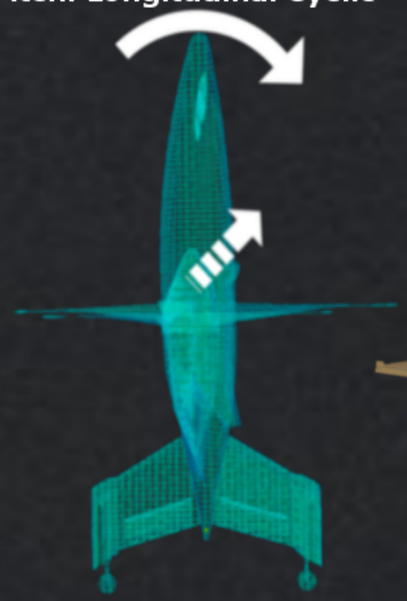

Yaw: Differential Longitudinal Cyclic

Avionics

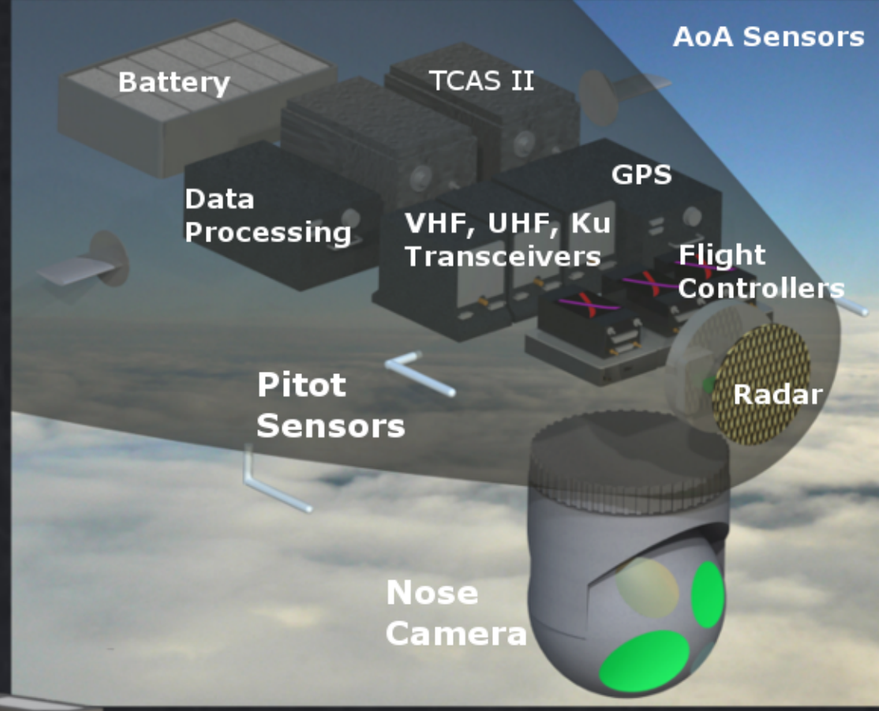

Mobile Ground Control Station

Triple Redundant Communications and Navigation

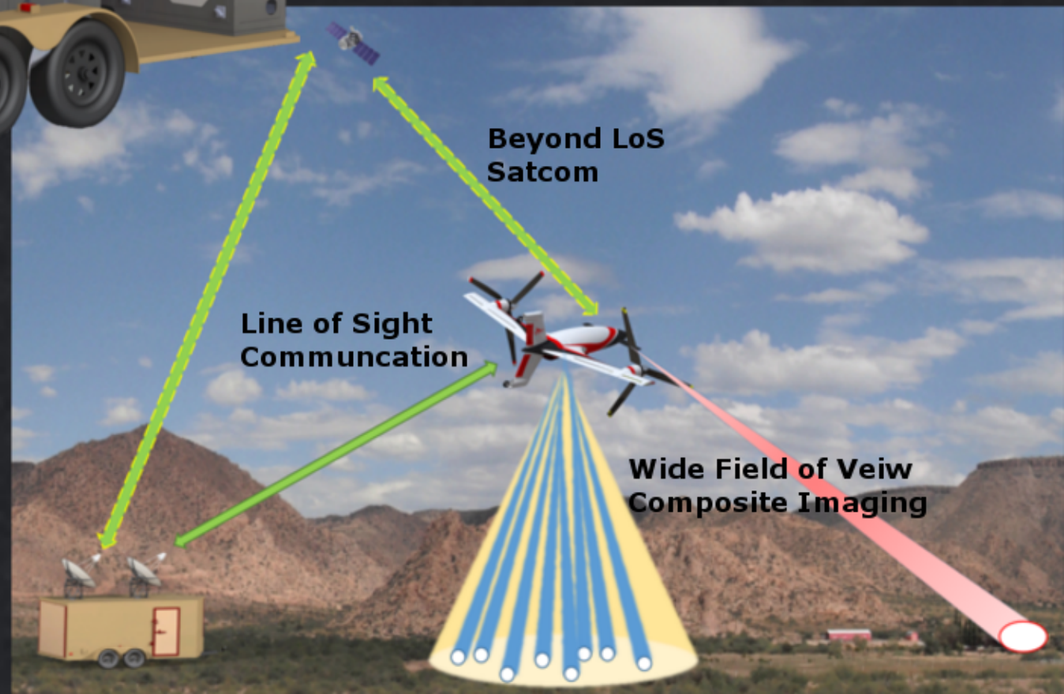

13 Flight Dynamics Evaluation Using FLIGHTLAB

The subsystems on the *Kestrel* are represented in the FLIGHTLAB model editor (FLME). The input characteristics of proprotors, control surfaces, fuselage, landing gear, and engine are obtained from preliminary design analysis and inserted into FLME. The rotor aerodynamics is modeled using a Peters-He Six State Inflow and the blade forces are computed assuming quasi-steady airloads. Rotor interference is modeled using 3-state Interference with wake contraction/expansion on the wing and control surfaces. The airframe is assumed to be a rigid-body and the full vehicle inertia terms were predicted using the CATIA model.

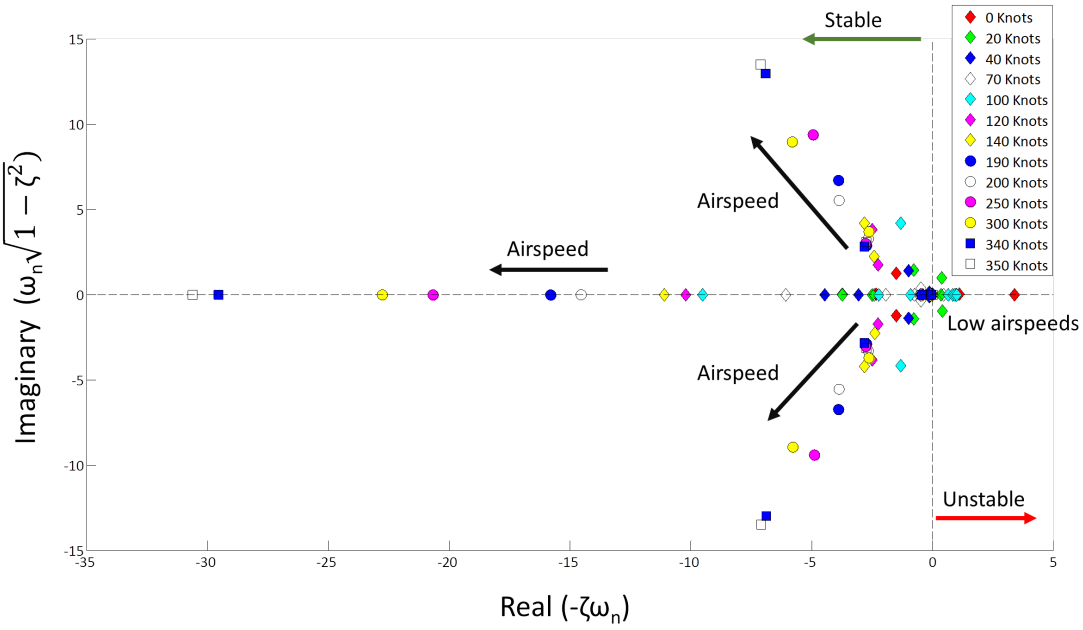

Figure 13.1: Open-loop pole stability roots in hover and forward flight.

13.0.1 Stability

As a first order analysis of the entire aircraft flight dynamics, the controls system of the *Kestrel* was simplified for the FLIGHTLAB model. The dynamics of the *Kestrel* was determined by a 6 degrees-of-freedom linearized FLIGHTLAB model with the general form:

$$\dot{x} = Ax + Bu \tag{3}$$

Where the state vectors are x = [u v w p q r ϕ θ] and the control inputs are u = [δ_{lat} δ_{lon} δ_{col} δ_{ped}]. The states [u v w] are the translational velocities, [p q r] are the rotational rates, and [ϕ θ] are the corresponding Euler roll and pitch angles.

From hover to low forward flight speeds, δ_{lat} refers to the differential collective of the proprotors, δ_{lon} is the longitudinal cyclic, δ_{ped} is differential longitudinal cyclic, and δ_{col} is the collective. For the FLIGHTLAB model, only the airspeed is used to determine the effectiveness of the control surfaces. When accelerating from low airspeeds, the control inputs (rotor collective and cyclic) are progressively applied to the aerodynamic control surfaces as the *Kestrel* enters fixed-wing mode. To simulate the transition flight mode, the Control Systems Graphical Editor (CSGE) model includes both rotor control and control surfaces and the mixing is dictated by airspeed.

A detailed analysis of the dynamic stability of the *Kestrel* was conducted. In the pole diagram in Fig. 13.2, $\zeta\omega_n$ represents the damping and $\omega_n \sqrt{1-\zeta^2}$ represents the damped frequency. It is evident that the *Kestrel* is inherently unstable in hover to low forward flight speeds up to 100 kts, where it mainly relies on rotor collective and cyclic. In hover, the vehicle has unstable longitudinal pitching oscillation and dutch roll modes, similar to traditional helicopters. As the airspeed increases from 100 kts, the control surfaces become effective and has a stabilizing effect on the vehicle. The remote pilot workload is reduced once the vehicle achieves 120 kts and the primary controls are through the control surfaces.

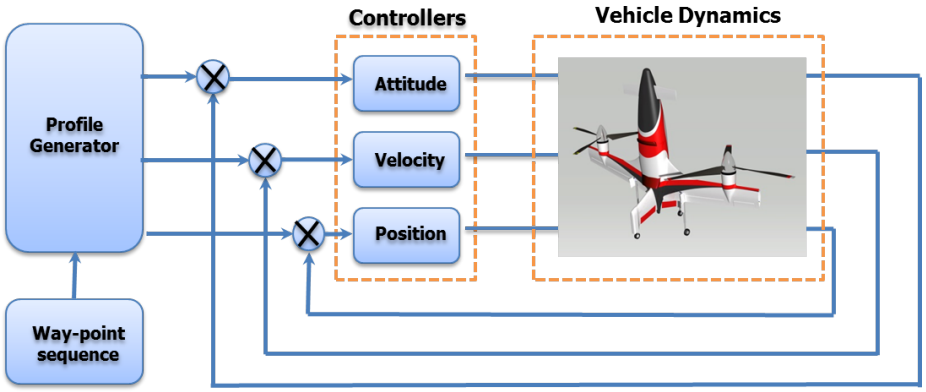

Figure 13.2: SISO controls architecture.

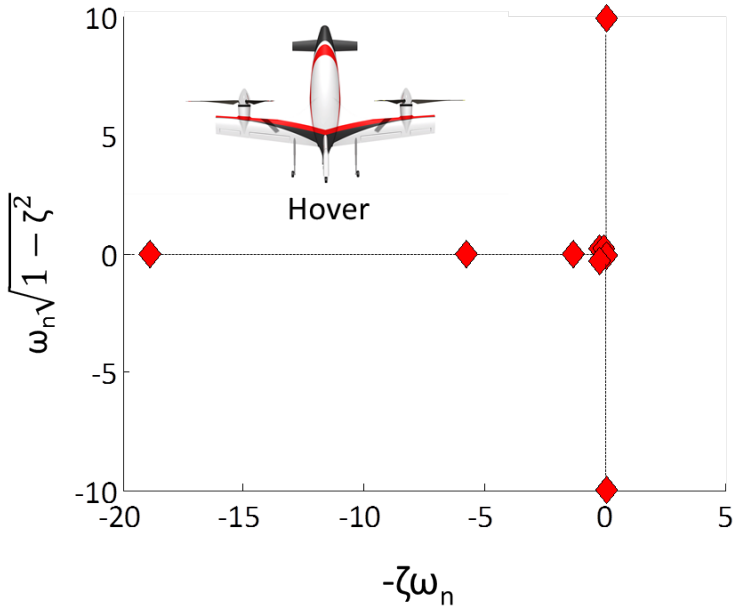

Figure 13.3: Closed-loop pole stability roots in hover.

13.0.2 Feedback Control Systems

Feedback control strategies were implemented using Flightlab to assess the stability of the *Kestrel* at hover and low airspeeds when equipped with a stability augmentation system. Hover represents the most unstable bare-airframe

flight mode, and was thus chosen to demonstrate the ability of basic feedback control to stabilize the vehicle.

The multi-input multi-output (MIMO) nonlinear system of the *Kestrel* has been decoupled into single-input single-output (SISO) sub-system. The sub-systems consist of attitude, velocity, and position channels which can be individually stabilized through feedback control. For this analysis, rate feedback control was implemented on the attitude subsystem and applied to the collective and cyclic controls.

Figure 13.3 shows the poles in hover after implementing closed-loop attitude stabilization. The poles have been shifted left hand plane, showing that the vehicle has been made stable. This validates both the low-speed control strategy and the feedback controller, showing that the bare airframe can be adequately mitigated using basic attitude feedback control.

13.1 Handling Qualities

The handling qualities requirements are specified by ADS-33E-PRF at mission tasks required outlined by the RFP. The handling qualities of the *Kestrel* were predicted using the complete nonlinear flight dynamics model in FLIGHTLAB, and evaluated at multiple flight conditions ranging from hover to cruise speed.

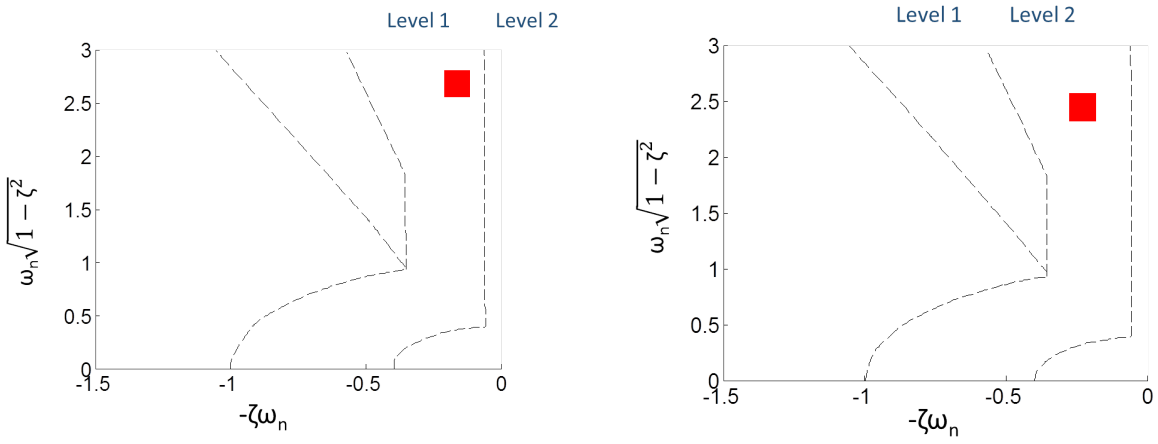

(a) Start of transition to horizontal flight (60 kts).

(b) Best range cruise speed (200 kts).

Figure 13.4: Lateral-directional stability.

The lateral-directional poles are shown in Fig. 13.5 for the start of transition from hover to forward flight (60 kts) and for best cruise airspeed (200 kts). Both sets of poles satisfy the Level 1 requirements, indicating that the predicted handling qualities is satisfactory without additional augmentations.

13.1.1 Bandwidth

Figure. 13.5 shows the predicted pitch and roll bandwidth assessed for the 'Target Tracking and Acquisition' ADS-33 criteria [40]. An evaluation of the flight stability of the vehicle was performed with only rate and velocity feedback. It was found that pitch, roll, and yaw dynamics are extremely sensitive to control inputs suggesting that flight dynamics of the *Kestrel* could be further improved by implementing attitude feedback control.

13.1.2 Quickness Criteria

The ratio of peak pitch (roll) rate to change in pitch (roll) attitude was predicted in pitch, roll, and yaw for over the best range cruise airspeed (200 kts). Figure 6(a) shows that the predicted pitch quickness satisfied the ADS-33 Level

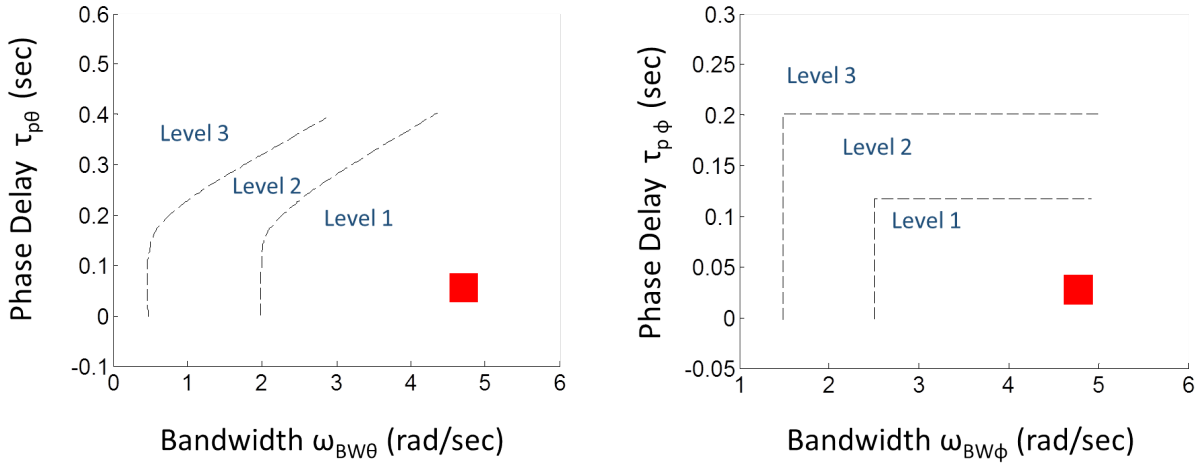

(a) Predicted pitch bandwidth.

(b) Predicted roll bandwidth.

Figure 13.5: Bandwidth for 'Target Tracking and Acquisition'.

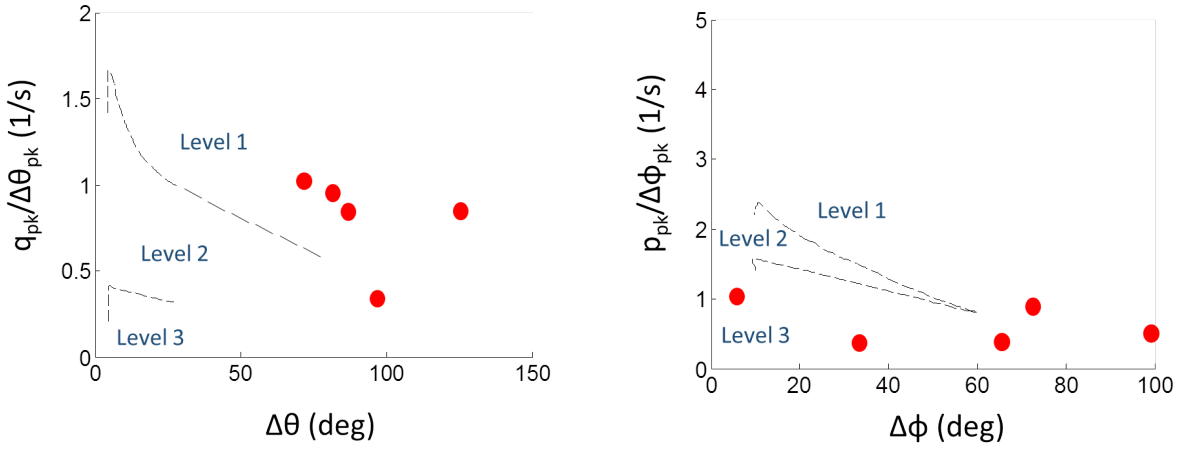

(a) Predicted pitch quickness.

(b) Predicted roll quickness.

Figure 13.6: Bandwidth for quickness.

1 requirements at most pitch attitude perturbations except in hover, which suggests that the c.g separation may not be large enough from the rotor tip-path-plane. For roll and yaw, the predicted quickness showed poor Level 3 handling qualities for small roll attitude, but improved to Level 1 at higher roll attitudes. Overall, simulation results suggest the *Kestrel* can adequately perform target tracking and acquisition missions with rate and velocity stability augmentation. Further improvements in performance can be achieved by implementing the complete feedback system that was outline in Section. 10.

14 Performance Analysis

Performance analyses were conducted for hover and forward flight conditions at MGTOW for the mission profile specified by the RFP. The *Kestrel* was designed to be efficient in both hover and forward flight regimes. Unprecedented cruise airspeeds are achieved by leveraging the dual speed rotor technology, which promote high propulsive efficiency. The propulsive efficiency reaches 87% at the maximum L/D airspeed and up to 72% at the maximum cruise speed. The zero-lift drag drag estimation for the entire air vehicle was performed using the *United States Air Force Stability and Control Data Compendium* (USAF DATCOM, referred to as DATCOM) [41]. Emergency glide and autorotation capabilities were also investigated. The performance analysis were conducted using proprotor performance and mission simulation tools developed by the design team.

14.1 Drag Estimation

Historical trends of flat plate drag area for tailsitters within the 10,000–12,000 lb gross weight range were not available. However, the equivalent flat plate drag area was approximated to be similar to a tiltrotor configuration because of the similarities in the proprotor-wing-fuselage layout between the tiltrotor and tailsitter. During the initial sizing, a total air vehicle equivalent flat plate drag of 12 ft^2 was estimated from historical trends [42].

The total drag for the aircraft was broken into the induced drag and zero-lift drag. The zero-lift drag was estimated by the methodology stated in DATCOM [41]. DATCOM is an industry accepted solution to calculate an aircraft's aerodynamic properties such as the stability and control derivatives, steady state lift, drag, and pitching moment. At subsonic speeds, DATCOM estimates the zero-lift drag by applying an interference correction factor to the skin-friction and pressure drag of the exposed wing, fuselage, canard, and tail. DATCOM computes the zero-lift drag build up by adding each component of the aircraft such as the wing, fuselage, nacelle, and tail, as shown in Table 14.1.

Table 14.1: Drag Break Down

Component	Drag Area (ft^2)	Percent Contribution
Fuselage	1.86	24.80%
Wing	3.61	44.30%
Canard	0.74	9.06%
Horizontal Stabilizer	0.57	6.95%
Vertical Stabilizer	0.57	6.95%
Nacelle	0.39	4.74%
Spinner	0.26	3.20%
Total	8.14	100%
Total with Interference Effects (120%)	9.77	100%

The total drag was assessed to be 8.14 ft^2. The final drag is assumed to be 120% of the calculated values due to miscellaneous components not accounted for within DATCOM. The miscellaneous components include pitot probes, antennas, door handles, and hinges. The total parasitic drag was determined to be 9.77 ft^2 and was used in subsequent performance analyses.

14.2 Download Penalty

When the *Kestrel* is in hover mode, the aircraft will have a download penalty from the downwash that acts on the wing and fueslage directly below the rotor. This downward force acting upon the aircraft structure will require the thrust produced by the rotors to be greater than the weight of the vehicle. However the downwash penalty for the *Kestrel* will be significantly lower than contemporary VTOL aircraft because the wing is along the direction of the rotor downwash. VTOL aircraft, such as a helicopter, typically have a download penalty of 5% of the gross weight,

primarily from the fuselage. Fixed wing aircraft with convertible rotors can require up to an additional 15% of the thrust penalty in hover [43]. The *Kestrel* was calculated to have a download penalty of 0.6% of the weight required in hover. The *Kestrel* has a significant performance benefit, by reducing hover thrust required between 4% and 14% over contemporary aircraft with a fixed wing and convertible rotors. With regard to *Kestrel*'s design gross weight of 11,000 lbs, this would translate to an additional thrust requirement of up to 1,540 lbs. Table 14.2 displays the download penalty of contemporary aircraft as compared to the *Kestrel*.

Table 14.2: Download Penalty for at 10,000 lb Gross Weight

Configuration	Download Penalty (lbs)	Percent of MTOGW
Helicopter, Single Main Rotor	500	5.0%
Tiltrotor	1,500	15.0%
Kestrel	60	0.6%

14.3 Hover Performance

The primary hover design point was at MTOGW, out of ground effect, at MSL ISA. The goal of the design with regard to hover performance was to maximize the power loading efficiency, as defined by Eq. 4. A secondary design point was to hover out of ground effect (HOGE) at a pressure altitude (h_P) of 6,000 ft, 95° F (ISA +36°) for the MTOGW.

$$k = PL\left(\frac{2\rho}{DL}\right)^{-\frac{1}{2}} \tag{4}$$

The *Kestrel* has large amounts of excess power, nearly 3,000 shp, in HOGE MSL ISA conditions, as shown in Fig. 14.1, because the power requirement was driven by the maximum cruise speed. The *Kestrel* was not limited by the transmission in hover because the transmission was also designed to the max power requirement. At MTOGW the *Kestrel* can hover in excess of 12,000 ft pressure altitude. As shown in Fig. 14.2, the *Kestrel* exceeds the high-hot requirement of 6,000 ft, 95° F at the design MTOGW and can hover at considerably higher altitudes as fuel is burned and thrust required is reduced with declining gross weight. The *Kestrel*'s ability to hover in high-hot conditions enables operations at high density altitudes such as in mountainous regions.

14.4 Forward Flight Performance

The power requirement for the *Kestrel* in forward flight was limited by the maximum cruise speed requirement set by the RFP. The mission analysis performed for the *Kestrel* determined that the optimum altitude for the best range cruise speed *(V_{BR})* was 9,180 feet density altitude. The maximum speed at 9,180 feet is 358 kts. Figure 14.3 shows the power requirement for forward flight. As shown in Fig. 14.3 the *Kestrel* requires minimal power at low speed, and is attributed to the dual speed rotor which enables the rotor to operate more efficiently for low speeds.

Figure 14.4 shows the lift-to-drag ratio L/D as a function of the airspeed. The *Kestrel* is capable of a L/D of 11.9 at the best range speed of 156 kts. The recommended cruise speed is the speed at the 99% efficiency of best range speed. The 99% efficient speed, also called the Carter speed, is selected because the power required versus airspeed near the best range speed is fairly flat; therefore the increase in speed will create a minimal power required penalty. The 99% efficient speed provides a 5% improvement in speed with a penalty of less than 1% range. The Carter speed of the *Kestrel* is at 164 kts with a L/D ratio of 11.8.

The *Kestrel* is capable of such high L/D ratios because of the wing aspect ratio of 10 and the high proprotor efficiency in forward flight (Section 4). The high aspect ratio wings reduces the induced drag, which at low speeds will be

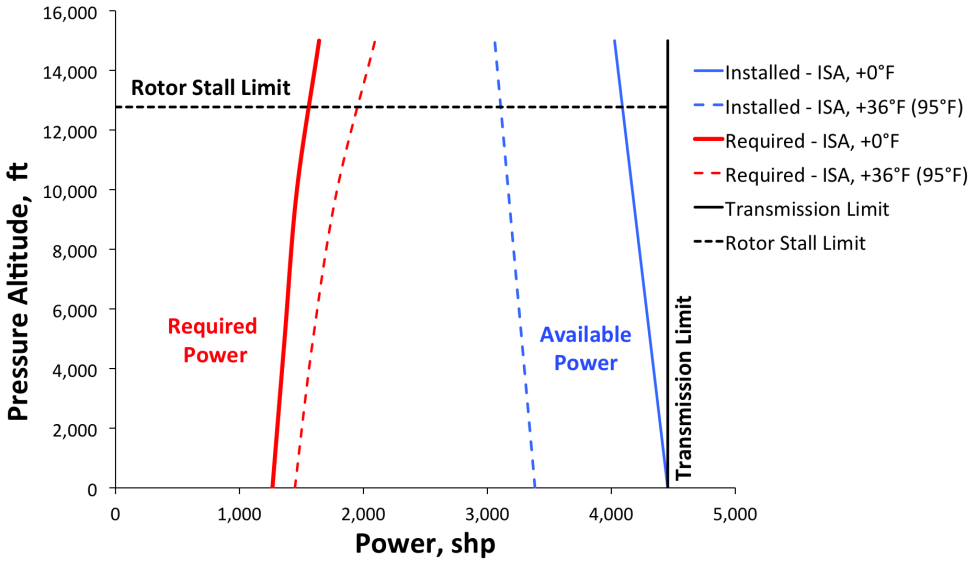

Figure 14.1: HOGE $P_{Required}$ and $P_{Available}$ at MTOGW

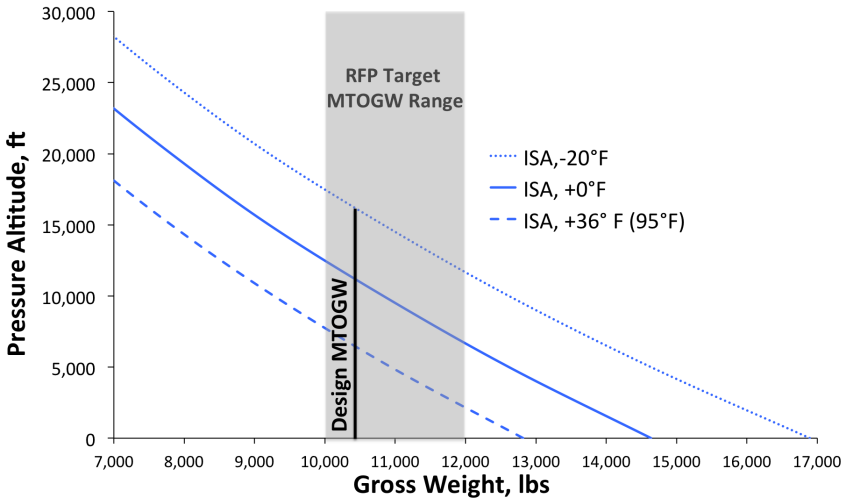

Figure 14.2: Weight-Altitude-Temperature Curve

relatively high due to the relatively high lift coefficient required.

14.5 Range and Endurance

The mission profile specified by the RFP as discussed in Section 2.1 specifies that segments 4 and 10 be flown at the velocity for best range (V_{BR}). *Kestrel* has a best lift-to-drag ratio of 11.9 at 156 kts as shown in Fig. 14.4. However, this is not representative of the complete vehicle's V_{BR} as the fuel efficiency must be considered. A turboshaft engine has a lower SFC at higher power settings and would favor a higher airspeed. The complete aircraft V_{BR} occurs at a point of tangency on the fuel flow rate versus airspeed curve to a straight line intersecting the origin, as shown in Fig. 14.5. V_{BR} for the *Kestrel* is 200 kts and gives a maximum ferry range of 1,618 nm or a radius of action of 809 nm if reserves are used in flight. The *Kestrel's* radius of action is over 100 nm greater than the larger AugustaWestland 609 tiltrotor [44].

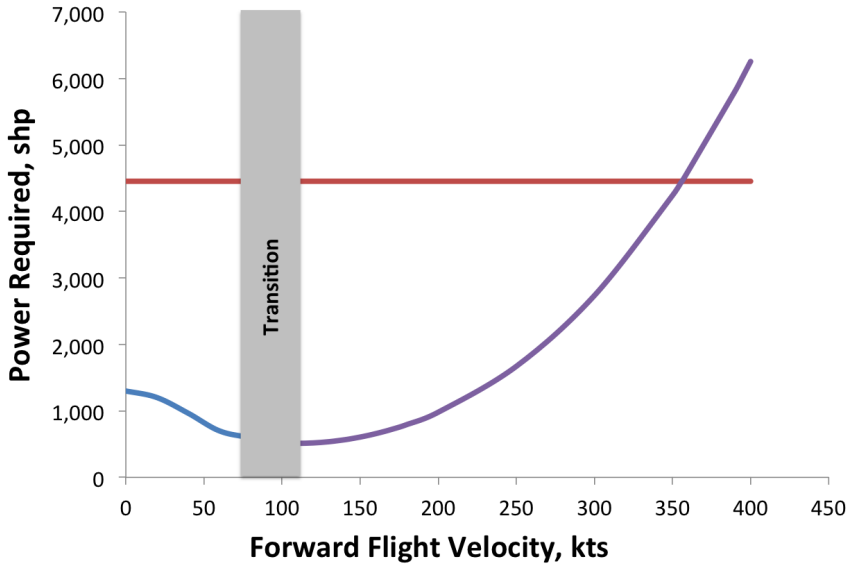

Figure 14.3: Power Required versus True Airspeed at MTOGW

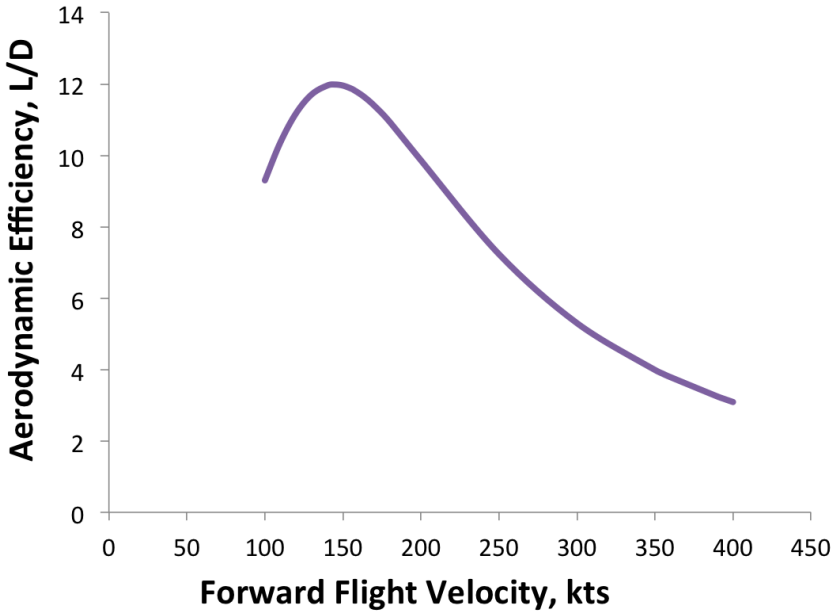

Figure 14.4: L/D versus True Airspeed

The velocity for best endurance (V_{BE}) is the velocity with the lowest fuel flow rate, which is 125 kts for the *Kestrel*, as shown in Fig. 14.5. This V_{BE} gives the *Kestrel* a maximum endurance of 10.78 hrs if reserves are used in flight.

14.6 Load Factor

The RFP specified that the minimum vertical load factor envelope shall be between -0.5 to +2.0 g, throughout the airspeed range. *Kestrel* abided by the structural safety margins of the 14CFR Part 27/29 and thus limited the structural load factors between -1 to 3.5. The vertical load factor throughout the speed range is shown in Fig. 14.6.

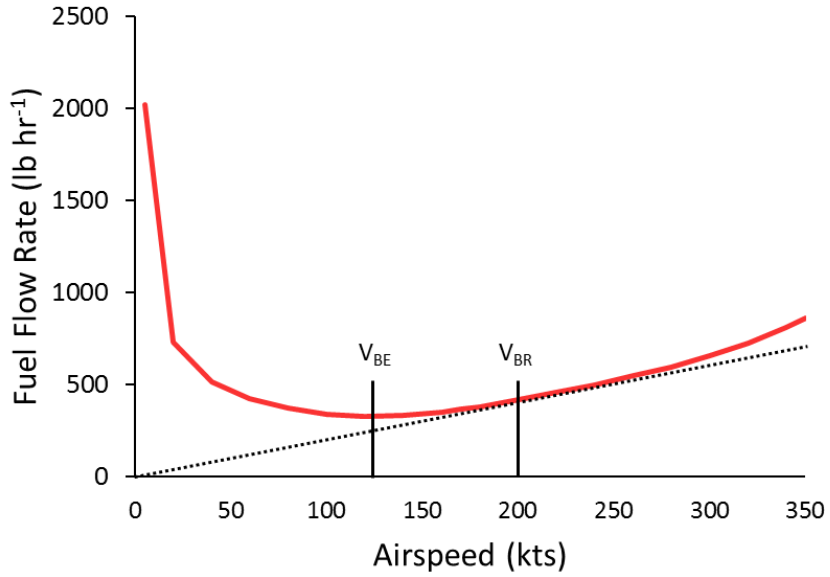

Figure 14.5: Fuel flow rate vs forward airspeed at 9,180 ft ISA.

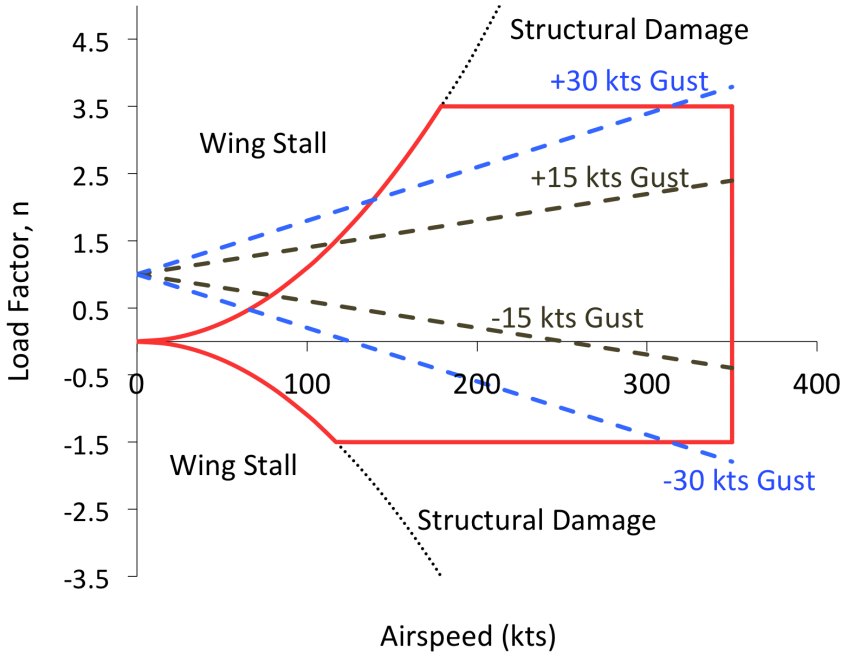

Figure 14.6: V-n diagram for *Kestrel*.

14.7 Glide and Autorotation

As stated previously in section 14.4, the *Kestrel* will have an advantageous L/D ratio in forward flight. Aircraft that exhibit high L/D in level forward flight conditions will also exhibit a high glide ratio. The glide ratio, which is numer-

ically equivalent to L/D, is the ratio of the aircraft's unpowered forward speed to its vertical descent. The glide ratio is beneficial during emergency procedures (EPs), when the aircraft must land in its airplane mode configuration. In the event of a forced belly landing the low high glide ratio will minimize the damage sustained to the aircraft. Although the proprotors would be damaged beyond repair the damage to the payload will be minimized due to the glide slope, which decreases the vertical descent rate, and the payload location on the top of the aircraft.

In the circumstances where the aircraft is forced to land while in its helicopter mode, the aircraft does so by autorotating. The ability to autorotate is dependent on the rotor flap moment of inertia I_R, the rotor speed Ω, the disk loading DL, and the weight of the aircraft W. This autorotation ability of the *Kestrel* can be evaluated by an autorotational index AI. The Sikorsky AI is defined in Eq. 5. *Kestrel* was determined to have an AI of 12 which is satisfactory for a multi-engine aircraft as shown by Fig. 14.7.

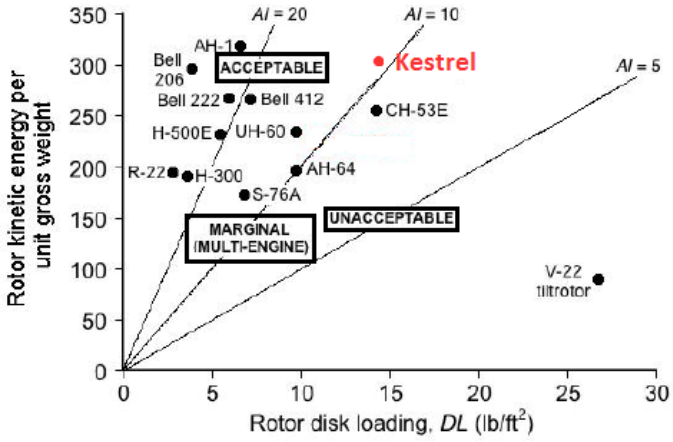

Figure 14.7: Comparison of autorotative index for various rotorcraft.

$$AI = \frac{I_b \Omega^2}{2W(DL)} \tag{5}$$

14.8 RFP Mission Performance

Figure 14.9 shows the fuel burned, power required, distance traveled, and time elapsed by the *Kestrel* for each segment of the mission profile specified by the RFP. Fig. 14.8 summarized the total time and distance of the mission. Also shown in Fig. 14.8 is hover efficiency, propulsive efficiency, and operating altitudes for the mission segments.

Mission Summary	
Mission Completion Time	232.6 min
Total Distance Traveled	734.5 min
Average Airspeed	189.5 kts

Operating Altitude ISA	
Segments 4,5,9,10,14	9,180 ft
Segments 1,2,7,12,13	SLS

Hover Efficiency	
Segment 2	82%
Segment 7	82%
Segment 12	82%

Propulsive Efficiency	
Segment 4	87%
Segment 5	72%
Segment 9	72%
Segment 10	87%

Figure 14.8: RFP mission profile performance summary.

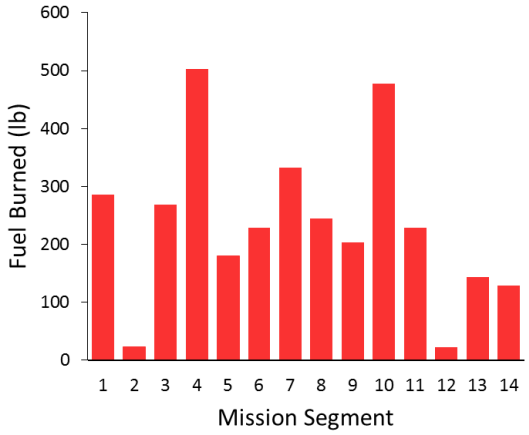

(a) Fuel burned for each mission segment.

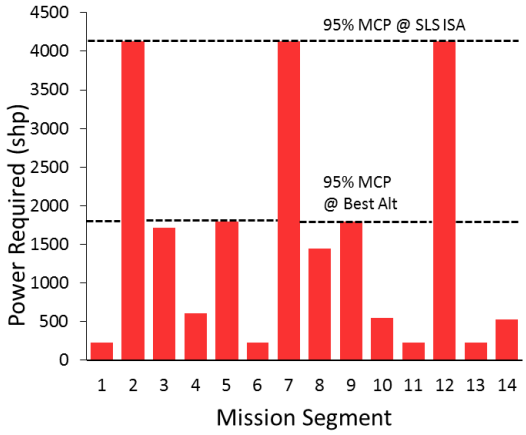

(b) Power required for each mission segment.

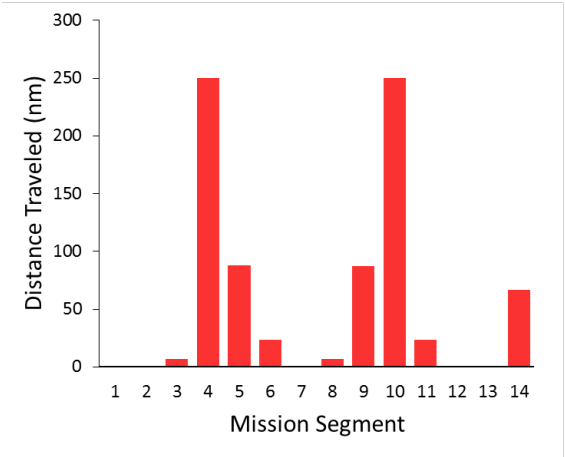

(c) Distance traveled for each mission segment.

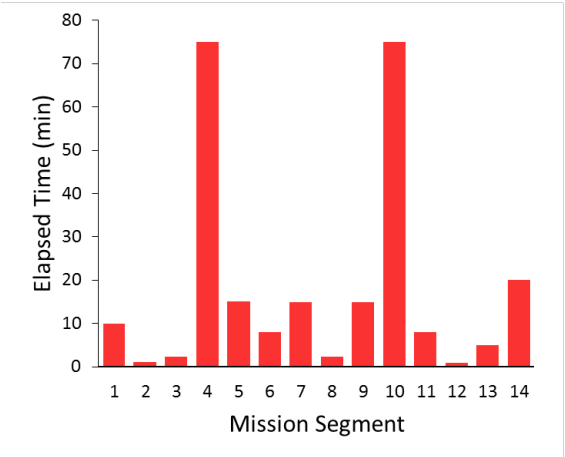

(d) Elapsed time for each mission segment

Figure 14.9: Mission profile performance data.

15 Concept of Operations (CONOPS)

The *Kestrel* is a technology demonstration platform with an extraordinary practical application. The *Kestrel* is also a force multiplier that is well suited for a variety of tasking, and can enhance the capabilities of other systems in service. The following details the Concept of Operations (CONOPS) for the aircraft.

15.1 Basis for Conceptual Operations

The *Kestrel* is a VTOL platform with, omnidirectional maneuverability, hovering, and landing on any flat surface, with superior forward flight capabilities and structural efficiency as compared to contemporary platforms. The *Kestrel* has a superior cruise airspeed of up to 350 kts, which can shorten the mission time and reduce time-on-target within a hostile environment. The speed capability does not compromise at the cost of range, forward flight efficiency, or useful payload. The *Kestrel* has a maximum L/D of 11.9 at its best range airspeed, with a useful load capability over 40% of the MTOGW. The *Kestrel* is a cross-pollination of efficient fixed-wing and rotary-wing aircraft that enables radically improved capabilities.

15.2 Intelligence, Surveillance, Reconnaissance (ISR) Capability

The *Kestrel* is an unmanned aircraft that can adopt to the rolez and responsibilities of as an Intelligence, Surveillance, and Reconnaissance (ISR) platform, that are too dangerous or repetitive for manned operations. The *Kestrel*'s range capability can maximize the distance a take off position can be from a potentially dangerous target location, such as inclement weather or a hazardous material spill. The *Kestrel* can provide rapid response and monitor events such as the 2011 Fukushima Daiichi nuclear disaster and keep response personnel out of harm's way. With a maximum endurance of 10.78 hours, an orbit of 3 *Kestrel*s could provide continuous coverage for intelligence gathering.

Weather stations can launch the *Kestrel* from a ground control center in fair weather and travel over bad weather to the center of a storm. The *Kestrel* has a large enough mission radius, of 809 miles, to fly to the center of the largest hurricane or tropical cyclone ever recorded on Earth (*Hurrican/Super Storm Sandy* [45] and *Typhoon Tip* [46], respectively). The Kestrel can also monitor the aftermath for disaster relief. Typhoon Haiyan, the 2004 Indian Ocean Tsunami, and the Deep Water Horizon incident, have proved the need for a VTOL aircraft with a large mission radius to assess damage and direct where rescue crews should respond. Figure 15.1 shows the mission radius of *Kestrel* as compared to the AW-609, an aircraft that is 50% heavier.

15.3 Cargo Delivery

The *Kestrel* can also fill the role as a cargo delivery platform. The unmanned aircraft system (UAS) can deliver day or night to locations deemed unsafe for manned flight without the risk of loss of life. The *Kestrel*'s speed and range capability are ideal for a fast-moving environment, such as battlefield or disaster relief. The *Kestrel* would be also for an ideal platform for repetitious cargo delivery tasking such as within the construction, logging, and firefighting industries.

15.4 Communication Relay

Many communication systems are limited by the line-of-sight (LOS) ranges, however the *Kestrel* is a force multiplier platform that will increase the capability of all communication networks it interfaces with. The *Kestrel* can fill the role as a flying cell tower to relay communications over the horizon for platforms that rely on LOS communications. Multiple *Kestrel*s can be linked together in series for an unlimited communication range. Figure 15.2 shows a visualization of two *Kestrel*'s in series aiding communication between a ship and a station outside of LOS

Figure 15.1: Radius of action with full payload and ferry range with full payload for the *Kestrel*.

Figure 15.2: *Kestrel*s aiding in communication links between a ship and a ground station.

15.5 Aerial Refuel

The *Kestrel*'s modular internal payload could also be outfitted with accessory systems to provide aerial refuel capability to other aircraft. The hard points on the main wing could be fitted with a Buddy-Refuel Pod and auxiliary fuel pods and the modular internal payload bay could be converted to hold auxiliary fuel tanks. Figure 15.3 shows a visualization of the *Kestrel* within its aerial refuel role.

15.6 Payload Interoperability

The *Kestrel*'s modular internal payload bay is located near the nose of the aircraft. The internal payload bay has clamshell doors as shown in Fig. 15.4. For easy access to the payload bay a ground support platform will come with

Figure 15.3: *Kestrel* operating as an aerial refueling platform.

Kestrel. This platform measures 8x10x0.5 ft with a curvature cutout that contours with the *Kestrel* fuselage. The platform is made of aluminum and steel, with a solid surface on top for ground crews to stand on, and forklift access holes running through the platform. A forklift will raise the platform, with 2–3 ground crew, and the awaiting to be installed payload on the platform; so that the ground crew may access the internal payload bay.

Inside the payload bay, aviation L-Track Rails run along the internal walls as shown in Fig. 15.4. Ground crew will be able to place cargo within the internal bay and fasten the cargo using aviation tie down straps, using the L-Track Rails as anchors.

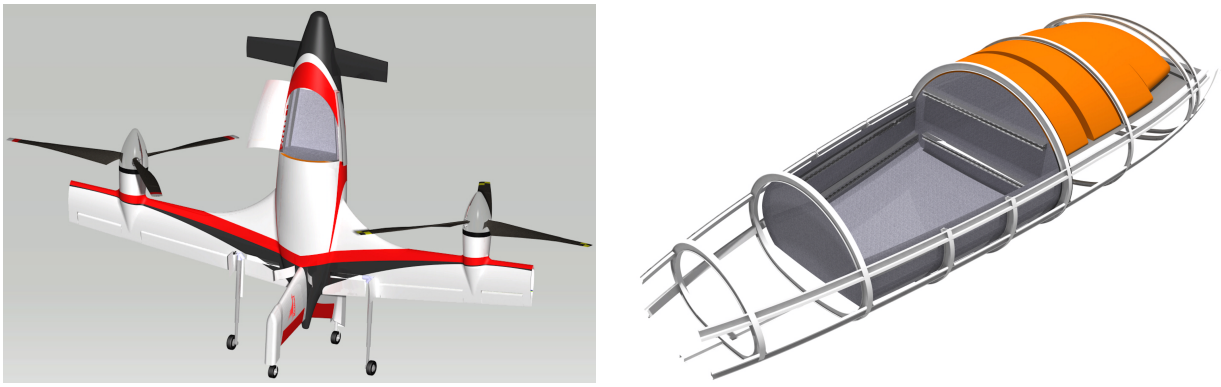

(a) (b)

Figure 15.4: *Kestrel*'s cargo bay.

16 Safety

The *Kestrel* is an unmanned platform so the concern over safety pertains to ground crew and people in the vicinity of the aircraft. The *Kestrel* is in compliance with the airworthiness standard set by the FAR Part 25 and 29.

16.1 Engine Failure

In the unlikely event of a single engine failure the interconnected drive shaft will drive both proprotors with one engine. The *Kestrel* will be able to transition from airplane mode and land normally with one engine inoperable (OEI) because, as described in Section 14, *Kestrel* has 962 shp of excess power at MSL. If both engines become inoperable in helicopter mode, the *Kestrel* has acceptable autorotation capability for a multi-engine aircraft as described in Section 14.7. If both engines fail when in airplane mode the *Kestrel* has a glide ratio of up to 11.9 which will provide the operators with time and range to plan a belly landing. Upon landing the composite proprotor blades will ”broomstraw” effectively disintegrating the blades and prevent further damage to the aircraft strcutre.

16.2 Fuel Tanks

The *Kestrel* has four fuel tanks located in the fuselage, aft of the internal payload bay, and one within the wing torque box. Each fuel tank has a self sealing fuel bladder to stop leaks in the event the fuel tank is punctured. The fuel tanks have been sized with an additional 10% volume, to air cushion the fuel in the event of a hard landing, which is compliance with FAR 29.952.

16.3 Fire Suppression

In the event of a fire the *Kestrel*, will deploy its solid propellent gas generator (SPGG) technology for suppression against flammable materials such as fuel, hydraulic fluid, and oil, which is in compliance with FAR 29.863. In the event of a manageable fire the *Kestrel* on the ground, the ground crews will be equipped with aviation fire extinguishers.

16.4 Ground Crew

The proprotors are located 15 ft above the ground which reduces the likelihood of injury to ground crew. Ground crew will however, need to be aware of the hot exhaust gases to prevent injury. To mitigate the risk of ground crew making contact with the exhaust gas and to prevent any damage to the runway or flight deck, the *Kestrel* will utilize coanda exhaust deflectors [48], similar to the one used on the MV-22, to safely disperse the exhaust gas from the aircraft.

17 Acoustics

The RFP does not state a definitive requirement for the acoustic characteristics of the aircraft. The aircraft must permit safe human operation below and in its immediate vicinity. Any aircraft intended for military or civilian use must meet strict acoustic requirements to reduce noise pollution and/or detection.

17.1 FAA Noise Requirements

Currently, there is no specific Federal Aviation Administration (FAA) noise certification standard for tailsitter aircraft. However, there are guidelines in reference to tiltrotors provided by Federal Aviation Regulations (FARs). Tiltrotors and tailsitters are similar in that the proprotor plane will be parallel to the ground in hover and low speed flight, and perpendicular to the ground in high-speed flight. Recently implemented changes to FAR Part 36 and the existing standards to the International Civil Aviation Organization (ICAO) require an aircraft noise measurement must be taken from one centerline noise position and two sideline positions. The flyover centerline noise measurement is located 492 feet (150 m) vertically below the aircraft; the two sideline points are symmetrically stationed on the ground at 492 ft (150 m) and perpendicular to the flight path.

The noise level limit for a 10,000 lb aircraft is between 95 and 99 EPNdB (Effective Perceived Noise Level in decibels) depending on the flight condition. Figure 17.1 shows the requirement graphically.

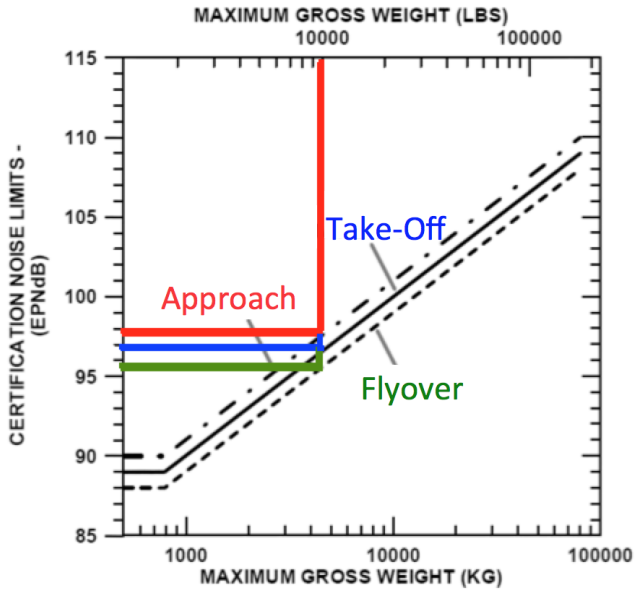

Figure 17.1: FAA Noise Limit Requirements (FAR 36.1103)

17.2 Noise Assessment

Rotor Noise estimations were obtained using an acoustics analysis developed at the University of Maryland base on Farasatts Formulation-1A of the Ffows–Williams–Hawkings (FWHA) equations. The FWHA model computes both the thickness noise and the loading noise. The thickness noise is caused by the displacement of the air by the rotor blade, thickness noise is a mainly a function of the thickness of the blades. The loading noise is from the blade loading. The thickness noise travels mostly in plane rotor and the loading noise travels directly below the rotor. This means that

when the *Kestrel* is traveling in airplane mode, the noise will be directed below and behind the flight path. For military applications this characteristic will decrease the acoustic detection when approaching a target. For civil applications, the *Kestrel* will mainly be heard while departing an area, which will reduce annoyance when flying overhead.

17.3 Noise Assessment in Helicopter Mode

The noise levels were calculated at the reference points stated in the FARs. Figure 17.2 shows the spherical contour plot for the thickness noise at a distance of 492 ft. The plot shows sound pressure levels measured in decibels. The sounds pressure levels were found to meet the requirements for all measurement points for departure, fly-over, and approach while in helicopter mode. The loading noise levels were also calculated and shown in Fig. 17.3 ; which was also found to be within regulation.

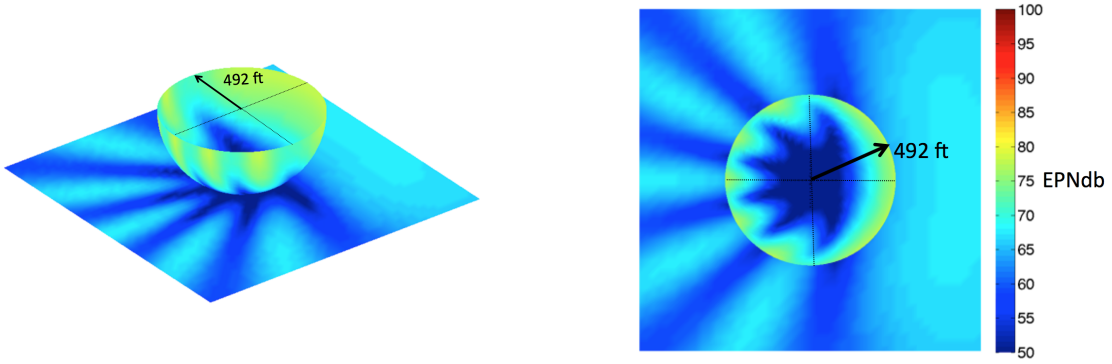

Figure 17.2: Thickness noise sound pressure levels, isometric and top view

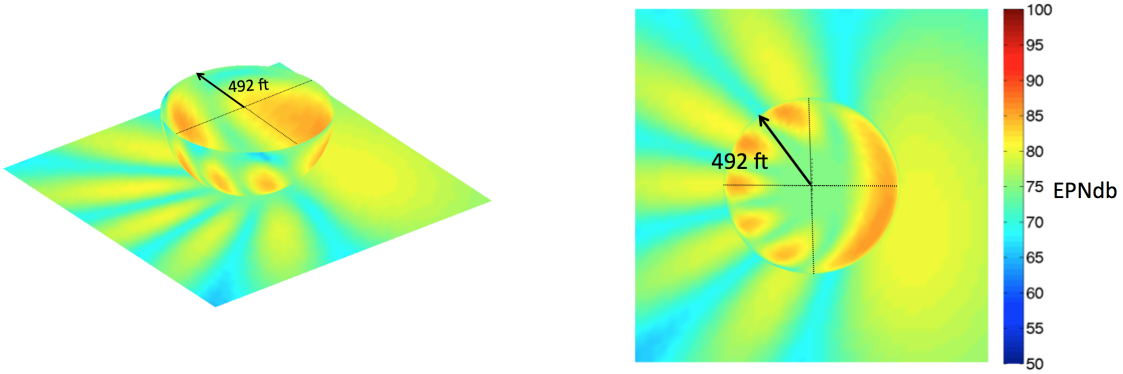

Figure 17.3: Loading noise sound pressure levels, isometric and top view

17.4 Noise Assessment in Airplane Mode

The noise levels for *Kestrel* were also calculated in airplane mode. For all operating conditions in airplane mode the *Kestrel* was found to have a lower noise measurement than when in helicopter mode, which can be attributed to the proprotor plane being perpendicular to the ground and operating at a lower blade loading compared to hover.

18 Life Cycle Cost

The life cycle cost of *Kestrel* can be broken into the following phases:

1) Development Cost
2) Acquisition Cost
3) Operational Cost

As this is a fixed price technology demonstrator program the main focus of the life cycle study was the acquisition cost and the operational cost. With respect to *Kestrel*, much emphasis was placed on minimizing the acquisition and operational cost while still fulfilling the RFP.

18.1 Acquisition Cost

The air vehicle cost analysis was based on the formula by Harris and Scully [47] and calculated in 1994 USD and adjusted according to the consumer price index (CPI) to 2014 USD. The empirical cost analysis model is based on the empty weight, number of rotor blades, engine power rating, and an additional empirical factor, H, made up of it's own subcomponents. The empirical factor H is based on the country of origin, air vehicle pressurization capability, landing gear type, engine type, number of engines, and number of main rotors. Each of these factors correspond to an empirical table lookup shown in Table 18.1. The calculation of H is shown in Eq. 6.

Table 18.1: Summary of Empirical Corrections

Country of Origin		Pressurized		Landing Gear	
U.S. Commercial	1.00	Yes	1.135	Fixed	1.000
U.S. Military	0.838	No	1.000	Retractable	1.104
France/Germany	0.860				
Russia	0.330				
Engine Type		**Number of Engines**		**Number of Main Rotors**	
Piston	1.000	Single	1.000	Single	1.000
Supercharged Piston	1.000	Multiple	1.352	Twin	1.046
Turbine Piston	1.180				
Gas Turbine	1.779				

$$H = Country * No.\ Engines * Engine\ Type * No.\ MainRotors * Landing\ Gear * Pressurization \tag{6}$$

Using the values presented in Table 18.1 the empirical factor, H, was calculated using Eq. 6. The original equation developed by Harris and Scully is shown in Eq. 7. The Harris and Scully base price for the air vehicle base price was adjusted for changes in inflation and CPI between the initial model development (1994) and present day (2014). The United States Bureau of Labor Statistics provided the adjustments for inflation and CPI.

$$Air\ Vehicle\ Base\ Price\ (1994\ USD) = 236.77 * N_b^{.2045} * W_{empty}^{.4854} * P_{Installed}^{.5843} * H \tag{7}$$

Eq. 7 calculates estimated baseline price for similar platforms and presented in Table 18.2. Although *AgustaWestland* is a British-Italian based company, for the purpose of this cost estimate study, *AgustaWestland* was given a similar weighting as aircraft originating from France and Germany. The AW-609 was initially developed by *Bell Helicopter* and *AgustaWestland*, therefore the aircraft was given an averaged weighting between U.S. Commercial and *AgustaWestland*. The actual baseline cost were obtained by Helicopter Blue Book [47] and is presented in Table 18.2.

Kestrel is estimated to have an air vehicle base line cost of $19.1 million which is greater than a helicopter but less than a tiltrotor within a similar weight class. Table 18.2 shows the empirical model developed by Scully and Harris

Table 18.2: Summary of Estimated and Actual Acquisition Costs

	AW-609	AW-139	EC-155	Kestrel
Calculated Baseline Price ($M)	25.5	11.0	10.6	19.1
Actual Baseline Price ($M)	30.0*	12.2	10.0	

* Projected Cost, not in production

accurately predicts the acquisition cost of various aircraft. An interesting note for this estimation method is that the K-MAX unmanned aircraft, produced by Lockheed Martin Corporation and Kaman Aerospace Corporation, is estimated to be $7.6 million while the actual price is quoted at $5.1 million. The original model developed by Harris and Scully may over estimate the acquisition cost of unmanned air vehicles.

18.2 Ground Control Station Costs

Kestrel is part of an unmanned air system (UAS) which in addition to the air vehicle includes the Ground Control Station (GCS) described in Section 12. Unmanned air systems are a relatively new sub sector of the aerospace industry and almost exclusively for military applications. Thus actual costs for a new ground control stations are difficult to ascertain. However, ground control stations are not expected to scale with the cost of the aircraft. A Universal Ground Control Station (UGCS) such as the AAI Textrons One System® is capable of controlling multiple unmanned platforms simultaneously. If the customer possesses an UGCS capable of interfacing with *Kestrel*, the GCS can be excluded from the life cycle cost.

18.3 Direct Operating Cost

The direct operating costs (DOC) are the costs that vary directly with respect to flight hours. The DOC encompasses the costs associated with the physical labor and materials to maintain the aircrafts airworthiness. The materials required to maintain the aircrafts airworthiness include the fuel, fuel additives, lubricants, and parts. The labor required includes the required maintenance and inspections.

The direct and indirect operating cost analysis used the *Conklin & de Decker Aviation Information* Life Cycle Cost program. The cost analysis generated financial data over 20 years of service life with 400 flight hours per year and annual 2.75% inflation. For comparison, the DOC for the EC-155 and *Kestrel* are shown in Fig. 18.1 and 18.2.

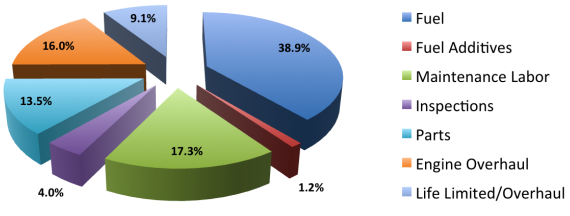

Figure 18.1: EC-155 DOC per Flight Hour

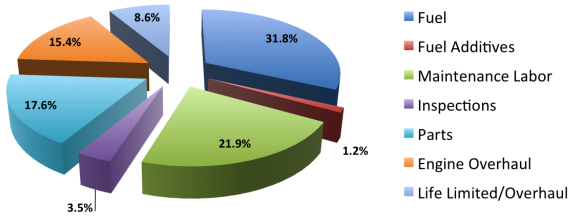

Figure 18.2: Kestrel DOC per Flight Hour

As shown inFig. 18.1 and 18.2 the dominant cost for the DOC is the fuel consumption for aircraft. *Kestrel* is a fuel efficient vehicle both in hover and forward flight but will average a fuel burn closer to contemporary helicopters due to the maximum cruise speed. For a detailed comparison, the direct operating cost was calculated for the EC-155, AW-139, and *Kestrel* and shown in Table 18.3

	Fuel + Additives	Maintenance Labor	Inspections	Parts	Engine Overhaul	Life Limited + Overhaul	Total
EC -155	1,199	410	55	438	336	143	2,220
AW-139	891	384	88	300	355	201	2,591
Kestrel	753	500	80	400	350	195	2,278

Table 18.3: Estimation of Direct Operational Costs (USD per Flight Hour)

18.4 Indirect Operating Cost

The Indirect Operating Costs (IOC) varies directly with the number of days the aircraft is committed to a tasking. These costs comprise of fixed costs and daily operating costs associated with the aircraft. The fixed costs include cost of buildings, management personnel, insurance, and depreciation. The daily operating costs include the salary and benefits for personnel to accomplish the task. Other miscellaneous indirect operating costs exist such as pilot training/currency requirements and the modernization/refurbishing of the aircraft. Figure 18.3 and 18.4 show the estimated IOC for the EC-155 and Kestrel.

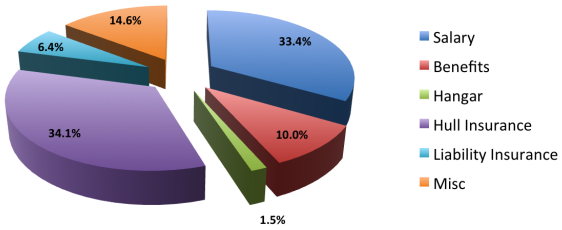

Figure 18.3: EC-155 Annual IOC

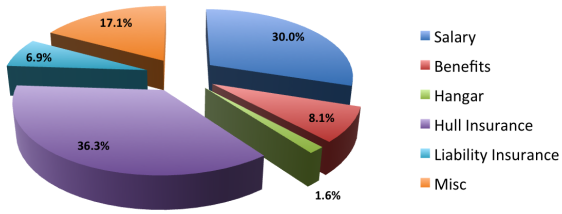

Figure 18.4: Kestrel Annual IOC

As shown in Fig. 18.3 and 18.4 the highest daily costs is the pilot salary and hull insurance. *Kestrel* as an unmanned platform introduces cost savings because it will not require a traditional pilots salary and benefits. *Kestrel* will have an Air Vehicle Operator (AVO) and depending on the mission a Sensor Operator (SO). The salary for both operators are based on seniority and experience level and are typically less than a traditional pilot. In general the SO will make less than an AVO because an SO does not require the same level of training and education of an AVO. The cost to provide health insurance, life insurance and disability benefits is far less than a traditional pilot due to the significantly decreased risk of death or injury. Hull insurance is calculated based on the acquisition cost and a percentage of the insured value. The liability insurance is currently rated at $25,000 per year. For a detailed comparison, the indirect operating cost was calculated for the EC-155, AW-139, and *Kestrel* and shown in Table 18.4.

	Salary	Benefits	Hangar	Hull Insurance	Liability Insurance	Misc	Total
AW-139	171,534	51,460	9,020	199,650	32,747	80,344	544,755
EC-155	171,534	51,460	7,810	175,514	32,747	74,888	513,953
Kestrel	143,000	38,595	7,590	173,184	32,747	81,488	476,604

Table 18.4: Estimation of Annual Indirect Operational Costs (USD)

19 Mini-Kestrel, a MAV Scale Design-Build-Fly Demonstrator

A Micro Air Vehicle (MAV) version of the Kestrel was developed in tandem with the full-sized vehicle to investigate scalability and as a technology demonstrator. The Mini-Kestrel has a 20 inch wing span and a 280 gram take-off weight. The design is shown in Fig. 19.1 along with a picture of the current prototype.

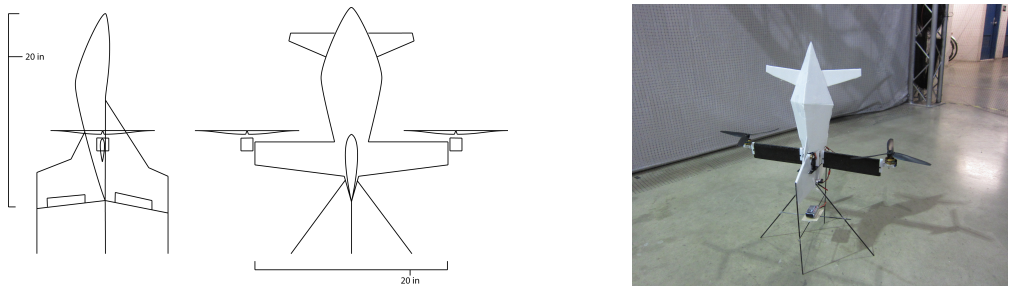

(a) Design schematic (b) Current prototype

Figure 19.1: The Mini-Kestrel MAV.

19.1 Airframe

The aerodynamic design of the Kestrel was adapted for the low Reynolds number flight regime encountered by small scale flyers. The Mini-Kestrel has a lower wing loading than the full scale vehicle and a lower aspect ratio wing. An Eppler 549 airfoil was chosen for the wing, and the design has larger vertical tail surfaces for improved gust rejection.

The combination of proprotor cyclic and aerodynamic surfaces used on the Kestrel had to be adapted for a MAV scale vehicle. For mechanical simplicity, a pair of tilting rotors are used in place of longitudinal cyclic control. For forward flight, the canard is fixed, leaving roll and pitch control to a set of mixed-input ailerons. The tilt rotor mechanics are built on a carbon fiber composite chassis with CNC machined delrin bearing blocks. The structure forms a central core for the fuselage, wings, vertical tail and simplified landing struts. The wings are constructed from carbon fiber/sandwich foam structure which houses a hollow member for electrical wiring to pass through. This ensures an aerodynamically clean surface on the wing. The central mechanism on the current prototype is shown in Fig. 19.2 .

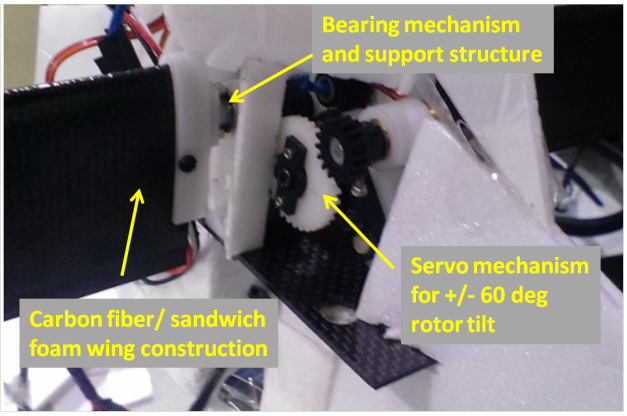

Figure 19.2: MAV central chassis and tiltrotor mechanism.

19.2 Avionics

Like the full-sized Kestrel, the MAV demonstrator uses a combination of inertial and aerodynamic sensing for flight control and transition guidance. The autopilot board uses an ARM Cortex M3 processor for data acquisition and flight control. An Invensense MPU 9150 IMU provides inertial measurements and a nRF24L01 radio is used for communications with a ground station. Radio The board weighs 1.3 grams and was designed at the University of Maryland [49,50]. Due to payload constraints, the MAV-scale aerodynamic sensing package is simplified to a reduced set of three embedded pressure ports over each canard surface for transition guidance. A set of Honeywell HSDCRR 1NDAA3 series pressure sensors mounted on the fuselage provide differential pressure measurements for airspeed and canard flow-state estimation. These are shown in Fig. 19.3.

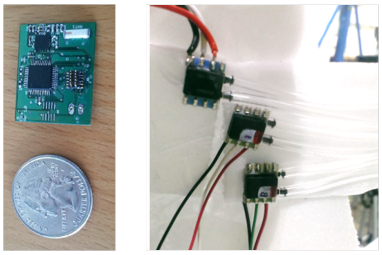

(a) ELKA Autopilot board and pressure sensors

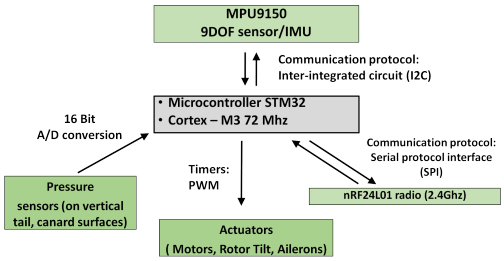

(b) Communication protocol

Figure 19.3: MAV Avionics.

19.3 Initial Flight Tests and Ongoing Work

The Mini-Kestrel was first flown in the Collective Dynamics and Control Laboratory (CDCL) indoor flight test facility. The current prototype was remotely piloted and demonstrated vertical take-off and hover capabilities. Still images from flight tests are shown in Fig. 19.4

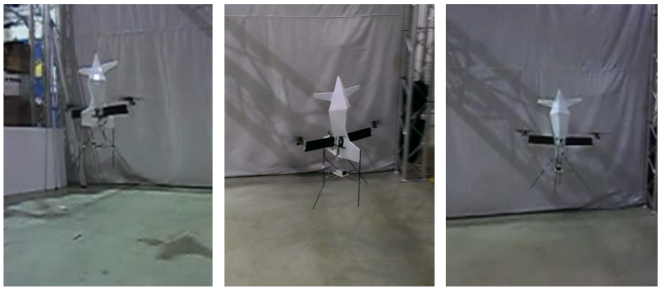

Figure 19.4: Mini-Kestrel in flight at the CDCL indoor test facility.

The current vehicle is still under development. Initial hover testing was carried out using a combined tiltrotor and wing configuration to simplify construction. The aerodynamic control surfaces are currently being installed for forward flight tests.

20 RFP Requirements

Table 20.1: Avionics equipment weights and power requirements.

RFP Requirements (Section 1.1)	***Kestrel* Performance**	**Achieved?**	**Performance Margin**	**Section**
Sustained high speed flight: 300-400 KTAS	Maximum continuous speed = 350 KTAS	Yes	Met requirement	3
Aircraft hover efficiency within 25% of ideal power loading	Hover efficiency= 18% of ideal power loading	Yes	Exceeded by 9.3%	4.11
Useful load fraction $\geq$40% gross weight, payload fraction $\geq$12.5% gross weight	Useful load fraction $\geq$40% gross weight, payload fraction $\geq$12.5% gross weight	Yes	Met requirement	10
Maximum gross weight: 10,000-12,000 lb with weight breakdown	Maximum gross weight: 11,000 lb	Yes	Met requirement	10
Aircraft cruise lift-to-drag ratio$\geq$10	Best range airspeed lift-to-drag ratio= 11.9	Yes	Exceeded by 19%	15.4
Utilize existing & available engine technology	Rolls-Royce/Turbomeca RTM322-01/9 turboshaft engine	Yes	Met requirement	2.2.1
Utilize technologically mature subsystems	All components of high technical readiness level (TRL)	Yes	Met requirement	4.10
Development of flight control laws	Robust H_∞ controllers	Yes	Met requirement	11.3
Performance and handling qualities analysis with FLIGHTLAB model	Level 1 handling qualities	Yes	Met requirement	13.1
Day VFR MEL avionics suite	VFR & IFR Avionics Suite	Yes	Met requirement	13.1.1
Minimum vertical load factor envelope of -0.5G to 2.0G throughout speed ranges	Structurally sound to meet load factor	Yes	Met requirement	14.6
Ability to carry out standardized flight profile	Fully capable	Yes	Met requirement	15.7
Scalability	Scaled design-build-fly flight demonstrator	Yes	Met requirement	19

21 Summary

The University of Maryland Graduate Team has designed the *Kestrel*, a novel tailsitter that combines the high hover efficiency of rotary-winged vehicles with the high speed capability of fixed-wing vehicles. The *Kestrel* meets all the performance requirements mandated by the 2014 AHS Student Design Competition RFP, including the sustained high speed flight at true airspeeds between 300 kts and 400 kts, system hover efficiency within 25% of the ideal power loading, lift-to-drag ratio of atleast 10, and useful load fraction of atleast 60% of the gross weight with a payload fraction no less than 12.5% gross weight. The proposed design concludes:

1. The Pareto efficiency analysis for the parametric study, coupled with the advanced proprotor blade airfoils allows for superior performance for hover and forward flight.
2. The autonomous capability with remotely-piloted option, are leveraged to utilize the tailsitter configuration which reduces the empty weight, mechanical complexity, and download penalty.
3. The dual-speed transmission, enable unprecedented forward flight efficiency for a vertical take-off and landing vehicle.
4. The fully autonomous transition, is augmented with stall detection pressures sensors, cyclic and collective pitch, and fixed wing control surfaces is path optimized for power efficiency and scheduled based on airspeed, stall detection and flight path angle
5. Aerodynamic considerations established a need for a two-speed gearbox. The Differential Dual-Drive two-speed gearbox concept has the ability to change proprotor speed smoothly without drivetrain shock or disruption of power. Because of the use of existing technologies, the team is confident that this dual-speed drivetrain will be a successful design.

22 References

[1] "Broad Agency Announcement: Vertical Take-Off and Landing Experimental Aircraft (VTOL X-Plane)," Defense Advanced Research Projects Agency, Tactical Technology Office, Arlington, VA, February 2013.

[2] Nagaraj, V. T., "ENAE634 Helicopter Design Lecture Notes: Concept Selection Methodology," University of Maryland, College Park, 2014.

[3] Tishchenko, M. N., and Nagaraj, V. T., "Preliminary Design of Helicopters: Notes on Tishchenko's Method for Initial Sizing of Helicopters," University of Maryland, College Park, 2014.

[4] Leishman, J.G., *Principles of Helicopter Aerodynamics*, 2^{nd} ed., Cambridge University Press, Cambridge, England, UK, 2006.

[5] Suhr, S. A., *Preliminary Turboshaft Engine Design Methodology for Rotorcraft Applications*, Master of Science Department of Aerospace Engineering, Georgia Institute of Technology, Atlanta, GA, 2006.

[6] Johnson, W., "NDARC – NASA Design And Analysis of Rotorcraft Validation and Demonstration," AHS Aeromechanics Specialists Meeting, San Francisco, CA Jan. 20–22, 2008.

[7] Turbomeca, "RTM 322," RTM 322 datasheet, Sept. 2012

[8] Smailys, H. M., Chabot, M., Chamoun, J., Chmiel, D., Jermyn, D., Kacker, S., Lefebvre, F., Litalien, C., Patel, K., and Stuttaford, P., "Advanced Technologies Applied to PT6C-67A Tiltrotor Engine Design," 57th Annual Forum Proceedings of the American Helicopter Society, Washington, D.C., May 2001.

[9] Leishman, J.G., *Principles of Helicopter Aerodynamics*, 2^{nd} ed., Cambridge University Press, Cambridge, England, UK, 2006.

[10] Noonan, K. W., Althoff, S.L., Samak, D.,K., and Green, M.D., "Effect of Blade Planform Variation on Forward-Flight Performance of Small-Scale Rotors," National Aeronautics and Space Administration, Langley Research Center, Hampton, VA, 1992.

[11] Prouty, R. W., *Helicopter Performance, Stability, and Control*, R. E. Krieger Publishing Company, Melbourne, 2002.

[12] Walker, T. D., and Baskin, B. K., "Drive Mechanisms for Variable Diameter Rotor Systems," Patent No. US 20110206513 A1m Sikorsky Aircraft Corporation, Stratford, Connecticut, Dec. 2010.

[13] Jane, F.T., *Janes All The Worlds Aircraft*, New York: McGraw-Hill,. 2013, pp. 439

[14] Gudmundsson, S., *General Aviation Aircraft Design Applied Methods and Procedures*, Butterworth–Heinemann, Oxford, 2014.

[15] Leishman, J. G., *The Helicopter: Thinking Forward, Looking Back*, College Park Press, College Park, Maryland, 2007.

[16] Peyran, R. J., and Rand, O., "The Effect of Design Requirements on Conceptual Tiltrotor Wing Weight, 55th Annual Forum of the American Helicopter Society, Montréal, Québec, Canada, 25–27 May 1999.

[17] Nixon, M., "Aeroelastic Response and Stability of Tiltrotors with Elastically Coupled Composite Rotor Blades," Doctor of Philosophy, Department of Aerospace Engineering, University of Maryland, College Park, Maryland, 1993.

[18] Johnson, W., "Dynamics of Tilting Proprotor Aircraft in Cruise Flight," NASA TN D-7677, 1974.

[19] Anderson, J. *Introduction to Flight*, Mcraw-Hill Higher Education, Crawfordsville, IN, 2008.

[20] Handschuh, R.F., Lewicki, D.G., and Stevens, M.A., "Variable/Multispeed Rotorcraft Drive System Concepts," NASA TM2009-215456, March 2009.

[21] Rotorcraft Engine and Rotor Speed Synchronization. Rotorcraft Engine And Rotor Speed Synchronization. Web. 04 Apr. 2014.

[22] Explain That Stuff, "Chainsaws-Centrifugal Clutch: How Does a Chainsaw Work?", http://www.explainthatstuff.com/how-chainsaws-work.html, [accessed 30 Apr. 2014].

[23] Budynas, R. G., and Nisbett, J. K., *Shigley's Mechanical Engineering Design*, McGraw-Hill, Singapore, 2011.

[24] U.S. Army, *Engineering Design Handbook - Helicopter Engineering Part One: Preliminary Design (AMCP706-201)*, Headquarters, U.S. Army Material Command, Alexandria, VA, 1974.

[25] U.S. Army, *Engineering Design Handbook - Helicopter Engineering Part Two: Detail Design (AMCP706-202)*, Headquarters, U.S. Army Material Command, Alexandria, VA, 1974.

[26] Alcoa, "Alloy 2099-T83 And 2099-T8E67 Extrusions," http://www.alcoa.com/hard_alloy_extrusions/catalog/pdf/Alloy2099TechSh [accessed 5 May 2014].

[27] Kureemun, R., and Bates., D. G., "Aircraft Flight Controls Design Using Constrained Output Feedback," American Institute of Aeronautics and Astronautics Guidance, Navigation and Control Conference and Exhibition, Montréal, Canada, 6–9 August 2001,.

[28] Martin, M. D., and Demo, G. J., *The history of the XV-15 tilt rotor research aircraft: from concept to flight*, National Aeronautics and Space Administration, Office of Policy and Plans, NASA History Division, 2000.

[29] Yeo, D., Atkins, E., Bernal, L., and Shyy, W., "Aerodynamic Sensing for a Fixed Wing UAS Operating at High Angles of Attack," AIAA 2012-4416, Proceedings of the AIAA Atmospheric Flight Mechanics Conference, Minneapolis, Minnesota, 13–16 August 2012.

[30] Yeo, D., Atkins, E., Bernal, L., and Shyy, W., "Experimental Validation of an Aerodynamic Sensing Scheme for Post-Stall Aerodynamic Moment Characterization," AIAA 2013-4979, Proceedings of the AIAA Atmospheric Flight Mechanics Conference, Boston, Massachusetts, 19–22 August 2013.

[31] Jung, Y., Shim, D., and Ananthkrishnan, N., "Controller Synthesis and Application to Hover-to-Cruise Transition Flight of a Tail Sitter UAV," AIAA 2010-7508, Proceedings of the AIAA Atmospheric Flight Mechanics Conference, Toronto, Ontario, Canada, 2–5 August 2010.

[32] Hrisihikeshavan, V., Bawek, D., Rand, O., and Chopra, I., "Control of a Quad Rotor-Biplane Micro Air Vehicle in Transition from Hover to Forward Flight," 69th Annual Forum of the American Helicopter Society, Phoenix, Arizona, May 2013.

[33] Handbook of Business Aviation, "AgustaWestland introduces Obstacle Proximity LiDAR System (OPLS) for enhanced safety," http://www.handbook.aero, [accessed 26 February 2014].

[34] Sierra Nevada Corporation, "Gorgon Stare - Persistent Wide Area Airborne Surveillance (WAAS) System Brochure," http://www.sncorp.com/pdfs/isr/gorgon_stare.pdf, [accessed April 2014].

[35] BAE Systems, "Autonomous Real-Time Ground Ubiquitous Surveillance Imaging System (ARGUS-IS) Brochure," http://bit.ly/1usFmXB, [accessed April 2014].

[36] US Army, "Combat Rotorcraft EMI Suppression Technology (CREST)," SITIS Archives - SBIR A04-080 (Army), www.dodsbir.net, [accessed April 2014].

[37] Jensen, D., "HUMS, Aviation Today Online," October 1, 2006, http://bit.ly/Unktk4, [accessed April 2014].

[38] TRACKIR by NaturalPoint, "TrackIR 5 Brochure," http://www.naturalpoint.com, [accessed April 2014].

[39] Elbit Systems of America, "JEDEYE Brochure," http://www.elbitsystems.com, [accessed April 2014].

[40] Johnson, W., *Rotorcraft Aeromechanics*, Cambridge University Press, New York, 2013.

[41] Finck, R. D., "USAF Stability and Control DATCOM (Rev. ed.)," Flight Control Division, Air Force Flight Dynamics Laboratory, Wright-Patterson Air Force Base, Dayton, Ohio, 1978.

[42] Harris, F. D., *Introduction to Autogyros, Helicopters, and other V/STOL Aircraft*, National Aeronautics and Space Administration, Ames Research Center, Moffett Field, California, 2011.

[43] Leishman, J. G., *The Helicopter: Thinking Forward, Looking Back*, College Park Press, College Park, Maryland, 2007.

[44] AugustaWestland, AugustaWestland 609 Technical Data, http://www.agustawestland.com/product/aw609, [cited 3 May 2014].

[45] National Weather Service Weather Forecast Office, "Superstorm Sandy Event Review," http://www.erh.noaa.gov/rnk/events/2012/Sandy/summary.php, [accessed 3 May 2014].

[46] Steward, S., "Most intense tropical cyclones," Research World, Delhi, India, 2012.

[47] Harris, F. D., and Scully, M. P., "Helicopters Cost Too Much, 53rd Annual Forum of the American Helicopter Society, Virginia Beach, VA, April 1997.

[48] Kurtze, G., Gruenzweig, and Hartmann, "Jet engine Sound Suppressor With Coanda Effect Deflector," US Patent No. US3386528 A, June 1968.

MAV

[49] Petricca, L.,Hrishikeshavan, V., Ohlckers,P., and Chopra,I.,"Design, Fabrication and Testing of an Embedded Lightweight Kinematic Autopilot (ELKA)," *International Journal of Inteligent Unmanned Systems*, (in press), Apr. 2014.

[50] Shrestha, S., Hrisihikeshavan, V., Benedict, M., Yeo, D., and Chopra, I., "Development of Control Strategies and Flight Testing of a Twin-Cyclocopter in Forward Flight ," AHS 70th Forum, Montral, Quebec.